APPENDIX 5A

GILBERT ASSOCIATES, INC., REPORT

TO

METROPOLITAN EDISON COMPANY

ON

SUMMARY OF AIRCRAFT IMPACT DESIGN

FOR

THREE MILE ISLAND NUCLEAR STATION
UNIT 1

This Report Contains:

25 pages of text
7 tables
42 figures

A/7

7

TABLE OF CONTENTS

TABLE OF CONTENTS

LIST OF TABLES

FIGURES

FIGURES

FIGURES

1 INTRODUCTION

The vital structures of the Three Mile Island Nuclear Station Unit No. 1 as listed in Section 5.1.3 of the Final Safety Analysis Report are designed to withstand the following hypothetical aircraft impact loadings[1]:

Case	Item	Weight	Velocity	Effective Area
A	Object	6,000 lbs.	200 knots	5 ft. diameter
B	Object	4,000 lbs.	200 knots	3 ft. diameter
C	Total Aircraft	300,000 lbs.*	200 knots	16 ft. diameter
D	Total Aircraft	200,000 lbs.	200 knots	19 ft. diameter

This report presents results of the aircraft impact study, which includes the analysis of the Reactor Building shell for various locations of the above loadings; and, the plate analysis for the Case D loading, which is the basis for wall and roof slab designs for vital structures other than the Reactor Building shell. The paper entitled "On the Stress Analysis of Structures Subjected to Aircraft Impact Forces" is applicable to this work except for the static analysis of flat plates and a minor deviation in the dynamic load factors.

Also presented are additional studies to determine if the aircraft impact loading will produce a loss of prestress force in the Reactor Building shell and, if the loss of prestress does occur, what effect this loss would have on the structure.

The final study presented is concerned with the possibility of the spalling of the anchors of the liner due to an aircraft impact on the Reactor Building shell.

2 DYNAMIC LOAD FACTORS

The technique used to analyze these structures is based upon establishing a dynamic load factor and applying this factor to a static solution. In determining the DLF curve the response of an undamped, linear elastic one-degree-of freedom system is used.

* The analytical check on the basis of this loading considered a uniform collapse resistance of the fuselage which indicated that the integrity of the Reactor Building would not be jeopardized. Further investigation indicated that the assumption regarding uniform deceleration is not conservative. When a revised description of deceleration for Case C was assumed, based on a variable distribution similar in principle to that shown in Figure 5A-35 for Case D, the analytical methods employed did not demonstrate that the Reactor Building would remain stable. As

described in Section 3.1.1.2, the check was made for the Case C aircraft based on a constant loading and was found to be less severe than the Case D aircraft analyzed is described in Section 3.1.1.3. Because of the extremely remote probability of the Case C aircraft impacting at the most unfavorable location and attitude, the Case D aircraft for impingement was finally adopted as the design basis.

The idealized total reaction vs time curve is as shown in Figure 5A-1. This total reaction vs time curve describes quite well the results obtained from Tables 5A-6 and 5A-7 and figures 5A-35 and 5A-36. The time variable t_n and the ratio factor for a Boeing 720 airplane (Figure 5A-1) are shown in Table 5A-1.

The equations for dynamic load factors (DLF) for an undamped linear elastic one-degree-of-freedom system[2] are shown in Table 5A-2 in terms of the fundamental period T. The dynamic load factor is defined as the ratio between the dynamic response at any time (t) and the static response to the peak load P.

The maximum response as a function of the period T for Boeing 720 impact is calculated by the equations of Table 5A-2 and shown graphically in Figure 5A-3. Since this maximum response curve is obtained, the analysis of plate and shell structures can now be analyzed statically once the dynamic load factor is chosen from Figure 5A-3 with reference to appropriate period T. Figure 5A-3 represents a revised curve obtained from plotting additional points at $\frac{5}{1000} - \frac{2}{100}$ cps frequency steps.

Basically this curve is similar to the previous one but does pick up some oscillation which has been considered in the design.

3 ANALYSIS

The analysis of the vital structures as defined in Section 5.1.3 of the Final Safety Analysis Report is divided into two concepts: Section 3.1, Shell Analysis; and Section 3.2, Plate Analysis of this appendix.

3.1 SHELL ANALYSIS

This analysis is used for the Reactor Building. The areas of impact that are considered to be the most critical are; Apex of the Dome, Dome to Girder Transition, Girder to Cylinder Transition, Impact at Grade.

3.1.1 APEX OF THE DOME

This analysis is divided into three parts.

3.1.1.1 Analysis For Case A & B Impact Loadings

A study of the protection against missiles resulting from a hypothetical aircraft impact was made. The hypothetical missiles are defined as follows:

Case	Weight	Velocity	Impact Surface
A	6,000 lb	200 knots	5 ft diameter
B	4,000 lb	200 knots	3 ft diameter

This study consisted of an investigation of the overall structural response due to central impact of the missile on a spherical dome as well as the resistance to penetration due to a local material failure.

3.1.1.1.1 Structural Response

a. Introduction

An upper bound of permanent displacements was determined resulting from direct central aircraft impingement on a spherical dome. The basic tool used was the displacement bound theorem for rigid-plastic continua[3]. The initial velocity distribution is determined on the basis of an inelastic collision between the missile and the structure.

b. Limit Analysis for Ring Loads

First we considered a simply supported spherical cap under a ring load (See Figure 5A-4). The intensity of the load is "P" per unit length (i.e. the total load = $2\pi Pa$). A lower bound on the limiting value of "P" is found by determining a stress field which satisfies equilibrium condition and which nowhere violates the yield condition.

To obtain a lower bound, we assumed that for $r \geq a$

$$N_\phi = 0, \quad M_\theta = M_o$$

where "M_o" is the fully plastic moment per unit length. On this basis it can be then determined that:

$$2\pi Pa = \frac{4\pi M_o \sin}{\cos \bar{\phi}} \quad \frac{1}{\ln \left[\frac{(1+\sin\alpha)}{(1+\sin\bar{\phi})} \quad \frac{(1-\sin\bar{\phi})}{(1-\sin\alpha)} \right]}$$

where "$2\pi Pa$" is the total ring load.

For this condition where $\frac{"a"}{R}$ approaches zero.

$$\frac{2\pi Pa}{M_o} = 1.81\pi$$

c. Determination of the Initial Velocity Field

From the elastic solution for a concentrated load at the apex of a shell investigators have determined that "r_e," the length over which the initial velocity distribution is felt is approximately $2\sqrt{hR}$ where "h" is the shell thickness.[4,5] Therefore the initial velocity is sensibly zero for $r = r_e$.

The initial velocity distribution is considered proportional to the elastic static deflection due to a concentrated load at the apex. Because it is difficult to determine these deflections in closed form for a spherical shell it was necessary to approximate the deflection by several functions each one of which were used to determine λM velocity of the missile immediately after contact. These functions included the following:

1. Linear variation
2. Simple trigonometric variation
3. Variation suggested by a simply supported circular plate under a central concentrated load.
4. Variation suggested by a clamped circular plate under a central concentrated load.

For these cases the numerical values of "λ", v_o and T_o are as shown on Table 5A-3.

where λ = fraction of responding dome mass as previously described

v_o = velocity of λM immediately after contact

T_o = initial kinetic energy of the dome

d. Application of the Displacement Bound Theorem

Using the displacement bound theorem it can be shown that

$$W_o^{U.B.} = \frac{T_o}{1.81\pi M_o}$$

where $W_o^{U.B.}$ is the upper bound of the deflection at r = 0.

"M_o," the fully plastic moment per unit length, is conservatively developed considering that at plastic collapse the tendons are not carrying any load and that only the 3/8 in. steel liner acts as reinforcement with a yield strength of 30,000 psi. Therefore M_o = 393,000 lb ft/ft which results in a conservative lower bound. Considering the previous cases for distribution of initial velocity, the upper bound of displacements are therefore as shown on Table 5A-4.

The average value of 0.97 inches for $W_o^{U.B.}$ is considered to be a reasonable and representative number for an upper bound deflection. It should be noted that this analysis provides only an order of magnitude determination of the upper bound of displacement and based upon comparison with actual displacement of a flat circular plate with "a/R = 0," that is a concentrated in lieu of a ring load, the upper bound errs on the high side.

The conclusion can be drawn on the basis of this analysis that the structural response of the dome does not produce a condition of collapse. This solution does not consider the problem of local material failures which could lead to a more serious problem than the overall structural response.

3.1.1.1.2 Local Material Failure

A study was made of the problem of local penetration making use of the modified Petry formula, wherein:

$$D = k\ Ap\ V'$$

where D = depth (in feet) of penetration

k = experimentally obtained material's coefficient for penetration

Ap = sectional pressure obtained by dividing the weight of the missile by its maximum cross-sectional area (expressed as pounds per square foot)

V' = velocity factor expressed as $\log_{10}\left(1 + \frac{V^2}{215{,}000}\right)$

where "V" represents the terminal or striking velocity in feet per second.

On the basis of "k" being equal to 0.0023 the penetrations are as follows:

Case A D = 0.128 ft = 1.54 in.
Case B D = 0.237 ft = 2.85 in.

both of which are less than the limit established for valid use of this equation. The material coefficient "k" has been determined by experimental results for reinforced concrete with different compressive strengths. Variation in material properties will affect the k-value used and thereby the depth of penetration. However, the thickness of the reinforced concrete used for aircraft protected structures exceeds the lower limit for use of the modified Petry formula. A study of missile penetration was made using the Ballistic Research Laboratories formula[22] which resulted in deeper penetration but well within acceptable limits.

The impact of detached aircraft elements such as engines etc., will hit at a distance away from the center of impact. The top and bottom surface of the shell (See Figure 5A-15) in this location will be in compression, and the combined flexural stress less than at the center of impact. The engines have not been considered to hit at center of impact, however, the effect of the whole Class D aircraft remaining intact has been evaluated as discussed in Section 3.1.1.3.

3.1.1.2 Analysis For Case C Impact Loading

A study was made of the protection against a hypothetical aircraft impingement by an aircraft weighing 300,000 pounds, traveling at a velocity of 200 knots and impacting over an area with an effective diameter of 16 feet. The stability of the reactor containment structure was verified by means of dynamic elastic analyses for the impingement of the total aircraft.

The effect of a large aircraft impingement against the apex of the reinforced concrete dome was studied by calculating the dynamic response of an elastic solid of revolution to time-dependent forces acting on the area of impact, as shown in Figure 5A-5. The magnitude and duration of the impact forces were determined according to the mass, structural characteristics, and vertical component of the velocity of the aircraft. The grid for the finite-element idealization of the dome is given in Figure 5A-6. Based on virtual work, the equilibrium equations for the entire structure are formulated as follows:

$$(m)\ddot{\vec{d}} + [\alpha\,(k) + 2\beta\,(m)]\,\dot{\vec{d}} + (k)\,\vec{d} = f$$

where:

(m) = mass matrix

$\alpha(k) + 2\beta(m)$ = damping matrix

(k) = stiffness matrix

$\vec{d}$ = displacement vector

Dots indicate time derivatives. These equations are integrated by means of a Predictor-Corrector method with a Runge-Kutta-Gill starting procedure using a computer program developed at Franklin Institute Research Laboratories. FIRL is acting as Consultant to GAI in connection with this problem.

Evaluation of the results, in conjunction with a procedure proposed by Dr. Steven Batterman and utilized in the study described herein to calculate limit (final) displacements in a rigid-perfect plastic shell will lead to safe estimates of the size and velocity of the largest aircraft that may impinge upon the containment building without jeopardizing its structural integrity.

An analysis was performed considering the following loading condition (Refer to Figure 5A-5 for nomenclature):

P_n = 200 psi

t_1 = 0

$t_2 = t_3$ 0.16 sec.

The diameter of the impact area was considered to be 16 feet. In order to obtain a preliminary indication of displacements, this analysis was performed on the basis of the conservative assumption of no internal damping. Also to simplify the solution, the steel liner was not considered.

The equivalent diameter of the fuselage of the B707 type aircraft is approximately 13.3 ft. The assumed impact area is considered to be reasonably indicative of the impact area of such an aircraft considering the significant distortion which will occur to the fuselage as well as the load distribution afforded by the concrete to the middle surface of the dome.

The loading pressure of the 300,000 lb aircraft without impact would be 10.4 psi. Therefore the loading considered represents a constant deceleration of the impacting aircraft of 20g. That means that the entire aircraft remains intact and all elements decelerate at 20g. This represents an equivalent load on the fuselage of the aircraft of 5,800,000 lb, which it is estimated would result in gross collapse of the aircraft.

The analysis indicates that the maximum displacements and stresses all of which occur at the center of impact (i.e. the apex of the dome) are as follows:

	Displacement (in.)	Stress (psi)
Maximum	-0.98	-2264 + 354
Static	-0.66	-1832 + 346

The displacement at the apex of the dome as a function of time is depicted in Figure 5A-7. This graphical representation of displacements indicates that the most severe duration of the loading is equal to or greater than 0.16 seconds. The static displacement is that produced

by the 200 psi loading applied for an infinite period. Figure 5A-8 depicts the displacements and stresses which occur at time 0.16 seconds after impact which is the instant of maximum displacement at the dome apex.

The loading considered in this analysis represents the case where the aircraft with all its engines, fuel tanks, and wings remains intact and the total resulting load is applied on the nose of the aircraft. It has been concluded that the resultant load due to one or both wings shearing off the fuselage and impacting against the dome will result in a less critical condition than that previously considered. The static displacement of the dome at the point of impact of one engine is approximately 0.1 inches. The displacement results from a loading equivalent to a 20g deceleration applied for an infinite period. The physical separation of engines is sufficient to produce only a minimal increase in displacements due to the fact that the wings or engines upon separation from the remainder of the aircraft would be traveling at significantly reduced speed.

The results obtained from the Analysis for Case C Impact Loading were not used for the final design of the Reactor Building Dome and Shell.

3.1.1.3 Analysis For Case D Impact Loading

A study was made of the protection against a hypothetical aircraft impingement by an aircraft weighing 200,000 pounds, traveling at a velocity of 200 knots and impacting over an area with an effective diameter of 19 feet using the same analytical techniques described in Section 3.1.1.2 of this appendix. The final design of the Reactor Building was based upon the case D Impact Loading Analysis.

The load-time curves for the 200,000 lb. aircraft as shown on Figure 5A-2 were used as the design basis and was derived from the geometry, structure characteristics, and mass distribution of the B720 type aircraft.

Two loading cases were considered; one in which the outboard engines, wing structure, and outboard fuel are separated from the aircraft at a prescribed time following impact (Table 5A-6 and Figure 5A-2), and one in which the aircraft is assumed to remain intact after the initial impact (Table 5A-7 and Figure 5A-2).

The reaction load can be derived as follows:

Linear Impulse = Linear Momentum

and: $-R\,\text{delta t} = \mu L \dfrac{[V - \text{delta } V]}{LM_2} - \dfrac{[\mu LV + \mu XV]}{LM_1}$

$\text{R delta t} = \mu L(\text{delta V}) + \mu X(V)$

$R = \mu L \dfrac{(\text{delta V})}{\text{delta t}} + \dfrac{\mu \text{delta X}}{\text{delta t}} (V)$

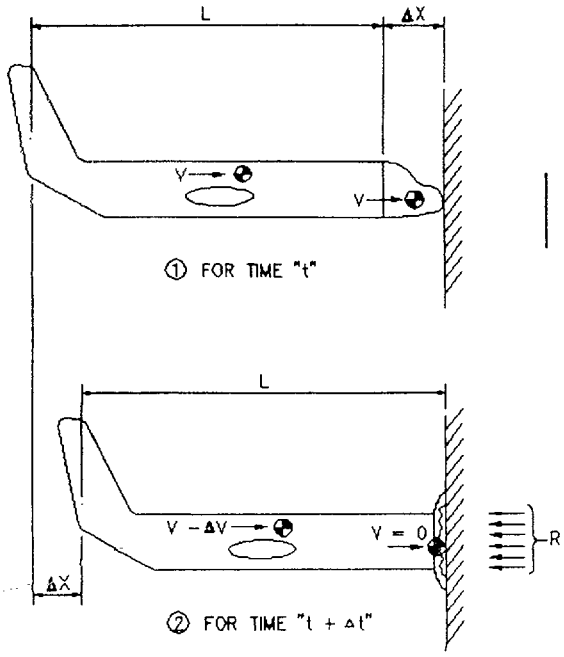

In the limit: $R = \mu La + \mu V^2$
and μL = M= mass of uncrushed aircraft
thus $\mu La = Ma = P_B$ (the unbalanced force on the uncrushed portion of aircraft)

therefore: $R = P_B + \mu V^2$

where:

R = Total reaction load on rigid surface in pounds

P_B = Load in pounds required to crush or deform fuselage longitudinally

μ = mass of aircraft per unit length (slugs/ft)

V = velocity in ft/sec of uncrushed portion of aircraft at any time or distance during the impact

Instrumented data from a full-scale C-119 aircraft impact into a vertical wall indicated that the results given by the above momentum exchange principle for a B720 aircraft were of the right order of magnitude; however, the actual reaction load (P_B) to the wall by the C-119 aircraft was not recorded. The rate of change of the aircraft velocity was determined, however, by high speed film analysis and compared with the rate of velocity change with the B720 aircraft as shown in Figures 5A-9 & 5A-10. This comparison shows that both aircraft decelerate at approximately the same rate; however, the B720 required more than twice as much crush distance because of its higher initial impact velocity.

The reaction load as a function of time is presented in Figure 5A-2 and 5A-35 for the B720. Note that the peak reaction occurs as the wing and fuselage are crushed between the front and rear spars. This is caused by the fact that the "μ^{V2}" is largest at this location ("μ" is very high here as shown by the mass distribution in Figure 5A-11). Also note that the fuselage deceleration is highest when the reaction load is rather low. This phenomena is caused by the reduced mass of the uncrushed portion of the aircraft being decelerated by the relatively constant buckling load (P_B) acting on the uncrushed portion. See Tables 5A-6 and 5A-7, and Figure 5A-2. The buckling load (P_B) of the fuselage is shown in Figure 5A-12*. The average diameter of the fuselage for the B720 aircraft is 13.3 feet. As can be seen from the load-time curve the peak load occurs after the wings have impacted against the dome. Considering that the wings constitute a large proportion of the total mass, it is considered justifiable to consider a portion of the wings that is in contact with the dome at the peak load as additional impact area. Considering this additional area and the load distribution afforded by the concrete to the middle surface of the dome, the effective diameter of the impact area is 19 feet.

The analysis indicates that maximum induced extreme compressive fiber stress of 7742 psi and displacement of 1.81 inches occurs at the center of the impact area.

For the two loading cases, the displacements of the apex of the dome as a function of time are shown in Figures 5A-13 and 5A-14. For comparison, the displacement of the points at a radius of 115.2 and 268.8 inches are also shown. Stresses due to the aircraft impingement and prestress near the apex and at a radius of 85 inches are shown in Figures 5A-15 and 5A-16.

The maximum combined extreme compressive fiber stress is approximately 9372 psi. This includes stresses due to aircraft related loads and the prestress loads. It has been recognized that biaxial stress conditions as produced in the Reactor Building due to prestress, increases the ultimate strength of concrete. Considering that the minimum cylinder strength of the concrete for the Reactor Building is based upon a 28 day curing time, an increase of 20 percent in strength can be justified (Reference 12) considering that the concrete will have cured more than two years when the plant is in operation. The present records of the 90 day compressive strength of the same concrete used in the shell is in agreement with this strength increase. The strength of concrete under biaxial stress when $\sigma\,\phi \cong \sigma\,\theta$ was determined by Rosenthal and Glucklich (Reference 26) to be $2.2f'_c = 2.2 \times 6000 = 13{,}200$ psi.

* Structural properties of the aircraft considered in Reference 1 were obtained from The Boeing Company.

The local radial tensile stresses around the dome tendon conduit was determined utilizing the Finite Element Method including in the model in the effect of the 5"ϕ, Schedule 40 steel tendon conduit. The model shown in Figure 5A-40 consist of an axisymetric solid of revolution. The loads applied to the model are:

a. Radial prestress from each of the three tendon layers

b. Meridional prestress

c. Meridional stresses due to aircraft impact

The resulting radial tensile or compressive stresses are shown on Figure 5A-41. The radial stresses shown in parenthesis are the results of the loads described above excluding the external dome pressure due to the crushed fuselage. The radial stresses have been adjusted for this external pressure. The stress concentration around the conduit was greatly absorbed by the steel conduit and thereby reduced the expected larger tensile and compressive stresses in the adjacent concrete. Two local areas of concrete tensile stresses exist on an axis 45° from the axis parallel with the dome surface. Any tensile cracking in this region would be limited by the confining compressive stresses. A local tensile crack in these regions of the concrete close to the conduit will increase the biaxial concrete compressive stress to approximately 9.150 psi <13,200 psi considering an average stress over the uncracked portion of concrete. This is the worst condition which exists approximately 8 inches from the dome surface, and is a conservative method for evaluating the load carrying capability of the concrete. In fact, essentially all concrete is subjected to triaxial compressive stresses which further increases the concrete capacity. A schematic showing the stress state of the dome in relationship to the conduit is shown in Figure 5A-42.

The maximum compressive stress at the center of the first tendon conduit is f_c = 5000 psi, with no radial tensile stresses.

The loading considered in this analysis of the dome were:

a. Prestress load
b. Radial tensile stresses due to tendon curvature
c. Stresses introduced due to aircraft impact.

Stresses in the dome at the edge of the loaded area of the aircraft are for wings and engines attached:

Meridional		Hoop	
f_c top =	- 6268 psi	f_c top =	-6419 psi
f_c bottom =	- 4931 psi	f_c bottom =	+128 psi
Shear v_c =	470 psi		

The concrete compressive stresses are acceptable; and the shear stress below that permitted by ACI 318-63, Chapter 26.

Stresses in the dome 36 inches out from the loaded area of the crushed aircraft for wings and engines attached (Figure 5A-37) are:

Meridional		Hoop	
f_c top =	-3600 psi	f_c top =	-5268 psi
f_c bottom =	-3440 psi	f_c bottom =	-342 psi
Shear v_c =	356 psi		

The concrete compressive stresses are acceptable; and the shear stress below that presented by ACI 318-63, Chapter 26. (Figures 5A-38 and 5A-39)

It is of interest to note that the high fiber stresses at the apex of the dome are reduced significantly to the location at the periphery of the loaded area and at a distance "d" from the periphery of the loaded area.

No special investigation has been made for the case of simultaneous impact of the partially disabled aircraft and the detached elements (outboard engines, wing structure, and outboard fuel) on separate locations. The impact of the aircraft with a 19 ft-0 in. diameter impact area is the most critical load case. It will be seen by inspection of Figure 5A-15 that detached elements will impact in areas at significantly lower stress level. It is considered improbable that the partially disabled aircraft can impact on the structures at a location that has been damaged by the previous impact of the detached elements. The impact of the entire aircraft on the dome has been analyzed and the results are shown in Figure 5A-16.

Therefore, the conclusion can be safety drawn that the dome will not collapse due to the established loading condition.

3.1.2 DOME TO GIRDER TRANSITION

This analysis is in accordance with the methods described in Section 5.2.4.1 and was made for Case D loading by a hypothetical aircraft described in Section 3.1.1.3. The non-axisymmetrical load is represented by a Fourier Series and has the general dimensions and shape as shown in Figure 5A-17. The stress resultants are shown in Figure 5A-18.

3.1.3 GIRDER TO CYLINDER TRANSITION (SPRING LINE)

Analyzed the same as 3.1.2 above. The stress resultants are as shown in Figures 5A-19 and 5A-20.

3.1.4 IMPACT AT GRADE

Analyzed the same as 3.1.2. The stress resultants are as shown in Figure 5A-21.

3.2 PLATE ANALYSIS

This analysis was made for the Case D loading by a hypothetical aircraft as described in Section 3.1.1.3.

3.2.1 FUNDAMENTAL FREQUENCY

It is readily seen in Figure 5A-3 that as long as the fundamental frequency of the plate is greater than 10 cps, or less than 6 cps, the dynamic load factor will be less than 1.32. In the present plate analysis, all of the slabs have the fundamental frequency greater than 10 cps. The fundamental frequency calculated for each slab (except two slabs which will be explained subsequently) is based on the assumption of simply-supported boundary conditions. This assumption will lead to a lower value of fundamental frequency for the current plates because their boundaries are actually restrained rather than simply-supported. The value of E employed in the dynamic analyses was equal to the static modulus, and no account was taken of the increase in E resulting from the dynamic load effect in order to compensate for any reduction of E due to high stress levels. This approach is felt to be conservative because (1) the structure fundamental frequencies fall to the left if the peak in the maximum DLF vs. frequency curve and (2) the area of impact, where the highest stress levels occur, is relatively small compared with the total structure. These low values of fundamental frequency will give a conservative dynamic load factor as can be seen in Figure 5A-3. Consequently, variation of the elastic properties and edge conditions from the assumed parameters would lead to a reduction of the magnitude of the dynamic response. When the dynamic load factor value falls below unity, a minimum factor of 1.0 is used. The theoretical background of calculating fundamental frequency of simply supported plate is straightforward and well documented. (References 2, 13, and 14). The well known formula of natural frequency is:

$$\omega_{mn} = \pi^2 \sqrt{\frac{D}{ph}\left[\left(\frac{m}{a}\right)^2 + \left(\frac{n}{b}\right)^2\right]}$$

where m and n denote the mode number; D is the flexural rigidity; p is the density; and a, b, and h, are length, width, and thickness of plate, respectively.

For the two exceptional plates where the boundary conditions are more likely to be fixed, the fundamental frequencies are calculated based on fixed boundaries. There is no exact solution of fundamental frequency for such cases; however, numerical approximations which are based on energy principle are available. (References 2, 15, and 16). The present calculations of fundamental frequency of fixed plate are obtained from the tables and suggested formulae in Chapter 5 of "Introduction to Structural Dynamics" (Reference 2).

After obtaining the fundamental frequency of each slab and the dynamic load factor, the remaining work is a statical slab analysis. This approximate dynamic analysis technique is equivalent to the assumption that the DLF's of all modes are equal to that of the fundamental mode. For the computation of maximum response for design purposes, this approach is conservative for the following reasons:

a. The fundamental periods of all the slabs fall to the left of the peak in the diagram of maximum DLF vs. period, thus indicating that the higher modes have smaller maximum DLF's.

b. The maximum DLF's of the various modes do not occur simultaneously.

c. The maximum bending moment results when the impact occurs at the center of the slab. For this case, the fundamental mode dominates the response.

d. The maximum transverse shear is obtained when the impact takes place near a supporting edge, in which case most of the load is transferred directly to the support with little dynamic participation of the slab.

In order to assess the validity of these assertions, the study reported in Reference 21 was recently extended to evaluate the dynamic response of a typical slab subject to impact at various locations (center, edge, and intermediate points). In this study, mode superposition, using up to 900 modes (30 harmonics in each coordinate direction), was employed with the expressions for the DLF given in Table 5A-2 to calculate the time history of the displacements and stress resultants at critical positions for the Boeing 720 impact. The maximum values of these quantities were compared with the corresponding static values, and it was found that for every one the ratio of maximum dynamic value to static value was less than the maximum DLF for the fundamental mode. Therefore, the design values obtained by factoring the static responses by the maximum fundamental DLF would in every case be larger than the actual maximum, indicating that this procedure will yield a conservative design.

3.2.2 FINITE-ELEMENT ANALYSIS FOR SLABS

The present finite-element analysis is based upon a rectangular plate element (Figure 5A-22) as developed in References 5A-16 and 5A-17. Each nodal point has 6 degrees-of-freedom. A comprehensive explanation of the satisfaction of the "completeness" and "compatibility" of the chosen displacement function is given in References 5A-18 and 5A-19. The convergence of the solution accuracy vs grid refinement is monotonic and rapid as evidenced in various References 5A-16, 5A-17, 5A-18, and 5A-19. For the problem of plate in bending, 16 elements discretization can lead the solution of deflections to a small error of less than five percent as compared with classical solutions. The element number used in the present calculation ranges from 25 to 64 for various slabs.

Since the finite-element method is much less restricted to the geometry and boundary conditions than the classical solution, the actual geometry and boundary conditions are represented in the present calculation without modifications.

As an illustration of the present slab analysis and design, an example of roof slab at the heat exchanger vault of the auxiliary building at Elevation 305 ft is chosen. The dimensions and boundary conditions are shown in Figure 5A-23(a). The dynamic load factor, based on the elastic undamped one degree-of-freedom assumptions, was found to be 1.188.

As shown in Figure 5A-23(a), nine critical impact positions, which produce the critical moments and shears at various sections, were examined. As a simplified demonstration, the moment diagrams along line AA are shown in Figure 5A-23(b). The top and bottom reinforcements corresponding to the moments in Figure 5A-23(b) were designed and shown on GAI Drawing 422030. The shear reinforcement designed for this slab is shown on GAI Drawing 422031. The shear reinforcements were designed on the basis of the aforementioned finite-element computer program output of shears.

The slab is a rectangle 121'-0 by 55'-0 by 6'-0 as shown on GAI Drawings 422030 and 422031. The slab is supported along all four edges and along the East-West centerline. For the purpose of this analysis, only the southern half has been considered. Moment curves have been plotted for the different impact positions. Five impact positions have been considered. An envelope was then constructed in order to obtain maximum moments at any point along section A-A, Figure 5A-23. This envelope was used to calculate the required reinforcement. A similar procedure was used to calculate the moments for another 4 strips of the slab in the North-South direction and 5 strips in the East-West direction.

3.2.3 DESIGN CRITERIA FOR REINFORCING

The wall and roof slabs exposed to aircraft impact have been designed according to the following criteria.

a. The main reinforcing is designed on the basis of bending moment diagrams obtained from computer printouts using Case D loading and according to the ACI 318-63, Ultimate Strength Design Method, Chapter 15.

b. The shear reinforcing is designed on the basis of the shear force diagram obtained from computer print-outs using the Case D loading and according to the ACI 318-63, Ultimate Strength Design Method, Chapter 17.

c. Anchorage for the reinforcing bars is provided by carrying the reinforcing bars past the theoretical cut-off point a distance sufficient to develop the ultimate strength of the bar.

d. The allowable bond stresses are calculated on the basis of ACI 318-63, Chapter 18.

e. No welding has been done on reinforcing bars.

f. In the design no special construction methods were specified.

3.2.4 DESIGN CHECK

It is recognized that the elastic analysis employed for the flat slabs is conservative and that the resulting design does have a capacity in excess of that implied by the load considered for slab design.

As a conclusion of this design, each wall and roof slab exposed to aircraft impact was checked utilizing the Yield Line Theory (Reference 25).

These aircraft-protected structures can withstand at least a load equal to 1.52 x (17,500,000) = 26,400,000 lbs. This load represents the maximum load as determined in the previous section, with the peak DLF = 1.52 as shown in Figure 5A-3.

4. ADDITIONAL DETAIL STUDIES

Some additional studies on the detail structural analysis of the aircraft impact on the containment vessel have been made:

a. Bearing failure of concrete in the neighborhood of anchors of tendons under direct impact.

b. Shear-off of the anchors of the dome tendons, vertical tendons, and hoop tendons.

c. Spalling due to aircraft impact on the outside wall.

d. Impact effects on equipment and components.

4.1 BEARING FAILURE OF CONCRETE UNDER DIRECT IMPACT

The bearing capacity of concrete, according to ACI-318-63, is 1.9 x 0.375 f'_c = 3560 psi. The aircraft impact force of 21,100 kips (assuming a dynamic load factor of 1.2), according to the 19 foot diameter (283.5 ft^2) circular normal impact area, produces an impact pressure of 21.1 x 10^6/283.5 x 144 = 517 psi. It is readily seen that the aircraft impact does not cause bearing failure as long as the total impact force is distributed on an area greater than 41.1 ft^2.(Reference 2) (corresponding to a bearing stress of 3560 psi). Thus, it may be concluded that bearing failure can be prevented as long as the impact force is distributed on an area greater than $\frac{41.1}{283.5} = 14.5$ percent of the normal impact area.

Intuitively, it is believed that no matter where the aircraft hits, the impact area should be at least 14.5 percent of the area of the case when the aircraft impacts on a flat wall.

The anchors of the dome and vertical tendons are embedded in concrete at least one foot in depth. No damage of the anchors is possible when the aircraft hits normal to the anchorages.

Although the hoop tendon anchorages are not embedded in concrete, the aircraft would have to hit in a tangential direction to the containment vessel to produce a bearing failure of the anchorage.

This being the case, it is unlikely that the total impact force will be concentrated over less than 14.5 percent of the normal impact area; therefore, a bearing failure of the concrete at the hoop tendon anchorages will not occur.

4.2 SHEAR-OFF THE ANCHORS

Three cases have to be investigated when considering the possibility of shearing-off the anchors of the tendons due to aircraft impact, particularly the impact of engines and sharp object.

4.2.1 CASE A: SHEAR-OFF THE ANCHORS OF VERTICAL TENDONS

The aircraft may travel in the direction shown in Figure 5A-26 such that the anchors of vertical tendons may be sheared-off. Based on the investigation conducted in Reference 1, the information is available that the maximum response of statically equivalent impact load is 21.1 x 10^6 lb (assuming conservatively a dynamic load factor of 1.2) and the maximum impact area is a 19 ft diameter circle (assuming the aircraft strikes normal to a flat wall). The shear strength at Section A-A shown in Figure 5A-27 governs whether or not the aircraft will shear the concrete and impinge at the anchors. The shear stress at Section A-A must be calculated for the worst condition of impact loading and compared with the shear capacity.

Considering the maximum aircraft impact area with a diameter of 19 ft, the maximum number of covered tendons are:

$$N = \frac{19\,\text{ft}}{\text{C. to C. dist. between anchors}} = \frac{19 \times 12}{30.5} = 7.47$$

As a very conservative estimation, the impact force on the area between two anchor centers is:

$$P = \frac{\text{Max. response}}{N} = \frac{21.1 \times 10^6}{7.47} = 2.83 \times 10^6 \text{ lb/tendon}$$

The area available for resisting the shear can be estimated from Figures 5A-27 and 5A-28.

A = 28" x 30.5" = 853 sq in.

It is reasonable to assume that the load applied above Section A-A is proportional to the area of impact. $\frac{[d \times 25]}{15 \times 25}\ 21.1 \times 10^6$ lbs.

where d = 2'-2".

The applied load = 3.1 x 10^6 lbs which results in a shearing stress across Section A-A equal to $\frac{3.1 \times 10^6 \text{ lbs.}}{25\ (12)\ 28} = 369\,\text{psi} < 600\,\text{psi}$

Ultimate shear strength of concrete f_{ult} = 600 psi. Although unlikely, it is, however, assumed that nine anchors are sheared-off by the aircraft impact. As illustrated in Figure 5A-29(a) it is seen that Section AA is of primary concern if vertical tendons fail under the impact. The moment m_1, caused by the aircraft impact, has to be resisted by the moment m_2. The moment caused by the aircraft impact is:

$$m_1 = 21.1 \times 10^3 \times 166.5 \times 12 = 4.2 \times 10^7 \text{ in-kips}$$

The moment due to the undestroyed tendon prestressed forces resisting, m_1 is:

$$m_2 - T(d_1 + d_2)$$

where T is the total prestressed forces on tension side of N.A., for the case when there is no tensile force in section AA. The tendons do not exceed their prestressed forces. Then,

$$T = 37 \times 2 \times 1090 = 8.06 \times 10^4 \text{ kips}$$

d_1 and d_2 are the distances from the neutral axis to the centers of gravity of the active tendons on the tension and compression sides of the neutral axis respectively as shown in Figure 5A-29(b). Therefore:

$$m_2 = T(d_1 + d_2) = 8.06 \times 10^4 \times 987 = 7.95 \times 10^7 \text{ (k-in)}$$

It is now concluded that even with a dynamic load factor 1.2 and a very conservative assumption that nine tendons are covered by the airplane impact and are destroyed, the safety factor for not causing tension at section AA is:

$$S.F. = \frac{m_2}{m_1} = \frac{7.95 \times 10^7}{4.2 \times 10^7} = 1.90$$

In order to shear-off nine vertical tendon anchorages, the aircraft must impact as shown in Figure 5A-26. A reasonable assumption is that the impact load will be concentrated above the ring girder. As a conservative estimate of the resulting forces, the forces shown on Figure 5A-18 due to the aircraft impact at the girder to dome transition were used. Figure 5A-18 shows that the maximum moments and shears occur in the dome. Therefore, the resisting prestress forces in the critical dome area are not affected by a loss of vertical prestress.

The shear stresses in the wall are of concern because the allowable shear stress reduces when the meridional axial force is lost due to the failure of nine vertical tendon anchorages. The shear stresses at three locations were determined and compared with an ultimate shear stress of $2\phi\sqrt{f_c}$ (ACI 318-63).

The three locations are:

a. Cylinder wall to ring girder transition

b. Base of wall

c. Ten feet above the base of the wall (Haunch to typical wall transition)

Although the shear stress at location a. exceeds 2 o $\sqrt{f'_c}$, the shear reinforcement required is less than that provided for the normal loading cases under no loss of prestress. The shear stresses at locations b. and c. are less than the ultimate shear stress.

4.2.2 CASE B: SHEAR-OFF THE ANCHORS OF DOME TENDONS

If the aircraft impact occurs as shown in Direction 2 of Figure 5A-30, the shear resisting capacity of the concrete at Section AA has to be greater than the impact force so that no force will be transferred to the anchors of the roof tendons. The shear resisting area, assuming a 19 ft width of impact area is:

$$A = 19 \text{ ft} \times 6.416 \text{ ft} \times 144 = 17{,}554 \text{ in}^2.$$

The total shear capacity of concrete against the vertical impact is:

$$F = 600 \times 17{,}554 = 10.53 \times 10^6 \text{ lb}$$

which is smaller than the aircraft impact load 21.1×10^6 lb (with a conservative assumed dynamic load factor 1.2).

It is reasonable to assume that the applied load is proportional to the area of impact. $\frac{[1.25 \times 19]}{15 \times 19}$ 21.1×10^6 lbs.

The applied load = 1.76×10^6 lbs which results in a shearing stress across section A-A of Figure 5A-30 = $\frac{1.76 \times 10^6 \text{ lbs}}{19\ (6.416)\ (144)}$ = 100 psi <600 psi.

Under the above analysis, the dome tendon anchorages will not fail in shear.

The dome tendons are composed of three layers lying on top of each other. Each layer is composed of parallel and equally spaced tendons (Figure 5A-31). As can be seen from Figure 5A-32, the orientation of the three layers is such that the tendons cross each other with a constant angle of 60 degrees. Since the dome tendons are so close to each other, crossing each other, and overlying each other is intuitively believed that no damage will occur to the dome even if a few tendons are assumed to be broken under the aircraft impact.

In addition to the previous logic, providing the failure of the dome tendon anchorages is caused by an aircraft impact as shown in Direction 2 of Figure 5A-30, the major portion of the impact load will be resisted by the cylindrical wall and not by the dome which has lost the prestress forces due to 8 broken dome tendons.

If the aircraft travels in the Direction 3 as shown in Figure 5A-30, it is seen that the concrete bearing failure is relatively small. Previously, a calculation has shown that as long as the actual impact area is at least 14.5 percent of the maximum theoretical impact area, no bearing failure will occur. Therefore, impact Direction 3 is of no critical concern.

4.2.3 CASE C: SHEARING-OFF THE HOOP TENDONS

The aircraft may travel in the direction shown in Figure 5A-33. Since there is no concrete cover to protect the anchor, direct impact on the anchors may shear-off several tendons. As shown in Figure 5A-33 the minimum vertical spacing between anchors on one side of the buttress in 33 inches. Each hoop tendon is anchored in one buttress, then passes by the adjacent buttress, and is finally anchored in the next adjacent buttress.The aircraft impact area has a minimum depth of 19 ft which can cover seven (i.e., $\frac{(19 \times 12)}{33} = 6.9$) anchors of hoop tendons. If the most conservative assumption is made that all of the seven anchors are sheared-off due to aircraft impact, one-half of the hoop prestress force in a cylindrical panel with a depth of 19 ft and a curve length of one third of the cylinder periphery would be eliminated. An analysis is made considering the containment vessel with normal prestress conditions with the exception that a cylindrical segment with a depth of 15 ft has only one half of the hoop prestress. The resultant axial forces and shears with half of the hoop tendon forces lost in the range between 800 inches and 965 inches above the base of the cylindrical wall are listed in Table 5A-5. It is seen that the out of plane shear and hoop force have changed due to the failure of the hoop tendons. The shear has increased considerably, but, is in the opposite direction of the shear due to aircraft impact, and therefore aids in resisting the aircraft impact. When the aircraft impact diminishes and the hoop tendons are still broken, the remaining shear is much less than the ultimate shear stress according to ACI 318-63.

The above analysis does not consider the moments caused by the loss of 8 hoop tendons. Referring to Figure 5A-34, which is a comparison of (1) the loading due to aircraft impact plus total prestress and (2) the loading due to aircraft impact plus total prestress minus the hoop prestress due to the loss of hoop tendons, it can be deduced that the resulting moments will tend to counteract the moments caused by the aircraft impact. When the aircraft impact diminishes, the axial compression due to the remaining prestress forces (see Table 5A-5) should be sufficient to overcome the tension due to the moments caused by the loss of hoop prestress.

Based on the above logic and conservative numerical calculation, it is believed that the aircraft impact in the direction shown on Figure 5A-33 does not jeopardize the stability of the structure.

4.3 SPALLING DUE TO AIRCRAFT IMPACT ON THE OUTSIDE WALL

Spalling is the kind of fracture which results from the interference between the incident compressional wave and its reflected counter-part. The mechanics of spalling can be described graphically as follows:

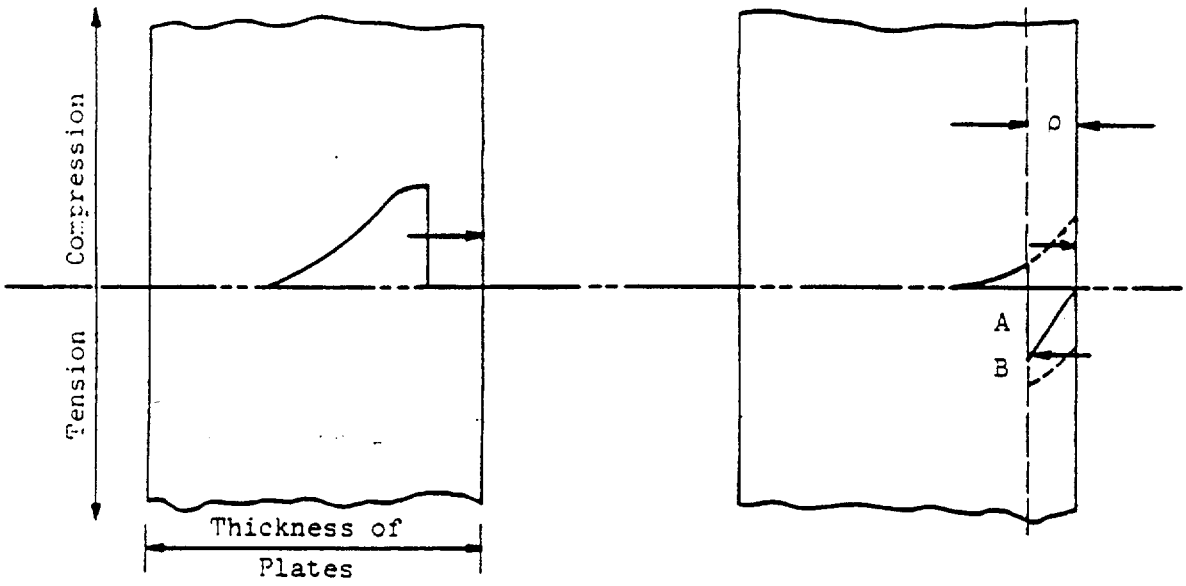

Compressive wave before reaching the free surface

Part of the compressive wave reflected back from the free surface

The spalling will occur at a distance ρ from the free surface, if the net tensile stress AB exceeds the tensile fracture strength of the material (References 23 and 24). From these we can see that the spalling is influenced by two factors, (a) the duration and shape of the stress pulse, and (b) property of the material acted on.

The plane dilatational wave will travel through the plate at the speed of $\sqrt{\frac{\lambda + 2\mu}{\rho}}$, were delta, μ are Lame's constants and ρ is the density of the material.

Transform $(\lambda + 2\mu)$ to a form in terms of Young's Modulus E, and Poisson's ratio ν, which engineers are more familiar with. We have:

$$\lambda + 2\mu = \frac{E\,(1 - \nu)}{(1 + \nu)\,(1 - 2\nu)}$$

For concrete, with E = 4,000 ksi, ν = 0.15, pg = 145 lb/ft^3, the wave velocity is:

$$c = 1.4 \times 10^5 \text{ in./sec} = 11{,}650 \text{ ft/sec.}$$

Hence, for the structure we are concerned with, the spalling may occur only for the stress pulse duration of the order of microseconds. The first unloading of our impact force occurs at 0.19 seconds. In other words, for a wall of 5 ft thickness, the wave has to travel back and forth almost 220 times before the impact force reaches the unloading point. Due to the internal friction, the stress wave is long dispersed before it can build up tensile stress in the structure. So the spalling effect is almost impossible to occur.

Nevertheless, the anchors on the containment vessel liner above grade will be deeply anchored into the concrete wall with one inch diameter bolts (form ties). These bolts have a capacity to resist 1.7 kips per foot of anchor. This measure further protects the liner anchors against failure due to spalling; even though such behavior is not anticipated, as previously described.

The design criteria for the liner anchors is described in Section 5.2.3.2.5 "Liner Anchor". The liner angle welds have been tested by 20 percent liquid penetrant test 100 visual inspection in accordance with the requirements of Section VIII of ASME Boiler and Pressure Vessel Code. Three specimens of the liner angle welds were tested by Pittsburgh Testing Laboratory and the factor of safety was found to be 2.7 against the worst possible load on the liner anchor.

4.4 IMPACT EFFECTS ON EQUIPMENT AND COMPONENTS

To eliminate the shock effect caused by an aircraft impact, the concrete floor slabs in the Control Building have been separated by a 2 inch wide joint from the exterior walls exposed to an aircraft impact. The concrete slabs are supported by steel beams which in turn are supported on elastromeric pads which act as vibration dampeners.

4.5 REFERENCES

1. Haley, Jr., J. and Turnbow, J., "Total Reaction Force due to an Aircraft Impact into a Rigid Barrier," AvSER Report prepared for Gilbert Associates, Inc. by Dynamic Science, Phoenix, Arizona, April 1968.

2. Biggs, J. M., "Introduction to Structural Dynamics," McGraw-Hill Book Co., N.Y. 1964, Section 2.3.

3. J. Martin, "Impulsive Loading Theorem For Rigid-Plastic Continua," J. Engineering Mechs. Div., ASCE, EM5, October 1964, pp. 27-42.

4. K. Forsberg and W. Flugge, "Point Load On a Shallow Elliptic Parabaloid," To Appear in Journal of Applied Mechanics.

5. A. Kalnins and P.M. Naghdi, "Propagation of Axisymmetric Waves in An Unlimited Elastic Shell," Journal of Applied Mechanics, 27, 1960, pp 690-695.

6. C. H. Norris 'et al': "Structural Design for Dynamic Loads," McGraw Hill, 1959.

7. J. N. Cernica and M. J. Charignon: "Ultimate Static and Impulse Loading of Reinforced Concrete Beams." ACI Journal, V. 50, No. 9, 1963, pp. 1219-1228

8. Walter Cowell: "Dynamic Properties of Plain Portland Cement Concrete." Naval Civil Engin. Lab., Port Huenema, Calif. Report NCEL 447, 1966.

9. H. Weigler and G. Becker: "Der Bauingenieur," Berlin, Vol. 36, No. 10, 1961, pp. 390-396.

10. J. Peter: "Zur Bewehrung von Scheiben und Schalen fur Hauptspannungan Schiefwinklig zur Bewehrungstrichtung, Doctoral Thesis, Technische Hochschule Stuttgart, 1964.

11. G. W.-D. Vile: "Strength of Concrete Under Short-Time Static Biaxial Stress." Proceedings of International Conference on Structural Concrete, London, 1965.

12. Fritz Leonhardt: "Prestressed Concrete Design and Construction" Wilhelm Ernst & Sohn, 1964, pp. 59.

13. Volterra, E. and Zachmanoglou, E., "Dynamics of Vibrations," Charles Merrill Books, Inc., Columbus, Ohio, 1965.

14. Timoshenko, S. and Young, D., "Vibration Problems in Engineering," 3rd Ed., D. Van Nostrand Co., Inc., 1955.

15. Harris, C. and Crede, C., "Shock and Vibration Handbook," McGraw-Hill Book Co., N.Y., 1961.

16. Bogner, F., Fox, R, and Schmit, L., "The Generation of Interelement-Compatible Stiffness and Mass Matrices by the Use of Interpolation Formulae, "Proc. Conf on Matrix Methods in Structural Mech., Dayton, Ohio, 1965.

17. Gallagher, R., "The Development and Evaluation of Matrix Methods for Thin Shell Structural Analysis," Ph.D. Dissertation, State University of New York at Buffalo, 1966.

18. Gallagher, R. and Yang H., "Elastic Instability Prediction of Doubly Curved Shell Structures," 2nd conference on Matrix Methods in Structural Mechanics, Wright-Patterson Air Force Base, Dayton, Ohio, Oct. 1968.

19. Yang, H., "A Finite-Element Formulation for the Instability Prediction of Doubly Curved Shell Structures," Ph.D. Dissertation, Cornell University, Ithaca, N.Y., Oct. 1968.

20. Timoshenko, S. and Goodier, J. N., "Theory of Elasticity," McGraw-Hill Book Co., 1951.

21. Riera, J. D., "On the Stress Analysis of Structures Subjected to Aircraft Impact Forces", Nuclear Engineering and Design, August, 1968.

22. Gwaltney, R. C., "Missile Generation and Protection in Light-Water-Cooled Power Reactor Plants" U.S. Atomic Energy Commission, DRNL-NSIC-22, September, 1968.

23. Rinehart, John S. and Pearson, John, "Behavior of Metals under Impulsive Loads" Dover, 1965.

24. Kolsky, H. "Stress Waves," Dover, 1963.

25. Wood, R. H. "Plastic and Elastic Design of Slabs and Plates," Ronald, 1961.

26. Rosenthal, I. and Glucklich, J., "Strength of Plain Concrete under Biaxial Stress," ACI Journal, November 1970.

TABLE 5A-1

TIME VARIABLE t_n

Boeing	t_1	t_2	t_3	t_4	t_5	t_6	α
	0.06	0.14	0.19	0.24	0.26	0.33	0.219

TABLE 5A-2

DYNAMIC LOAD FACTORS (DLF)

$$DLF_{(0 \text{ to } t_1)} = \left(\frac{t}{t_1} - \frac{T}{2\pi t_1} \sin \omega t\right) \alpha$$

$$DLF_{(t_1 \text{ to } t_2)} = \left(1 + \frac{T}{2\pi t_1} [\sin \omega(t-t_1) - \sin \omega t]\right) \alpha$$

$$DLF_{(t_2 \text{ to } t_3)} = DLF_2 + \left(\frac{2(t-t_2)}{t_p} - \frac{T}{\pi t_p} \sin \omega(t-t_2)\right)(1-\alpha)$$

$$DLF_{(t_3 \text{ to } t_4} = DLF_2 + \left(1 - \frac{2t-t_3}{t_p} + \frac{T}{\pi t_p} [2 \sin \omega(t-t_3) - \sin \omega(t-t_2)]\right)(1-\alpha)$$

$$DLF_{(t_4 \text{ to } t_5)} = DLF_2 + \frac{T}{\pi t_p} \left(-\sin \omega(t-t_4) + 2 \sin \omega(t-t_3) - \sin \omega(t-t_2)\right)(1-\alpha)$$

$$DLF_{(t_5 \text{ to } t_6)} = DLF_5 - \left(\frac{t-t_5}{t_6-t_5} - \frac{T}{2\pi(t_6 - t_5)} \sin \omega(t-t_5)\right) \alpha$$

$$DLF_{(\text{after } t_6)} = DLF_5 - \left(1 + \frac{T}{2\pi (t_6 - t_5)} [\sin \omega(t-t_6) - \sin \omega(t-t_5)]\right) \alpha$$

where:

$$\omega = \frac{2\pi}{T} \text{ (radians/sec)}$$

TABLE 5A-3

KINETIC ENERGY OF THE DOME

r_e = 37.0'

	λ	V_o (fps)	T_o (ft-lbs)
Case 1	0.1667	5.8	0.182×10^6
Case 2	0.172	5.6	0.172×10^6
Case 3	0.228	4.3	0.133×10^6
Case 4	0.130	7.4	0.23×10^6

TABLE 5A-4

UPPER BOUND DISPLACEMENTS

$r_e = 37.0'$

Case	$W_o^{U.B.}$ (inches)
1	0.995
2	0.925
3	0.715
4	1.245
Average	0.97

TABLE 5A-5

COMPARISON OF STRESS RESULTANTS FOR PRESTRESS LOADINGS

ELEV.*	OUT OF PLANE SHEAR $Q(10^2)$ lbs/in		MERIDIONAL FORCE $N\phi$ (10^5) lbs/in		HOOP FORCE $N\theta$ (10^5) lbs/in	
	(1)	(2)	(1)	(2)	(1)	(2)
800	-0.33	18.508	-.3730	-.3730	-.7166	-.5628
816	-0.32	14.446	-.3730	-.3730		-.5519
833	-0.309	10.589	-.3730	-.3730	-.7157	-.5429
849		6.892	-.3730	-.3730		-.5362
866		3.308	-.3730	-.3730		-.5320
882	-0.219	-0.22	-.3730	-.3730	-.7151	-.5305
899		-3.74	-.3730	-.3730		-.5317
915		-7.314	-.3730	-.3730		-.5355
932		-10.99	-.3730	-.3730		-.541
948		-14.83	-.3730	-.3730		-.5505
965	-0.010	-18.86	-.3730	-.3730	-.7150	-.5610

* INCHES ABOVE THE BASE CYLINDRICAL WALL

(1) WITHOUT LOSING TENDON

(2) OF HOOP TENDON FORCES LOST

Table 5A-6
Reaction Load (R) Calculations
Case 1: With Wing and Engines Detached
(C = 200 kts = 338 fps; M = 200,000 lb. = 6200 slugs)

TIME	STRENGTH OF FRAME	MASS /FT	MASS CRUSHED	MASS LOST	MASS INTACT
0.0	0.0	0.	0.	0.	6200.
0.010	0.154	5.	9.	0.	6191.
0.020	0.307	9.	23.	0.	6168.
0.030	0.459	12.	35.	0.	6132.
0.040	0.565	18.	49.	0.	6083.
0.050	0.565	22.	69.	0.	6014.
0.060	0.565	25.	81.	0.	5933.
0.070	0.565	28.	89.	0.	5844.
0.080	0.565	28.	94.	0.	5750.
0.090	0.565	28.	93.	0.	5658.
0.100	0.565	28.	92.	0.	5566.
0.110	0.565	28.	91.	0.	5474.
0.120	0.565	28.	91.	0.	5383.
0.130	0.565	28.	90.	0.	5293.
0.140	0.629	28.	89.	0.	5204.
0.150	0.817	47.	109.	0.	5095.
0.160	1.007	62.	187.	0.	4909.
0.170	1.193	86.	236.	336.*	4336.
0.180	1.378	112.	319.	0.	4017.
0.190	1.550	156.	401.	962.**	2654.
0.200	1.550	167.	501.	0.	2153.
0.210	1.550	157.	485.	0.	1669.
0.220	1.550	89.	405.	0.	1264.
0.230	1.550	33.	128.	0.	1136.
0.240	1.550	32.	88.	0.	1048.
0.250	1.550	31.	79.	0.	969.
0.260	1.550	30.	72.	0.	897.
0.270	1.550	29.	64.	0.	832.
0.280	1.550	28.	57.	0.	776.
0.290	1.495	27.	50.	0.	726.
0.300	1.438	27.	43.	0.	683.
0.310	1.389	26.	36.	0.	646.
0.320	1.347	25.	30.	0.	616.
0.330	1.313	25.	24.	0.	592.
0.340	1.287	25.	18.	0.	574.
0.350	1.269	24.	12.	0.	561.
0.360	1.259	24.	7.	0.	555.
0.367	1.257	24.	2.	0.	553.

MAXIMUM REACTION LOAD = 17.213 LBS*10.0E 6

* Inboard engines stopped without significant deformation at barrier.
** Outboard engines, wing structure, and outboard fuel are separated from wing.

Table 5A-6
Reaction Load (R) Calculations
Case 1: With Wing and Engines Detached
(C = 200 kts = 338 fps; M = 200,000 lb. = 6200 slugs)

TIME	DECEL	VEL CHANGE	VELOCITY	CRUSHED LENGTH	IMPACT CORCE	DECEL G'S
0.0	0.0	0.0	338.00	0.0	0.0	0.0
0 010	24.9	0.13	337.87	3.41	0.71	0.77
0.020	49.8	0.37	337.50	6.79	1.30	1.55
0.030	74.9	0.62	336.87	10.16	1.84	2.33
0.040	92.9	0.86	336.02	13.49	2.60	2.89
0.050	93.9	0.93	335.08	16.85	3.07	2.92
0.060	95.2	0.95	334.14	20.19	3.38	2.96
0.070	96.7	0.96	333.18	23.53	3.65	3.00
0.080	98.3	0.98	332.19	26.89	3.65	3.05
0.090	99.9	0.99	331.20	30.21	3.62	3.10
0.100	101.5	1.01	330.20	33.51	3.60	3.16
0.110	103.2	1.02	329.17	36.81	3.57	3.21
0.120	105.0	1.04	328.13	40.09	3.54	3.26
0.130	106.7	1.06	327.07	43.37	3.51	3.32
0.140	120.8	1.09	325.99	46.60	3.57	3.76
0.150	160.4	1.41	324.58	49.85	5.72	4.99
0.160	205.1	1.84	322.74	53.12	7.41	6.37
0.170	275.1	2.32	320.42	56.34	10.05	8.55
0.180	343.0	3.08	317.34	59.53	12.63	10.66
0.190	584.0	4.99	312.34	62.68	16.81	18.15
0.200	719.8	6.47	305.87	65.77	17.20	22.37
0.210	928.8	8.10	297.77	68.76	15.46	28.87
0.220	1226.3	10.78	286.99	71.68	8.91	38.11
0.230	1364.3	13.07	273.92	74.49	4.05	42.40
0.240	1479.0	14.36	259.56	77.18	3.71	45.97
0.250	1600.4	15.40	244.17	79.70	3.40	49.74
0.260	1728.7	16.65	227.52	82.06	3.10	53.73
0.270	1862.5	17.96	209.56	84.25	2.82	57.89
0.280	1998.3	19.12	190.44	86.23	2.57	62.11
0.290	2060.6	20.35	170.09	88.03	2.29	64.04
0.300	2107.2	20.84	149.25	89.63	2.03	65.49
0.310	2149.7	21.29	127.96	91.02	1.81	66.82
0.320	2187.4	21.91	106.05	92.20	1.63	67.99
0.330	2218.7	22.04	84.01	93.15	1.49	68.96
0.340	2243.2	22.32	61.69	93.88	1.38	69.72
0.350	2260.4	22.30	39.39	94.38	1.31	70.26
0.360	2270.2	22.66	16.73	94.66	1.27	70.56
0.367	2272.4	16.81	-0.08	94.73	1.26	70.63

MAXIMUM REACTION LOAD = 17.213 LBS*10.0E 6

See Figure 5A-31, Reaction Load and Fuselage Deceleration.

5A-7
Reaction Load (R) Calculations
Case 2: With Wing and Engines Attached
(V. = 200 kts = 338 fps; M = 200,000 lb. = 6200 slugs)

TIME	STRENGTH OF FRAME	MASS /FT	MASS CRUSHED	MASS LOST	MASS INTACT
0.0	0.0	0.	0.	0.	6200.
0.010	0.154	5.	9.	0.	6191.
0.020	0.307	9.	23.	0.	6168.
0.030	0.459	12.	35.	0.	6132.
0.040	0.565	18.	49.	0.	6083.
0.050	0.565	22.	69.	0.	6014.
0.060	0.565	25.	81.	0.	5933.
0.070	0.565	28.	89.	0.	5844.
0.080	0.565	28.	94.	0.	5750.
0.090	0.565	28.	93.	0.	5658.
0.100	0.565	28.	92.	0.	5566.
0.110	0.565	28.	91.	0.	5474.
0.120	0.565	28.	91.	0.	5383.
0.130	0.565	28.	90.	0.	5293.
0.140	0.629	28.	89.	0.	5204.
0.150	0.817	48.	110.	0.	5094.
0.160	1.007	84.	217.	0.	4877.
0.170	1.193	111.	318.	0.	4559.
0.180	1.378	134.	300.	0.	4168.
0.190	1.550	156.	458.	0.	3711.
0.200	1.550	167.	505.	0.	3206.
0.210	1.550	157.	492.	0.	2714.
0.220	1.550	141.	450.	0.	2264.
0.230	1.550	123.	391.	0.	1873.
0.240	1.550	102.	314.	0.	1559.
0.250	1.550	94.	273.	0.	1286.
0.260	1.550	82.	232.	0.	1054.
0.270	1.550	50.	161.	0.	893.
0.280	1.502	41.	104.	0.	789.
0.290	1.426	33.	79.	0.	709.
0.300	1.358	27.	58.	0.	652.
0.310	1.296	25.	44.	0.	608.
0.320	1.242	24.	37.	0	571.
0.330	1.196	24.	31.	0.	540
0.340	1.159	24.	26.	0.	514.
0.350	1.129	24.	20.	0.	494.
0.360	1.107	24.	15.	0.	480.
0.370	1.094	24.	9.	0.	470.
0.380	1.088	24.	4.	0.	467.
0.381	1.088	24.	0.	0.	467.

MAXIMUM REACTION LOAD = 17.580 LBS*10.0E 6
See Figure 5A-32, Reaction Load and Fuselage Deceleration.

5A-7
Reaction Load (R) Calculations
Case 2: With Wing and Engines Attached
(V. = 200 kts = 338 fps; M = 200,000 lb. = 6200 slugs)

TIME	DECEL	VEL CHANGE	VELOCITY	CRUSHED LENGTH	IMPACT CORCE	DECEL G'S
0.0	0.0	0.0	338.00	0.0	0.0	0.0
0 010	24.9	0.13	337.87	3.41	0.71	0.77
0.020	49.8	0.37	337.50	6.79	1.30	1.55
0.030	74.9	0.62	336.87	10.16	1.84	2.33
0.040	92.9	0.86	336.02	13.49	2.60	2.89
0.050	93.9	0.93	335.08	16.85	3.07	2.92
0.060	95.2	0.95	334.14	20.19	3.38	2.96
0.070	96.7	0.96	333.18	23.53	3.65	3.00
0.080	98.3	0.98	332.19	26.89	3.65	3.05
0.090	99.9	0.99	331.20	30.21	3.62	3.10
0.100	101.5	1.01	330.20	33.51	3.60	3.16
0.110	103.2	1.02	329.17	36.81	3.57	3.21
0.120	105.0	1.04	328.13	40.09	3.54	3.26
0.130	106.7	1.06	327.07	43.37	3.51	3.32
0.140	120.8	1.09	325.99	46.60	3.57	3.76
0.150	160.4	1.41	324.58	49.85	5.89	4.99
0.160	206.4	1.85	322.73	53.12	9.79	6.42
0.170	261.7	2.33	320.40	56.34	12.56	8.13
0.180	330.5	2.95	317.45	59.53	14.84	10.27
0.190	417.7	3.74	313.71	62.68	16.93	12.98
0.200	483.5	4.49	309.22	65.80	17.56	15.03
0.210	571.1	5.21	304.01	68.83	16.03	17.75
0.220	684.6	6.26	297.75	71.84	14.05	21.28
0.230	827.5	7.54	290.21	74.78	11.93	25.72
0.240	994.1	9.19	281.03	77.67	9.64	30.90
0.250	1205.2	10.96	270.06	80.43	8.39	37.46
0.260	1470.6	13.34	256.72	83.06	6.98	45.71
0.270	1736.3	16.12	240.59	85.55	4.45	53.96
0.280	1904.9	18.16	222.43	87.84	3.54	59.21
0.290	2010.6	19.61	202.83	89.97	2.80	62.49
0.300	2083.4	20.50	182.33	91.90	2.26	64.76
0.310	2133.4	21.10	161.23	93.62	1.94	66.31
0.320	2176.6	21.77	139.46	95.14	1.71	67.65
0.330	2216.2	21.97	117.49	96.42	1.53	68.88
0.340	2252.6	22.35	95.14	97.49	1.38	70.01
0.350	2283.6	22.46	72.68	98.32	1.26	70.98
0.360	2308.2	22.97	49.71	98.93	1.17	71.74
0.370	2324.4	23.17	26.54	99.31	1.11	72.24
0.380	2330.9	23.28	3.26	99.46	1.09	72.45
0.381	2331.0	3.26	-0.01	99.46	1.09	72.45

MAXIMUM REACTION LOAD = 17.580 LBS*10.0E 6
See Figure 5A-32, Reaction Load and Fuselage Deceleration.

F I G U R E S

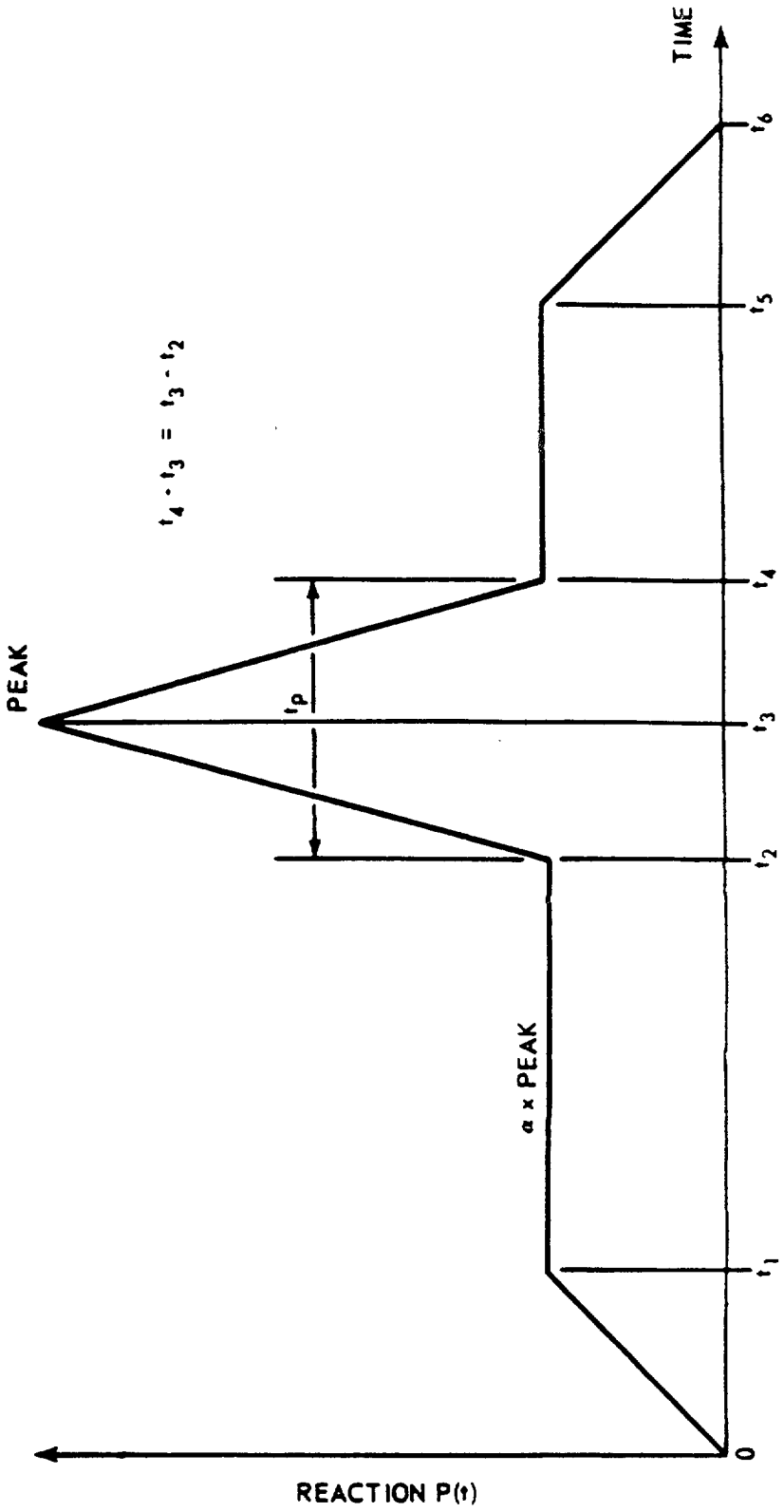

GPU Nuclear	Update -1
TMI Unit-1	7/82
Total Reaction vs Time Curve	
	Fig. 5A-1

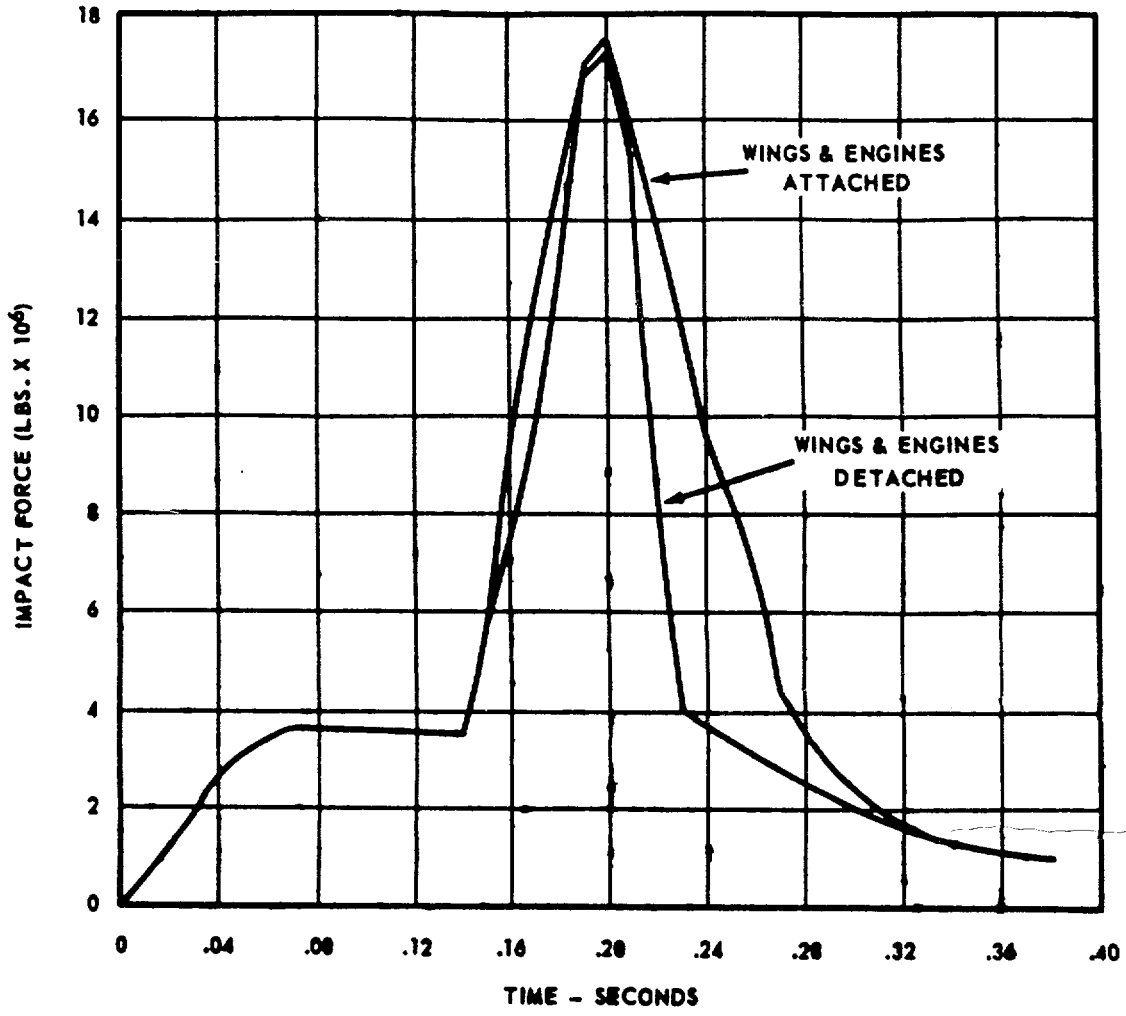

GPU Nuclear
TMI Unit-1

Update -1
7/82

Load Time Curve for 720 Aircraft at 200 Knots

Fig. 5A-2

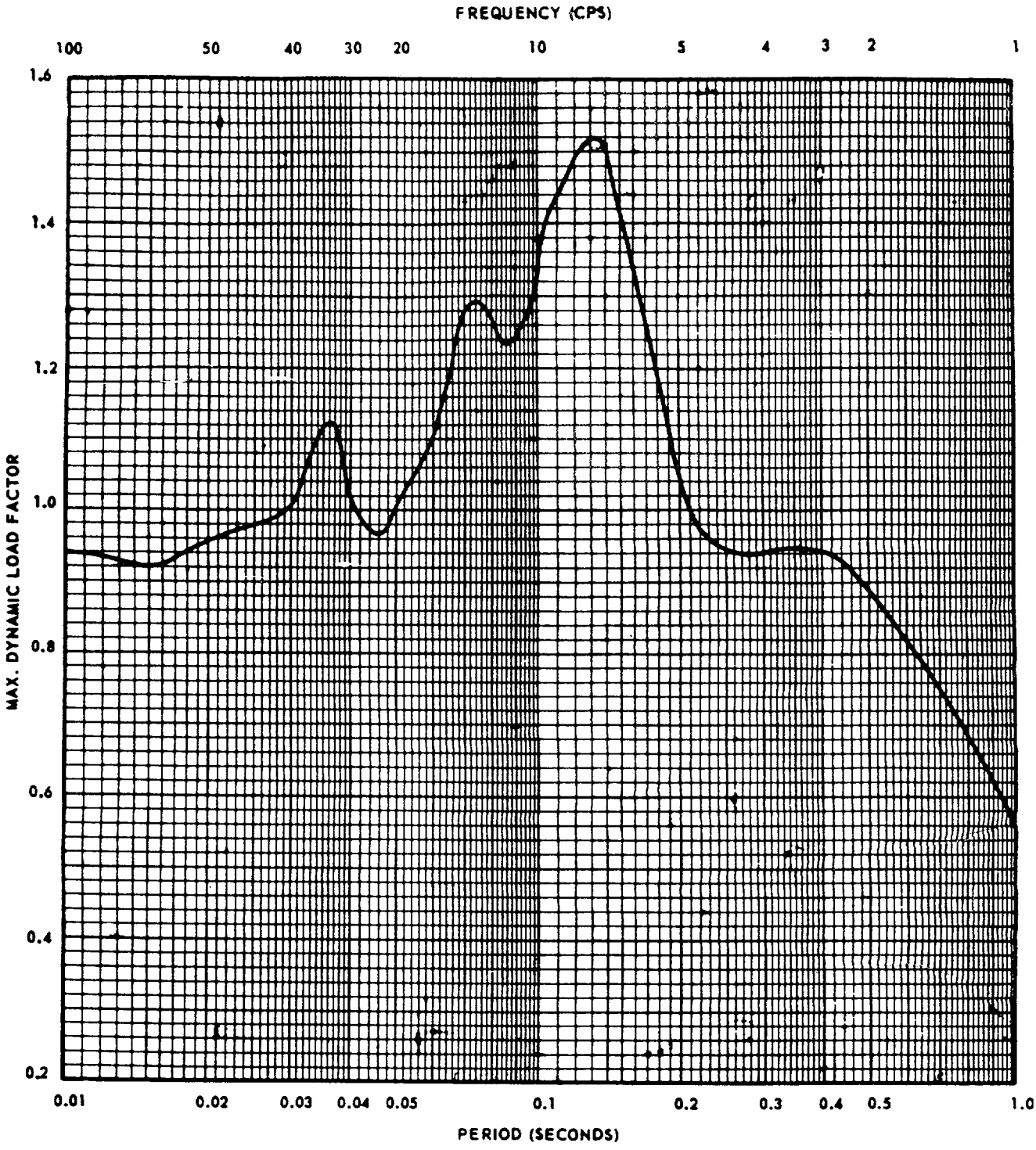

GPU Nuclear — Update -1

TMI Unit-1 — 7/82

Maximum Dynamic Load Factor vs Period or Frequency of a One-Degree-Freedom System under the Impact of Boeing 720

Fig. 5A-3

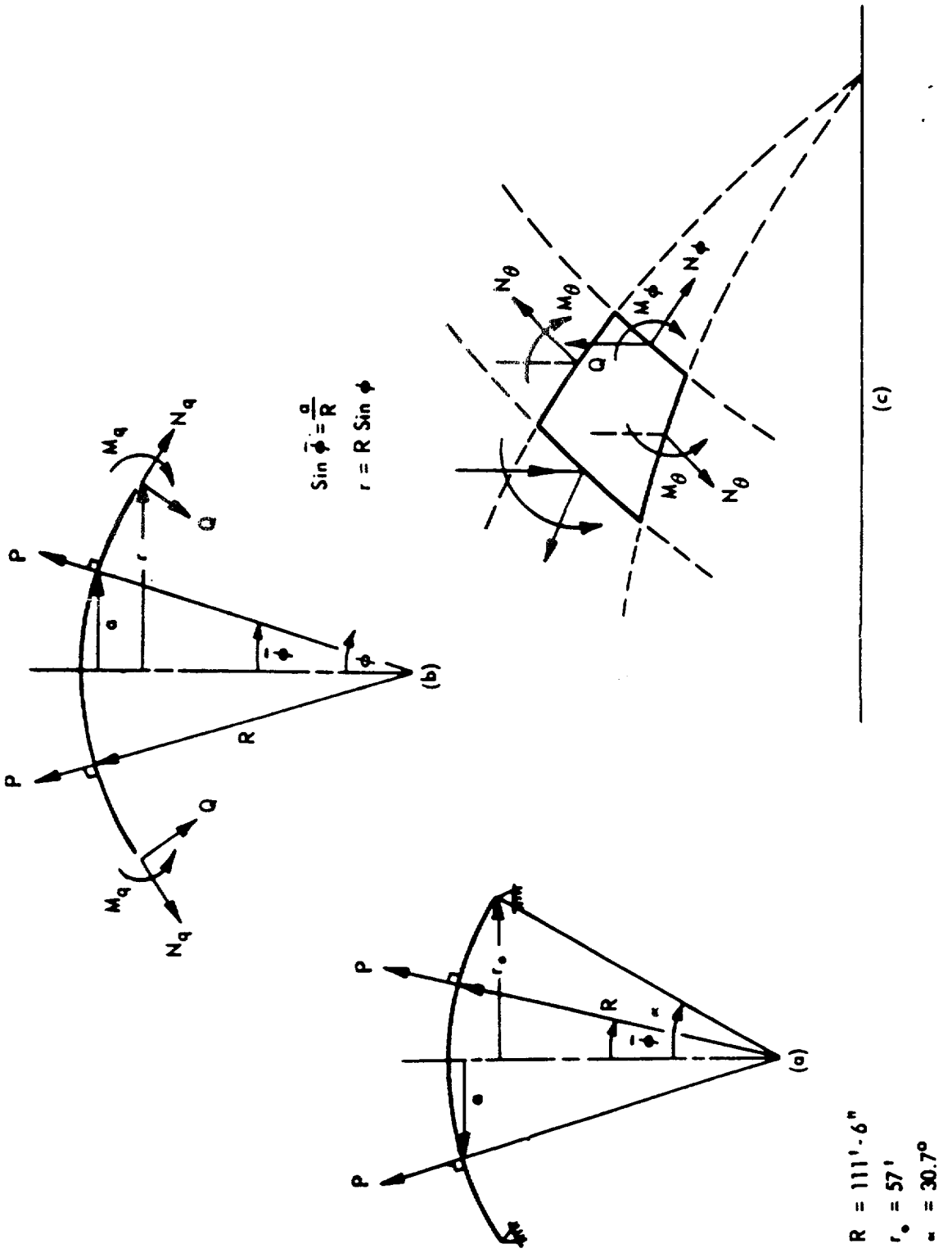

GPU Nuclear	Update -1
TMI Unit-1	7/82
Spherical Cap under a Ring Load	
	Fig. 5A-4

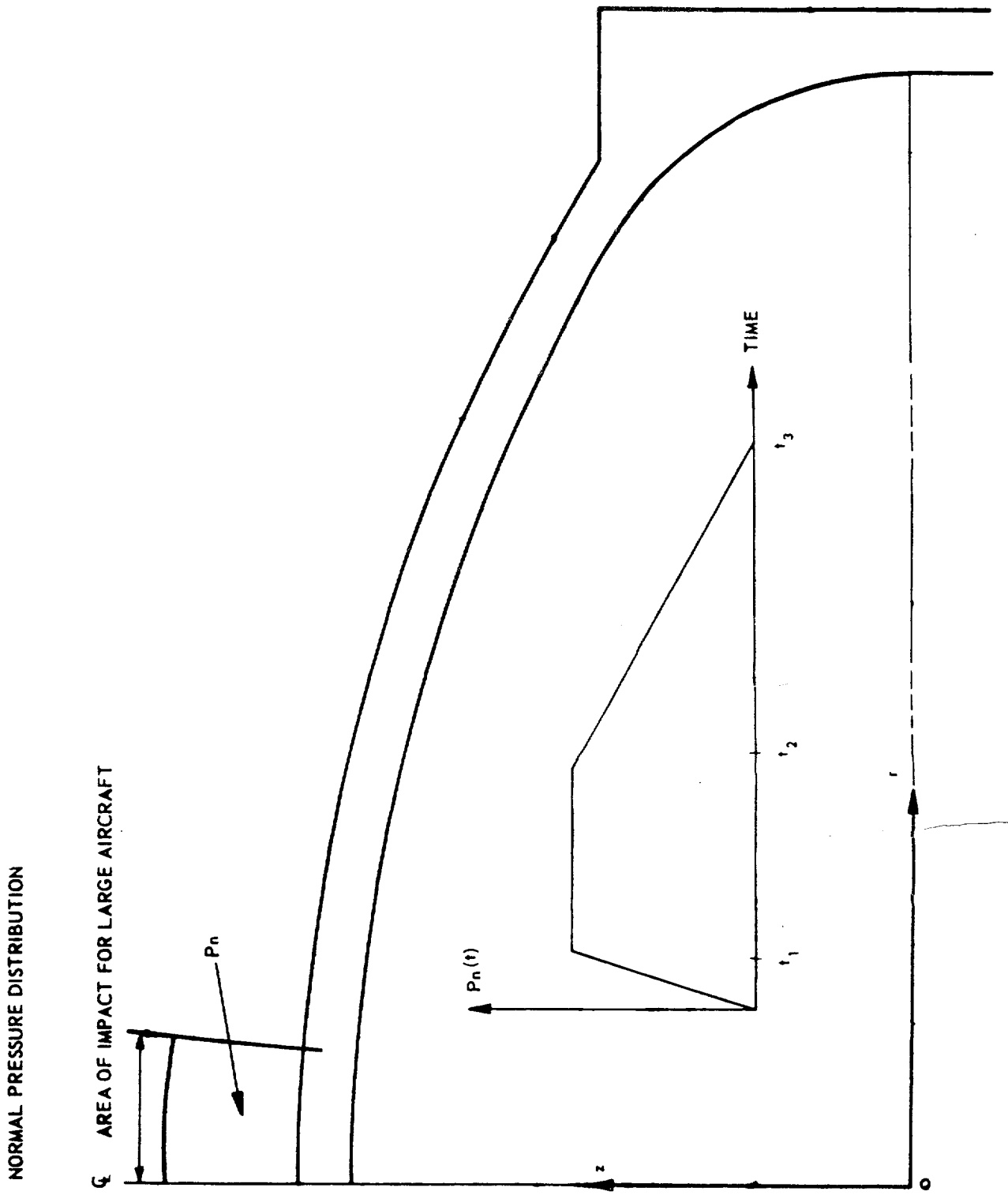

GPU Nuclear	Update -1
TMI Unit-1	7/82

Spacial and Time Distribution of Load on Shell

Fig. 5A-5

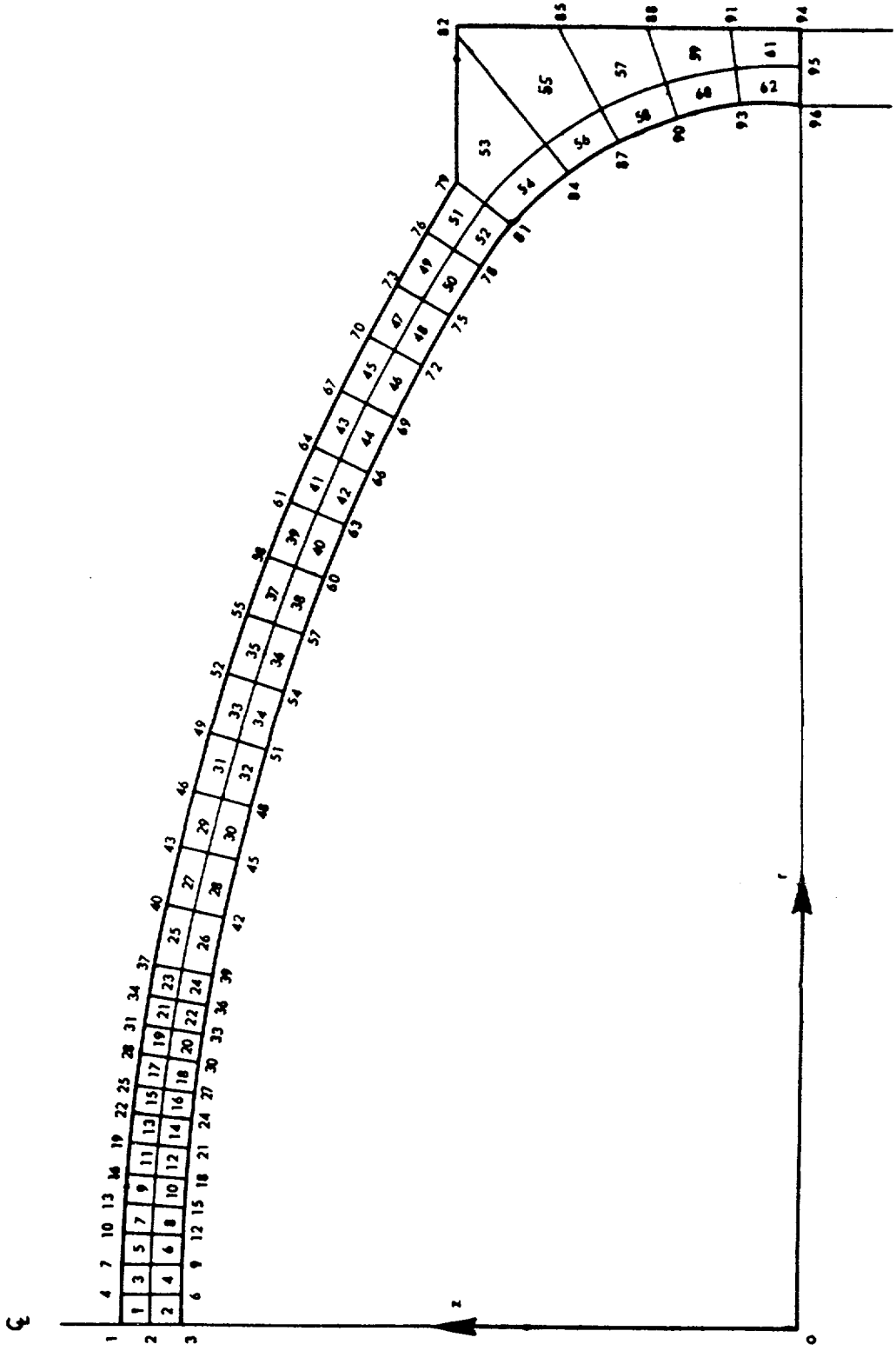

GPU Nuclear Update -1

TMI Unit-1 7/82

Grid for Dynamic Finite Element Analysis of Aircraft Impingement on Dome

Fig. 5A-6

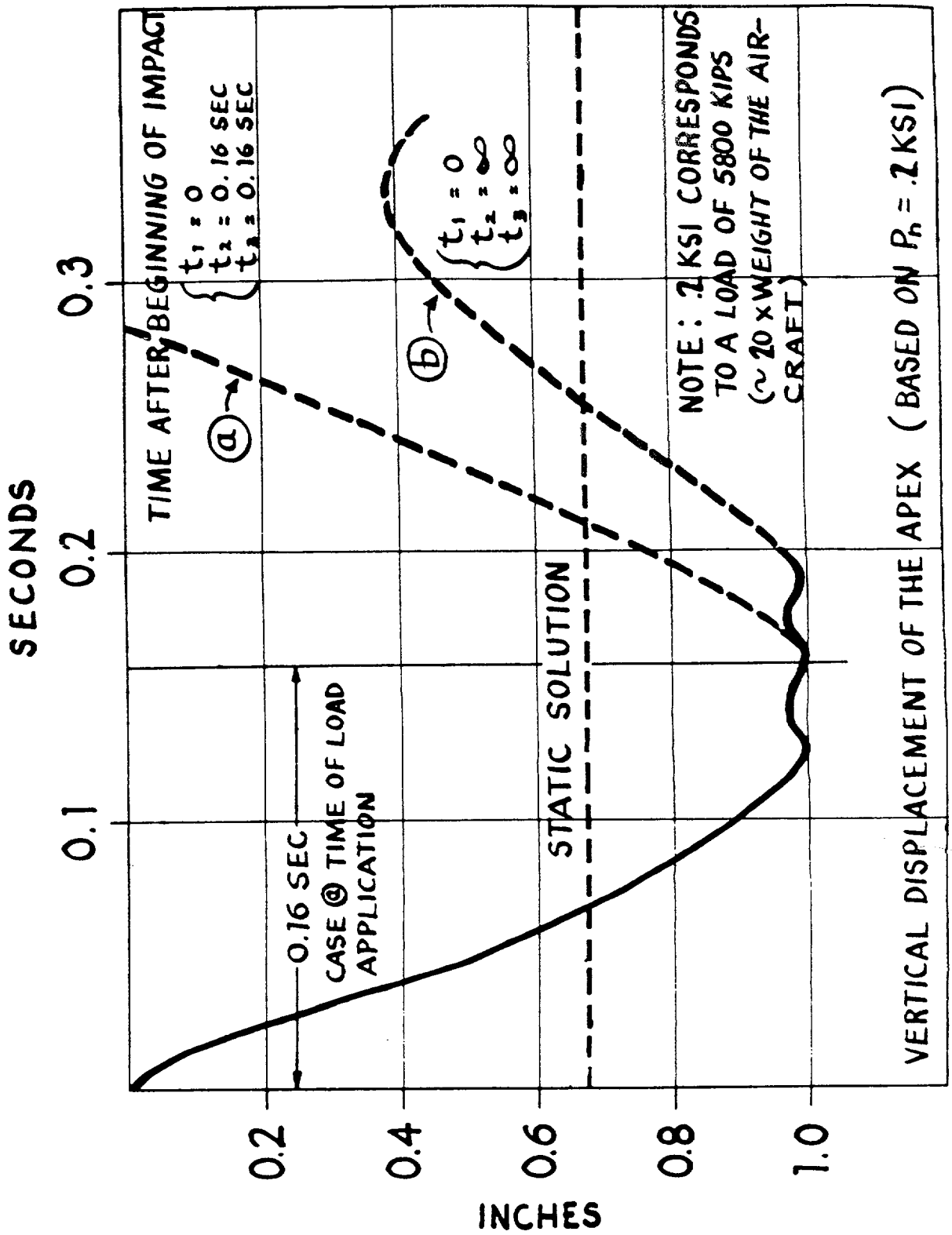

GPU Nuclear
TMI Unit-1

Update -1
7/82

Effect of Aircraft Impingement on Dome of Containment Structure-Constant Deceleration

Fig. 5A-7

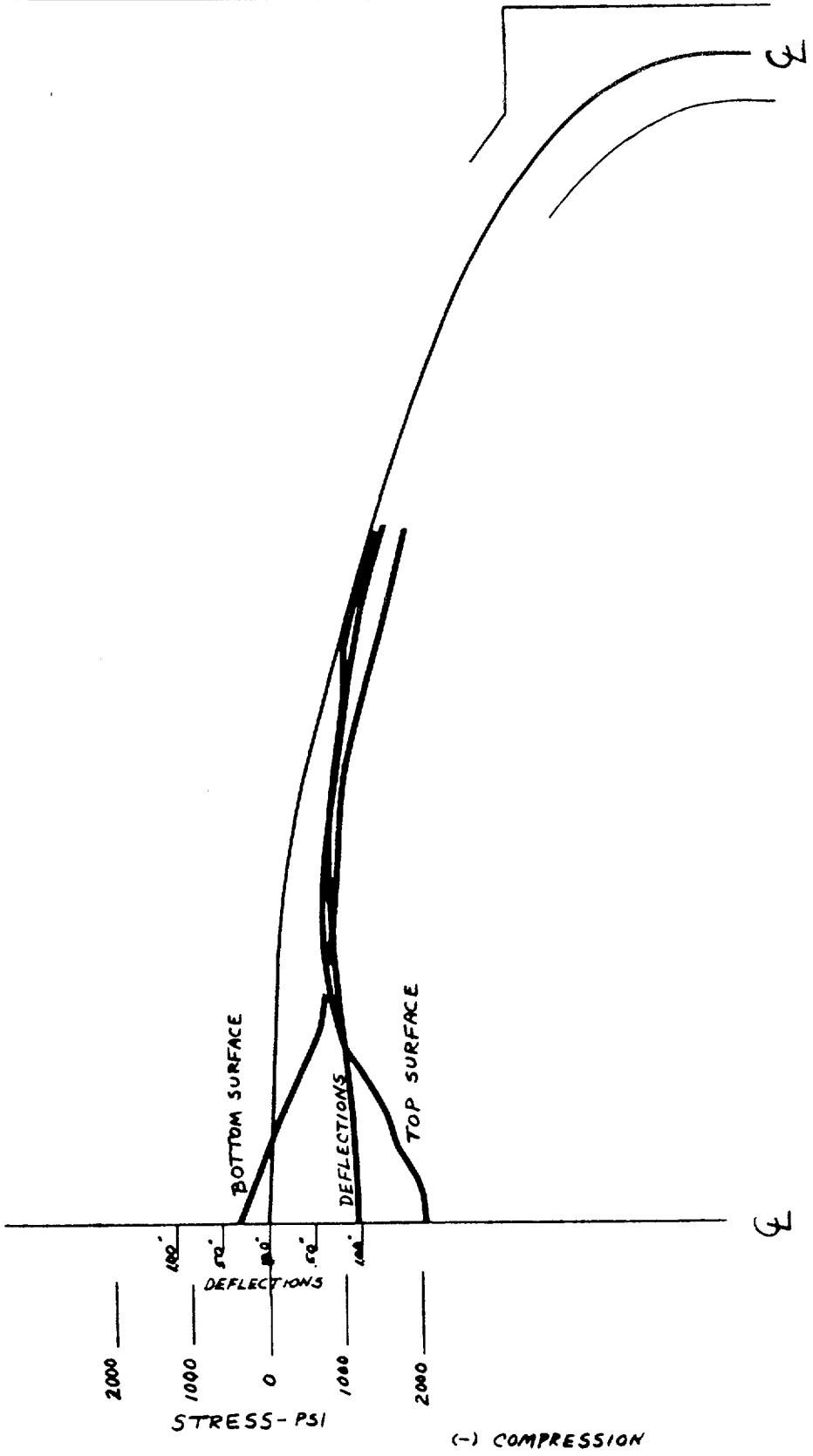

GPU Nuclear Update -1

TMI Unit-1 7/82

Deflections and Stresses for Aircraft Impingement for Time = 0.16 Seconds Constant Deceleration

Fig. 5A-8

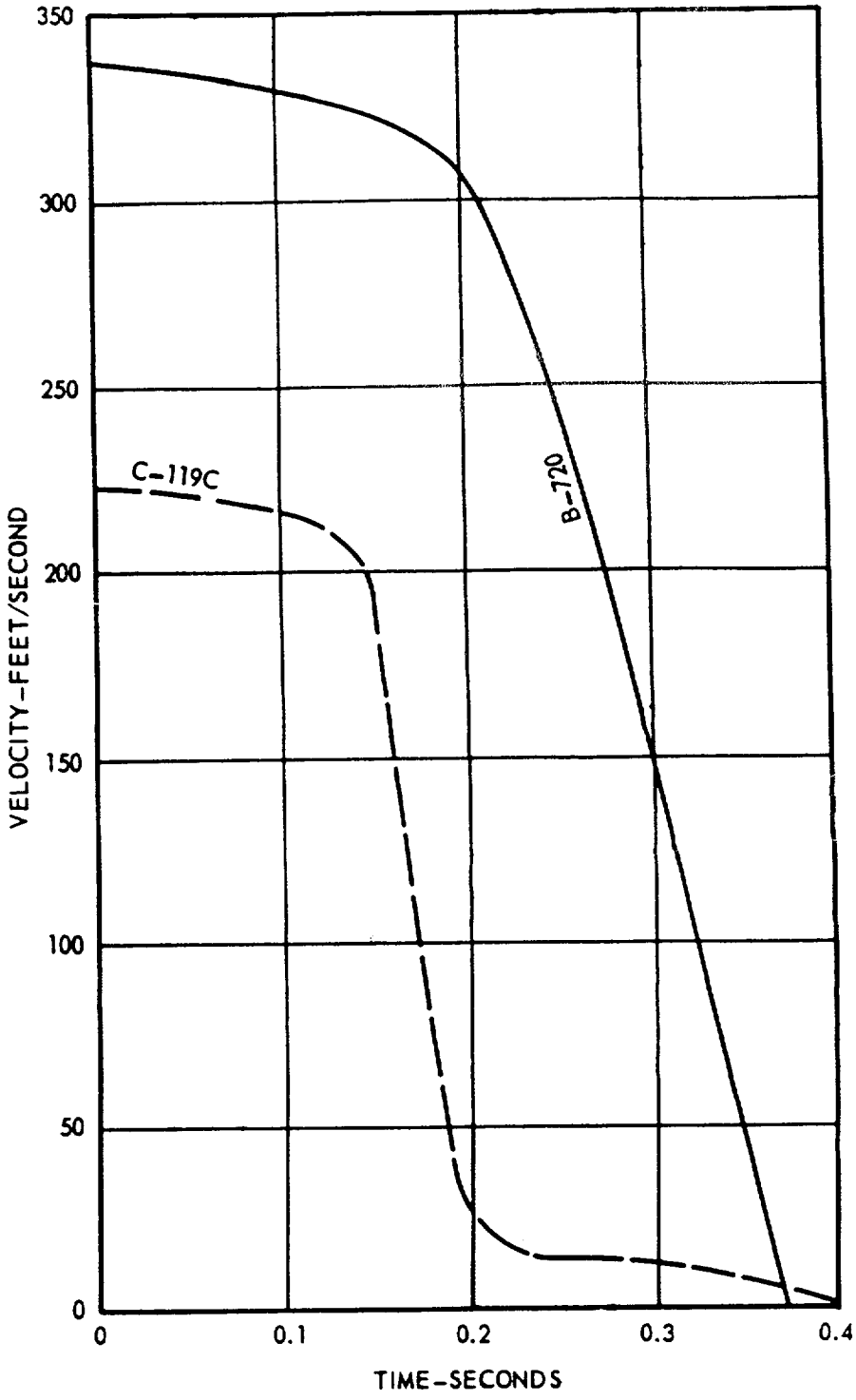

GPU Nuclear
TMI Unit-1

Update -1
7/82

Velocity Diagram for 720 Aircraft at 200 Knots Impact Speed with Wings and Engines Detached

Fig. 5A-9

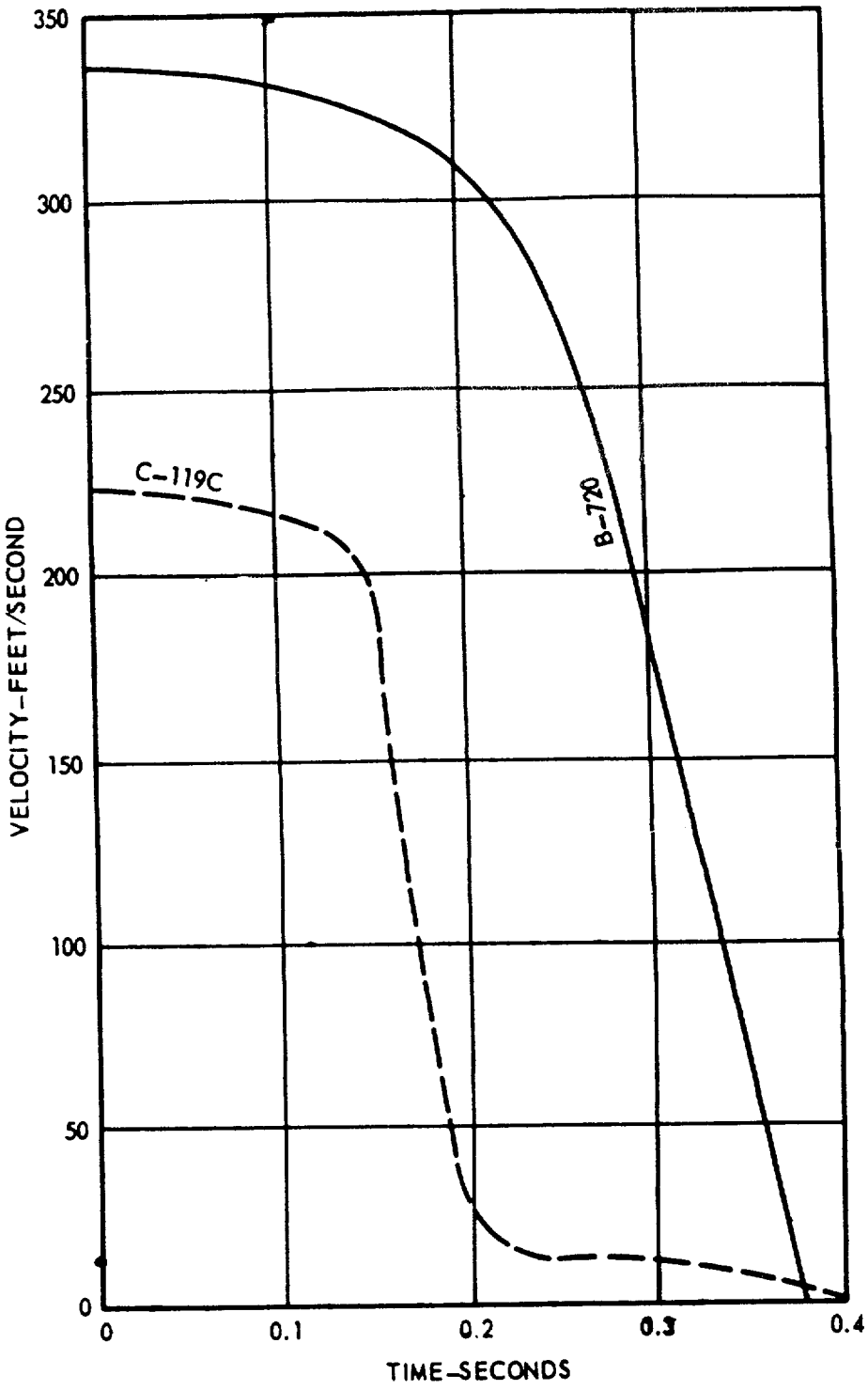

GPU Nuclear
TMI Unit-1

Update -1
7/82

Velocity Diagram for 720 Aircraft at 200 Knots Impact Speed with Wings and Engines Attached

Fig. 5A-10

AIRCRAFT WEIGHT BREAKDOWN

FUSELAGE	-	51,000 LB
EMPENNAGE	-	5,680
NOSE GEAR	-	700
MAIN GEAR	-	5,380
INB. ENG.	-	10,800
OUTB. ENG.	-	10,300
WING STR.	-	29,700
		113,560 LB
PASS. & BAGS	-	13,000
CARGO	-	10,000
FUEL	-	63,440
G. W.	-	200,000 LB

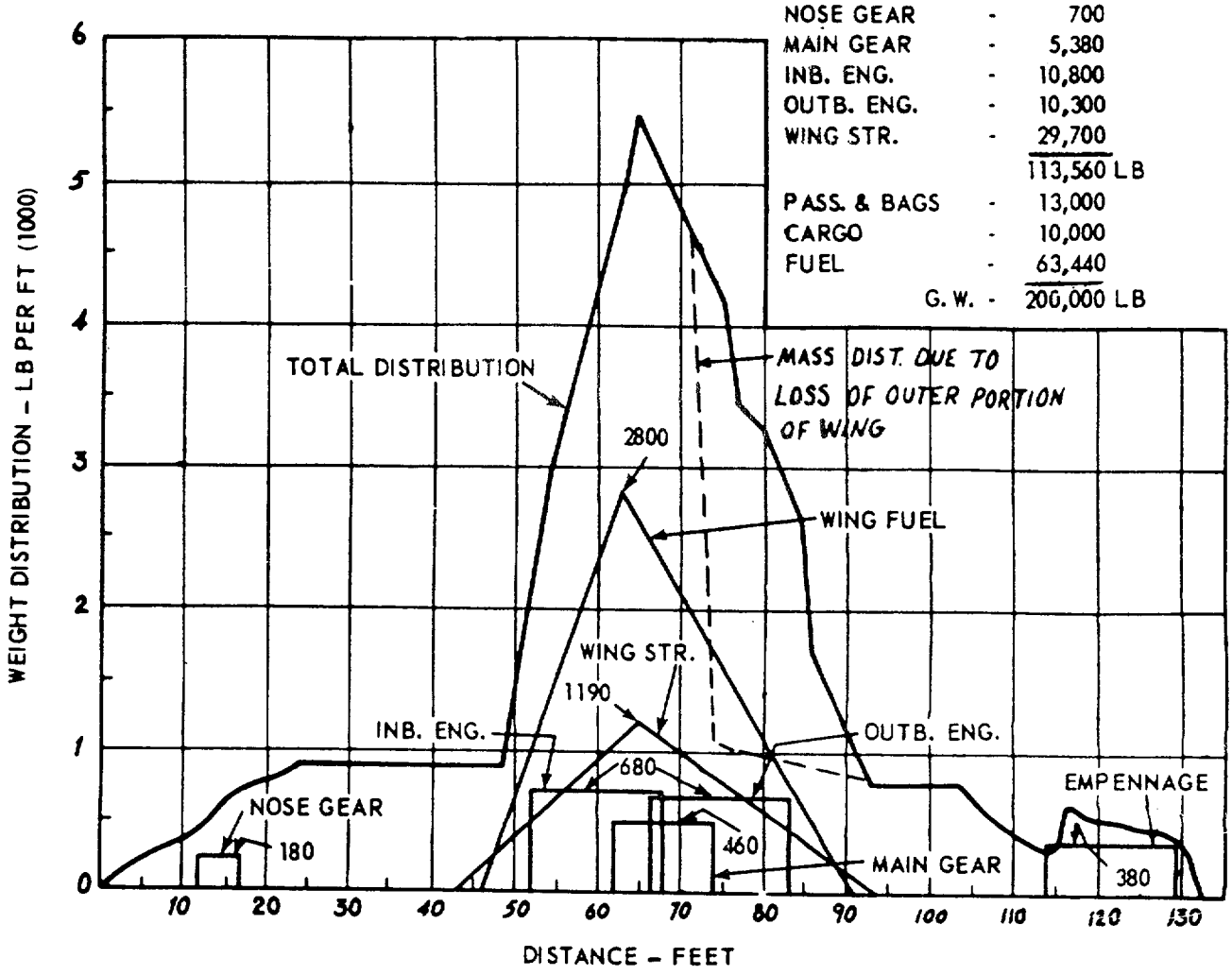

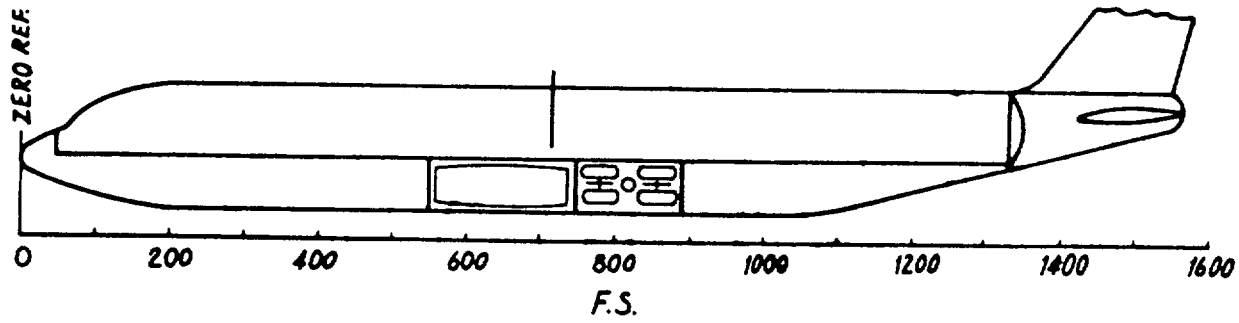

GPU Nuclear | **Update -1**
TMI Unit-1 | **7/82**

720 Aircraft Mass Distribution

Fig. 5A-11

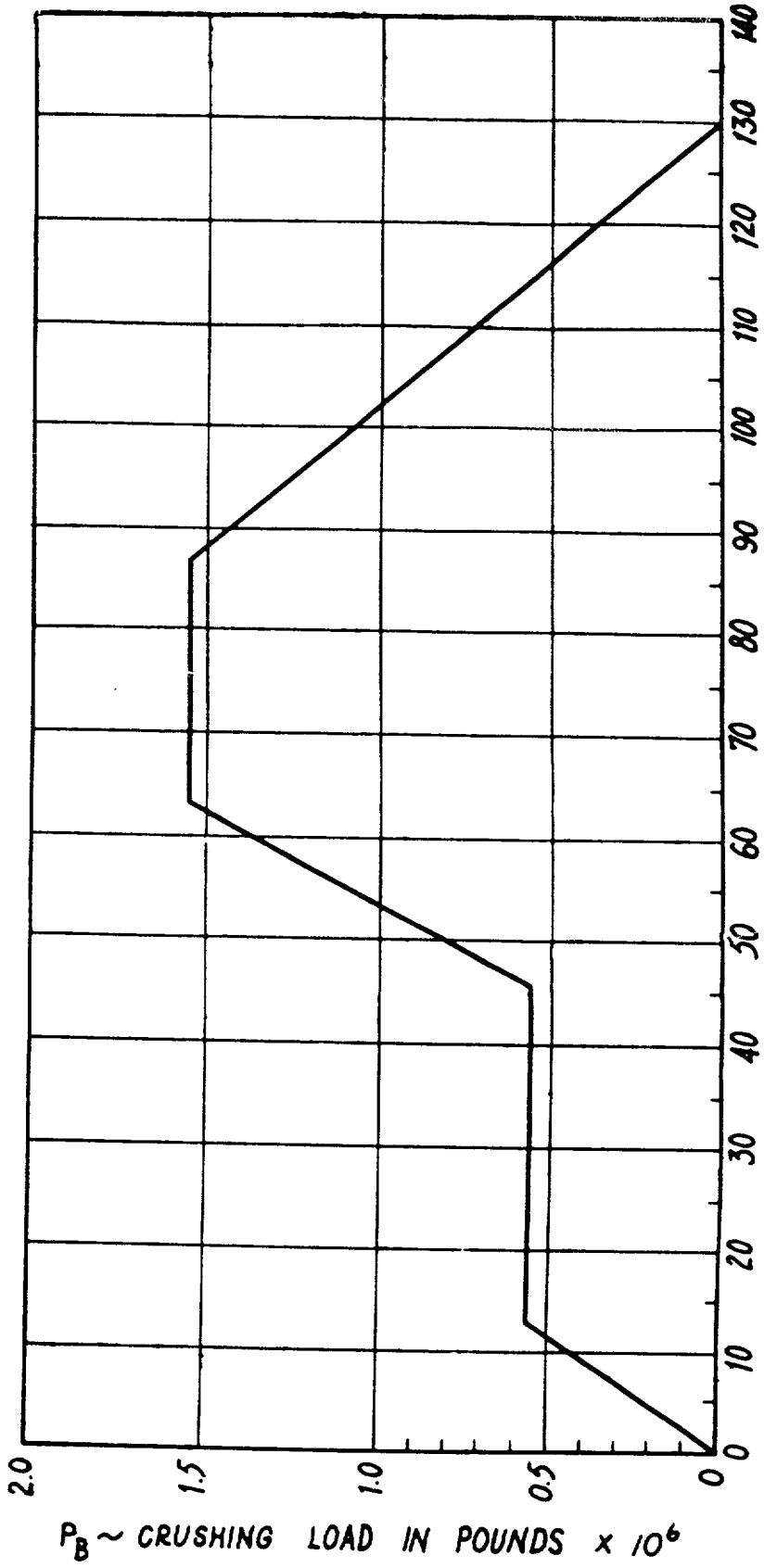

GPU Nuclear
TMI Unit-1

Update -1
7/82

Boeing 720 Fuselage Buckling (Crushing) Load

Fig. 5A-12

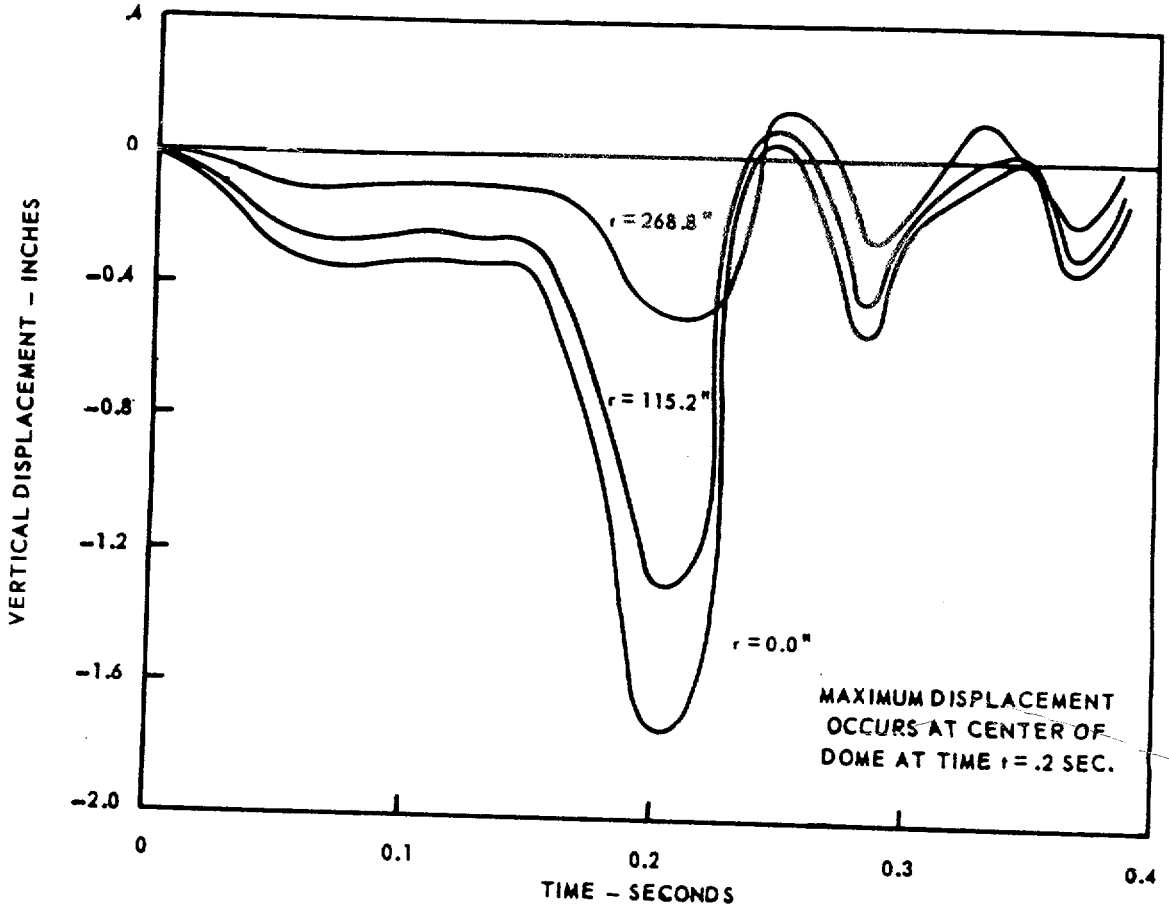

p. 5A.FIG-13

GPU Nuclear — Update -1

TMI Unit-1 — 7/82

Time Variation of Shell Vertical Displacements with Wings and Engines Detached

Fig. 5A-13

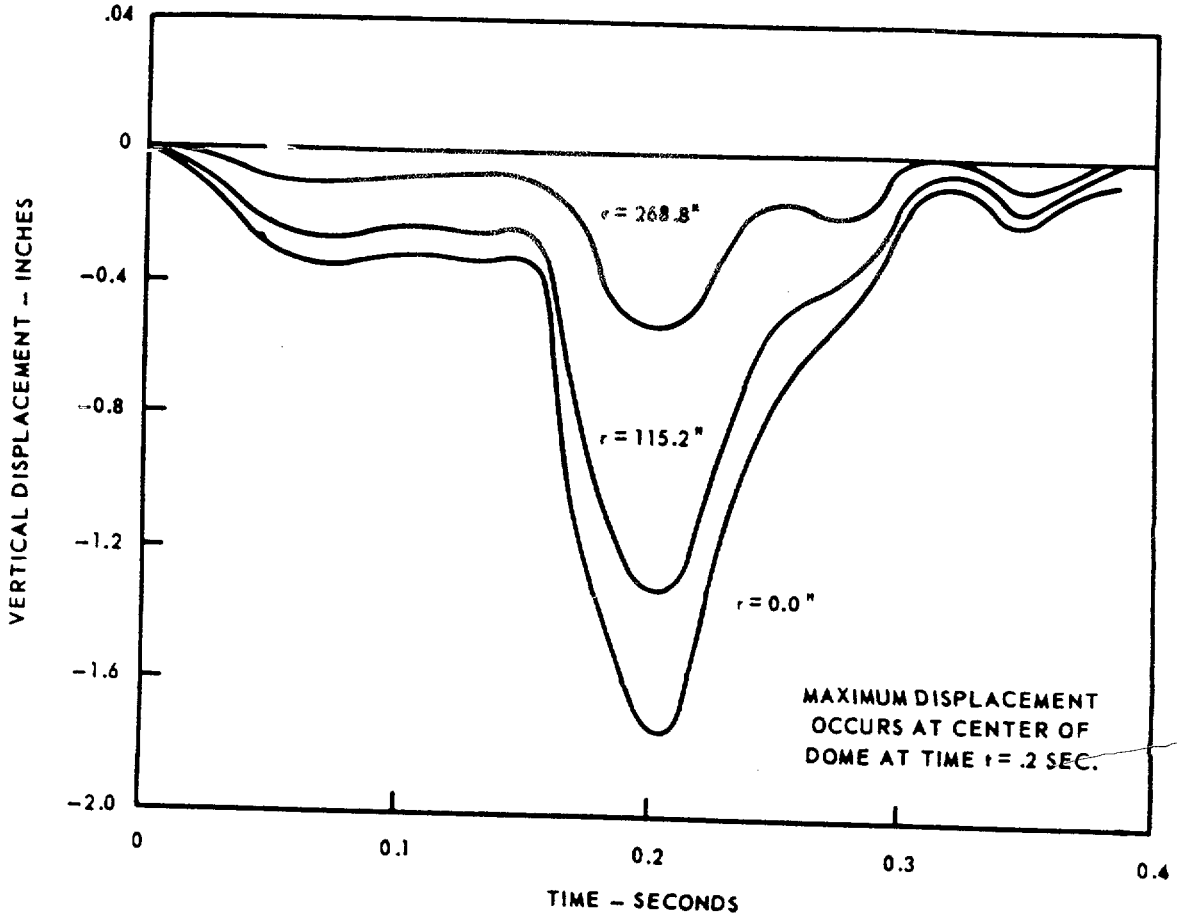

GPU Nuclear
TMI Unit-1

Update -1
7/82

Time Variation of Shell Vertical Displacements with Wings and Engines Attached

Fig. 5A-14

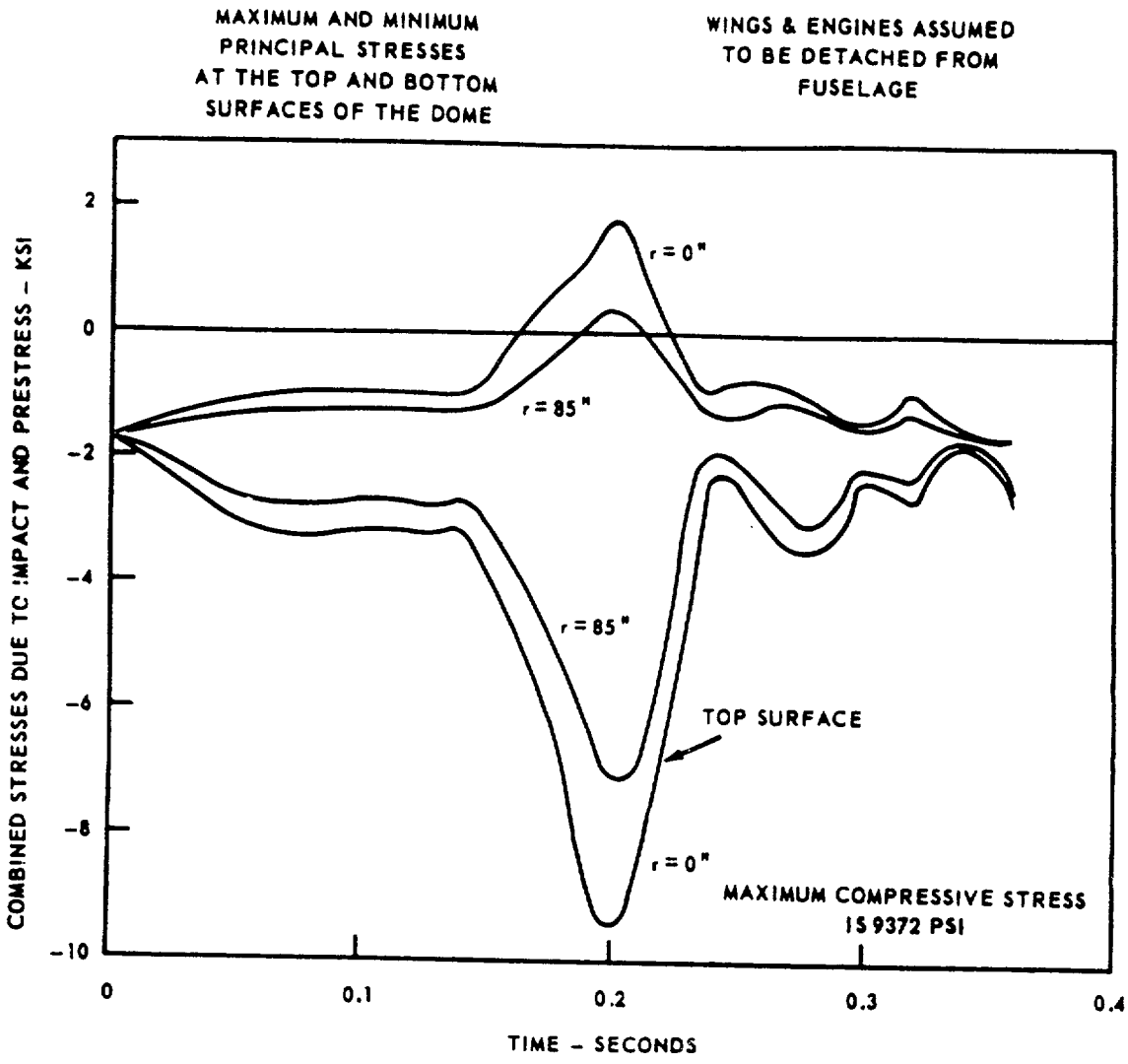

p. 5A.FIG-15

GPU Nuclear
TMI Unit-1

Update -1
7/82

Time Variation of Shell Surface Stresses Aircraft with Wings and Engines Detached

Fig. 5A-15

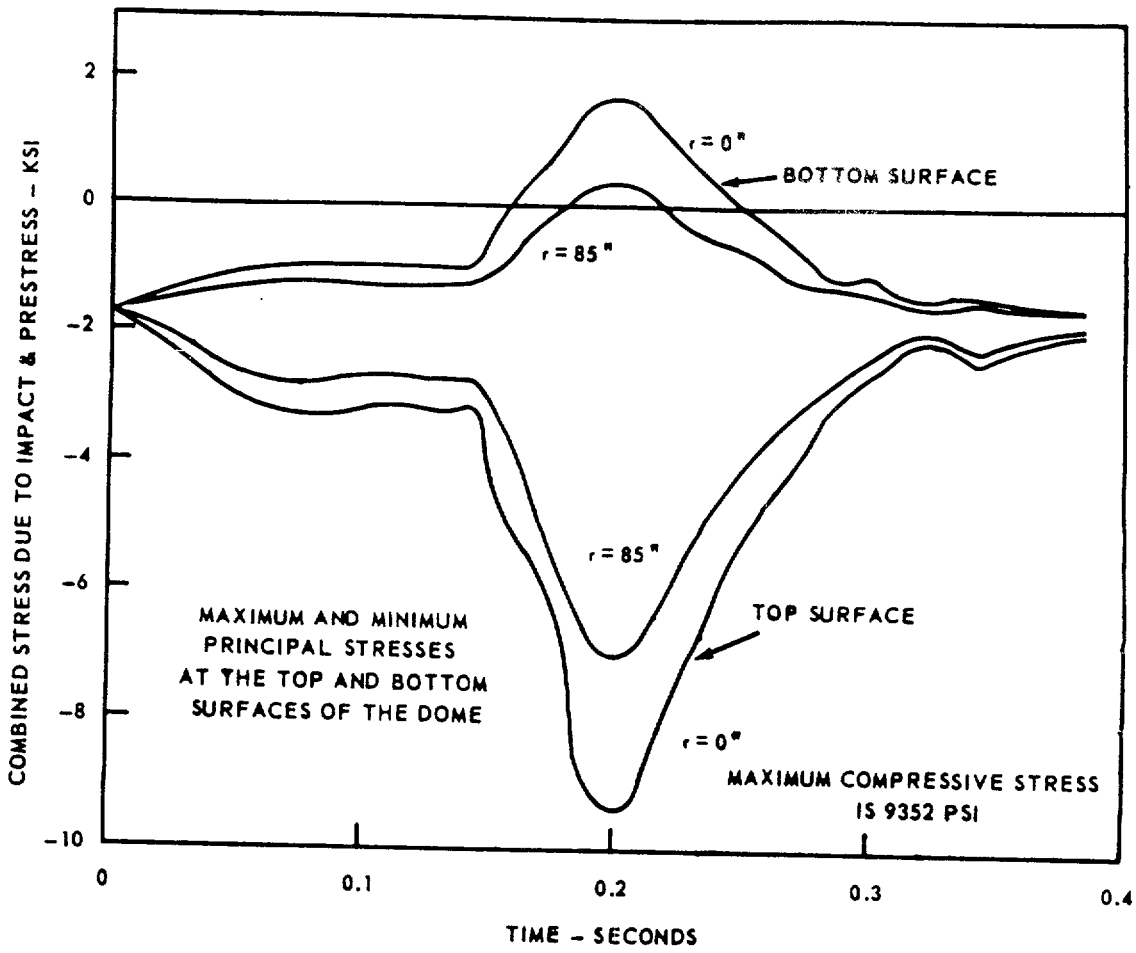

GPU Nuclear

TMI Unit-1

Update -1

7/82

Time Variation of Shells Surface Stresses Aircraft with Wings and Engines Attached

Fig. 5A-16

FOURIER SERIES = .07955 - .1575 COS θ + .1558 COS 2θ - .1446 COS 3θ + .133 COS 4θ
- .1208 COS 5θ + .1058 COS 6θ - .0894 COS 7θ + .0722 COS 8θ
- .0551 COS 9θ

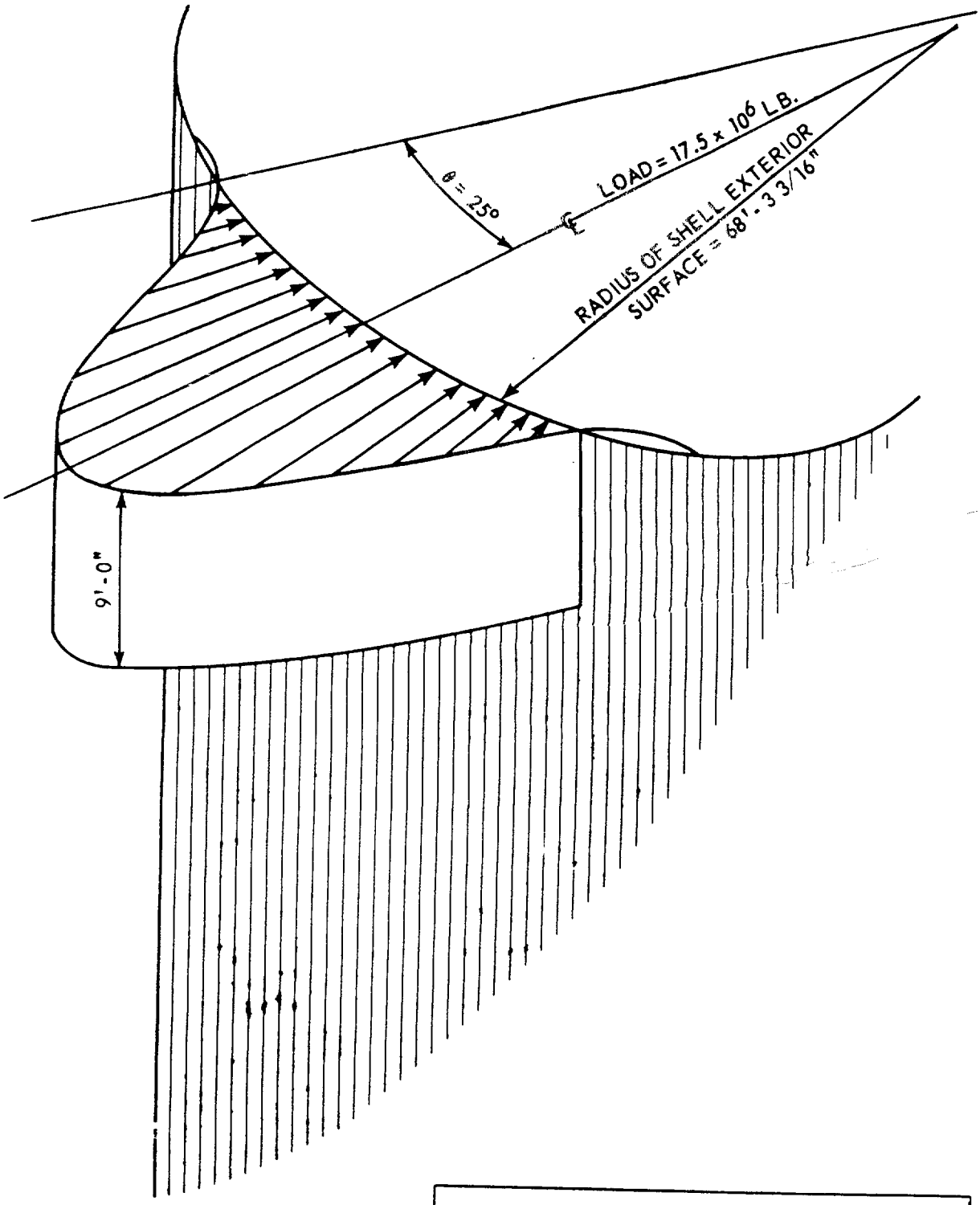

GPU Nuclear
TMI Unit-1

Update -1
7/82

Pressure Distribution for Aircraft Impact

Fig. 5A-17

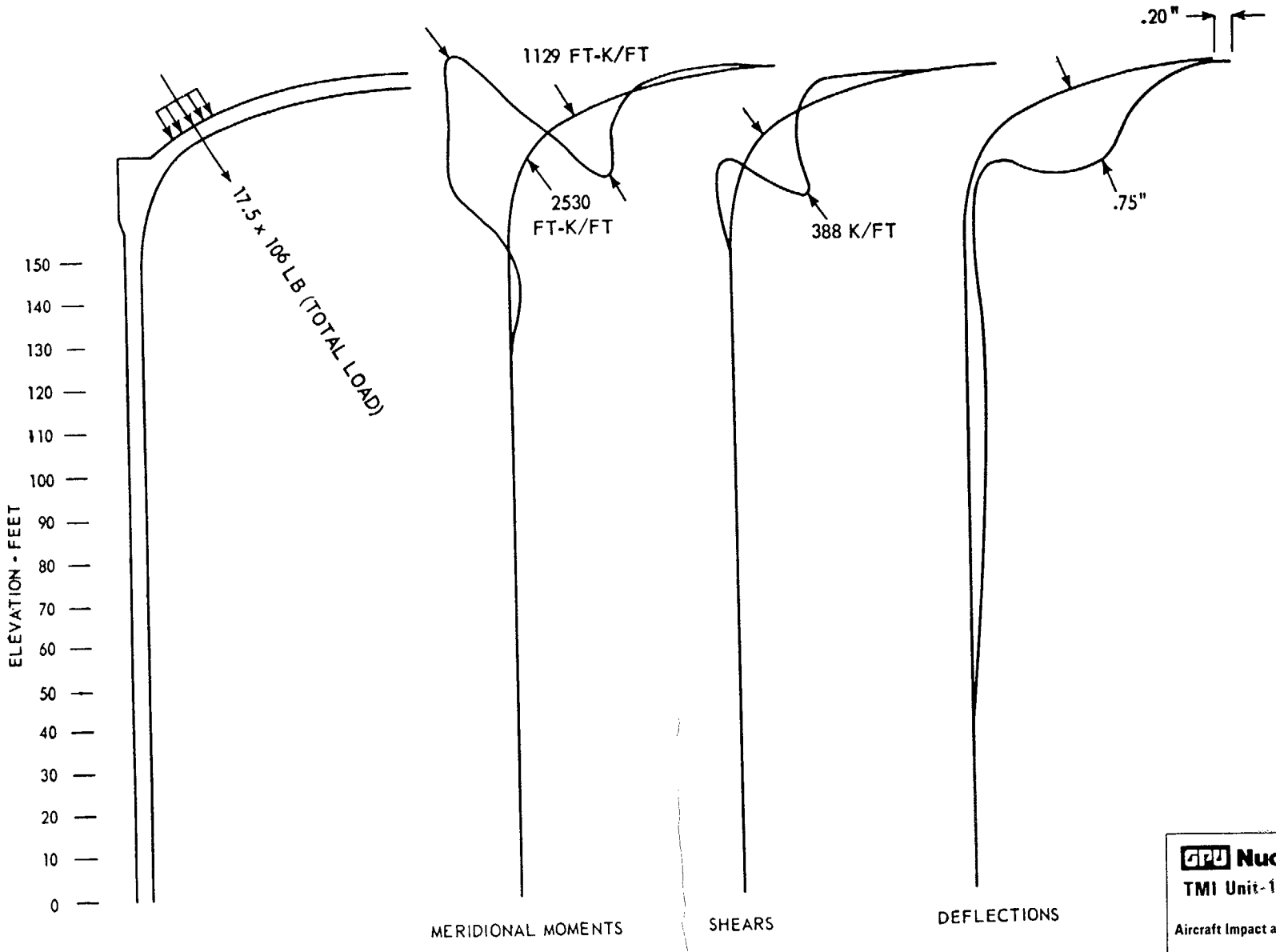

GPU Nuclear
TMI Unit-1

Update -1
7/82

Aircraft Impact at Girder to Dome Transition

Fig. 5A-18

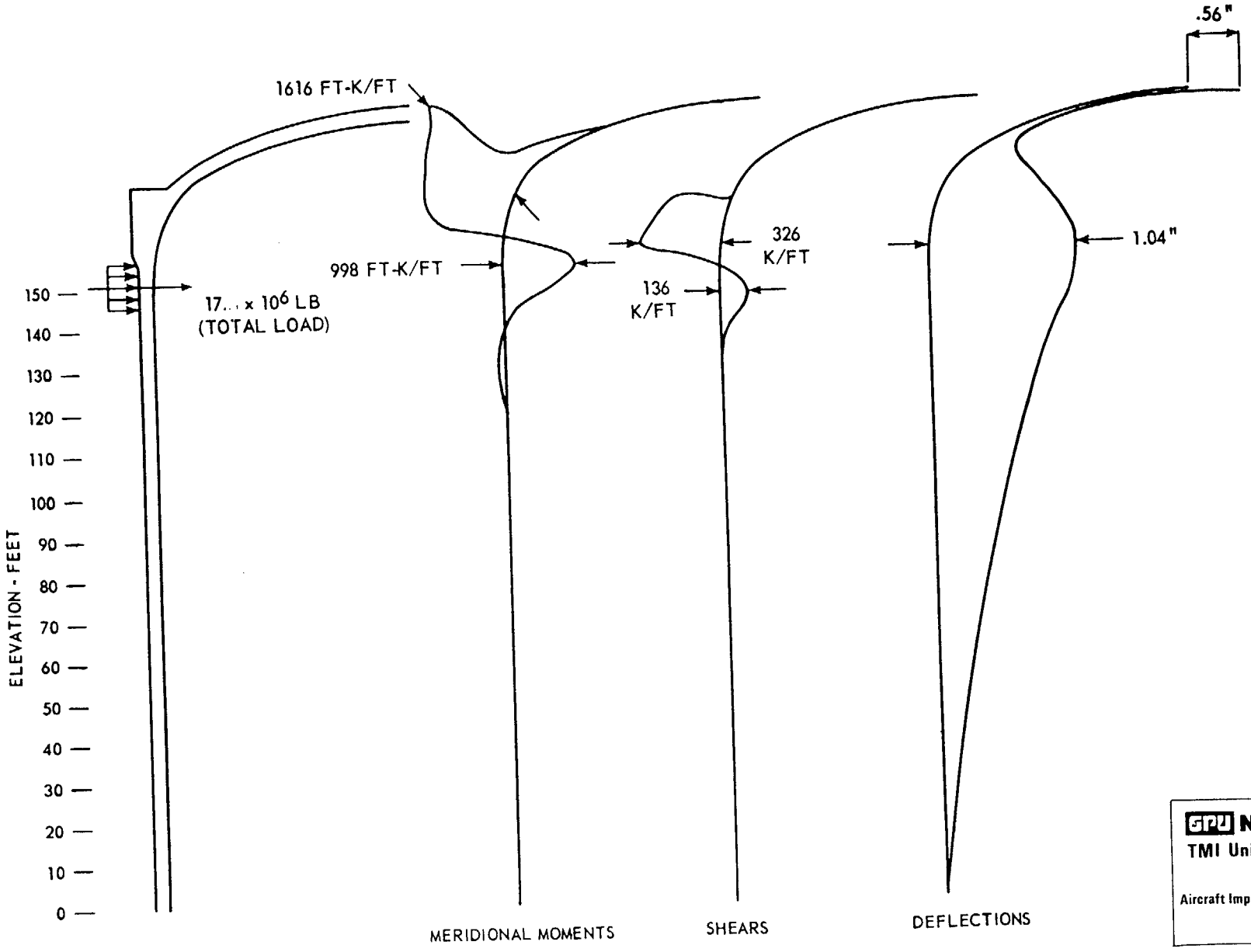

GPU Nuclear
TMI Unit-1

Update -1
7/82

Aircraft Impact at Spring Line

Fig. 5A-19

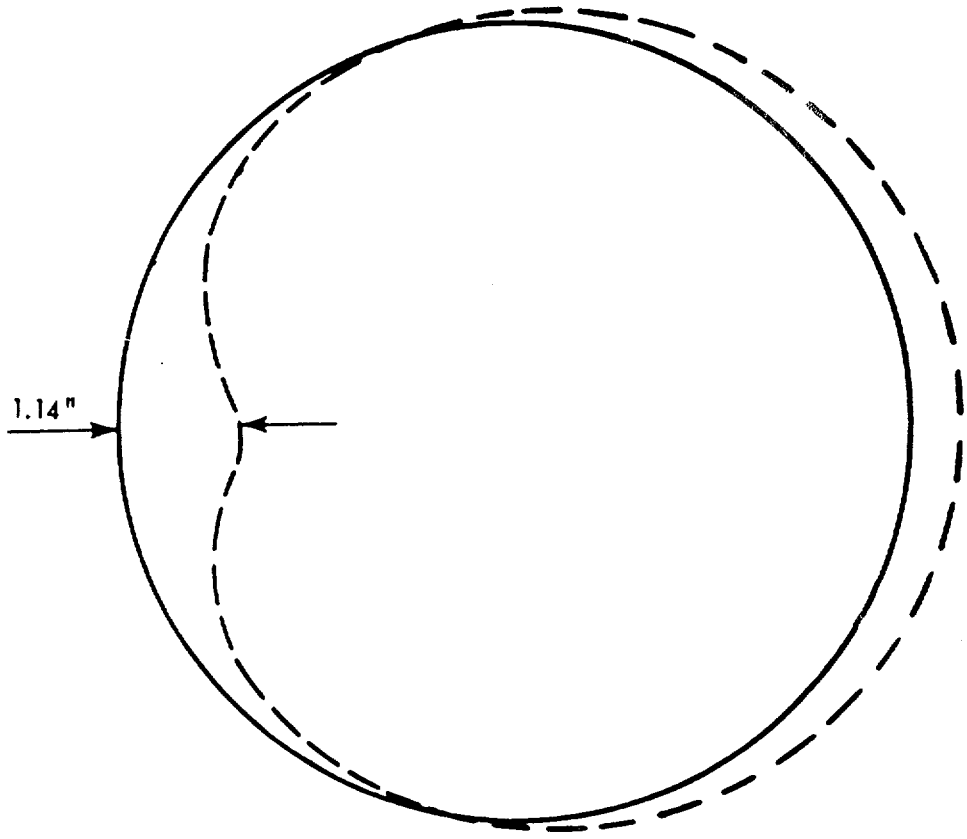

ELEV. 149'-1"

p. 5A.FIG-20

GPU Nuclear
TMI Unit-1

Update -1
7/82

Radial Deflection Impact at Spring Line

Fig. 5A-20

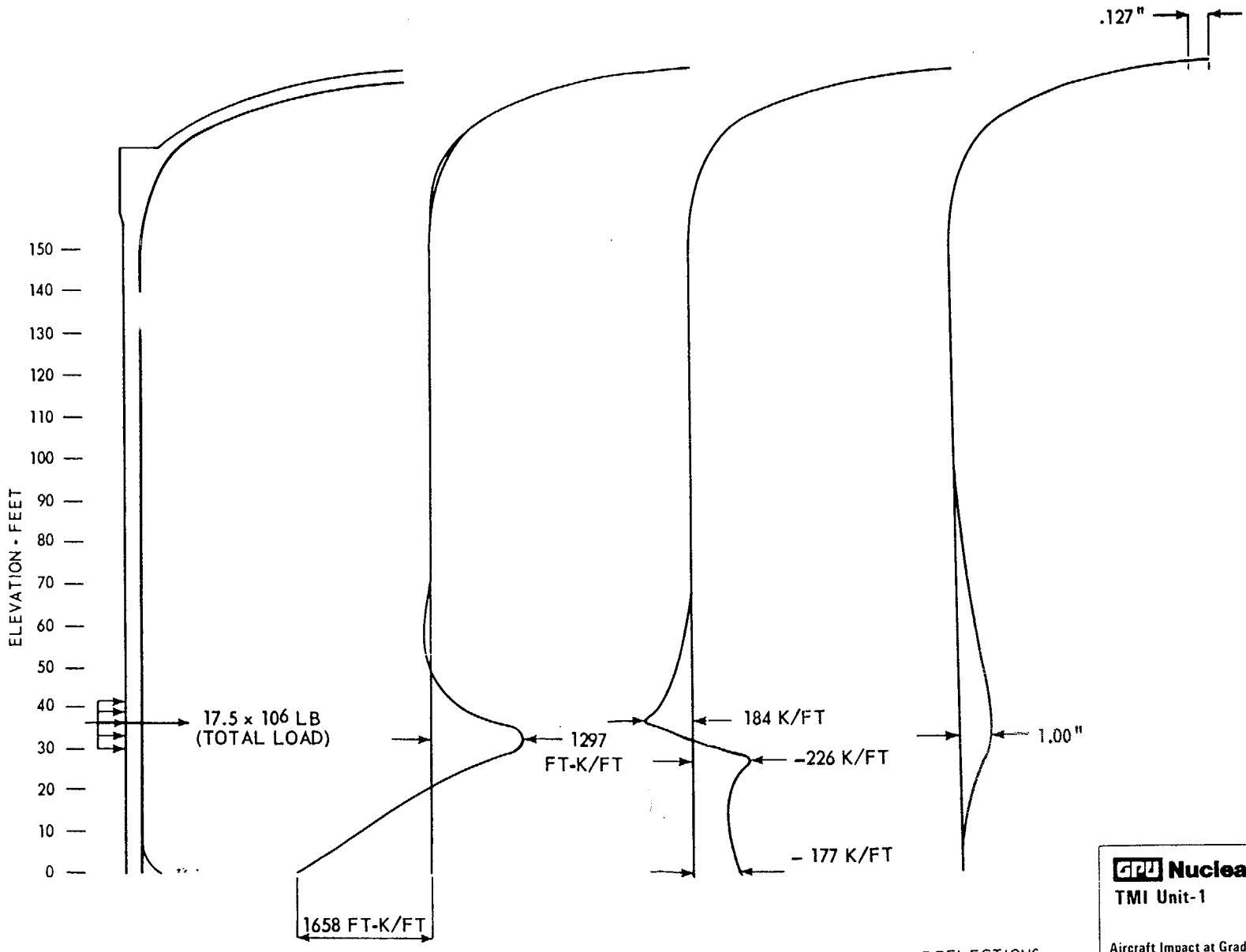

GPU Nuclear
TMI Unit-1

Update -1
7/82

Aircraft Impact at Grade

Fig. 5A-21

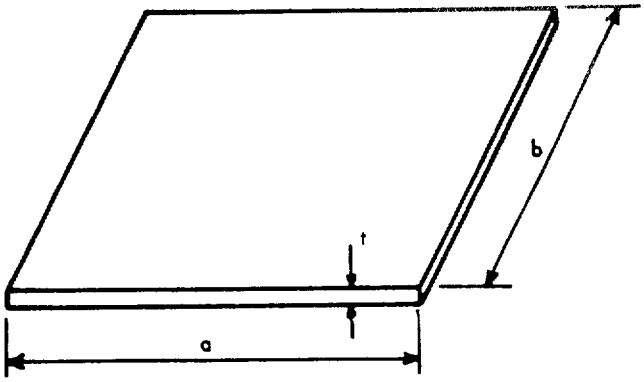

(a) GEOMETRY

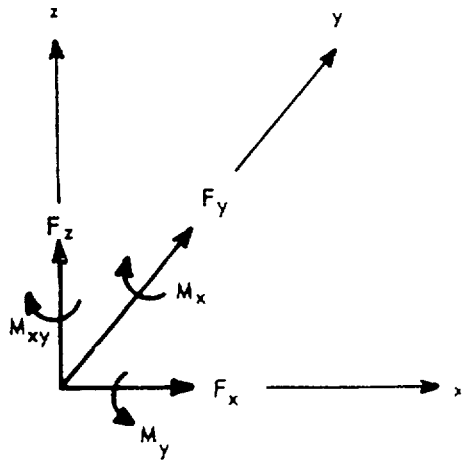

(b) SIX FORCE COMPONENTS AT NODAL POINT

GPU Nuclear
TMI Unit-1

Update -1
7/82

Rectangular Finite Element

Fig. 5A-22

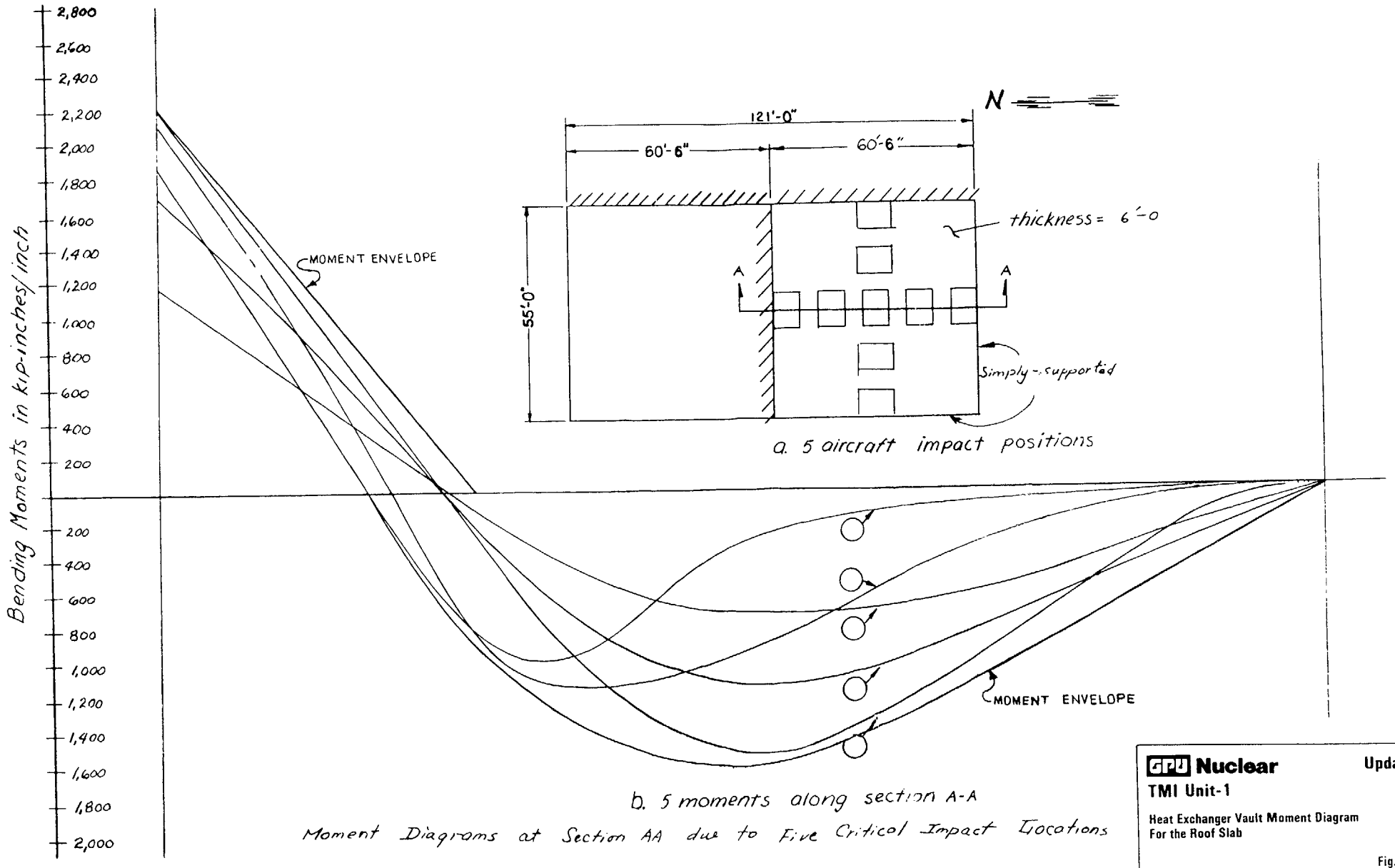

Moment Diagrams at Section AA due to Five Critical Impact Locations

GPU Nuclear
TMI Unit-1

Update - 1
7/82

Heat Exchanger Vault Moment Diagram
For the Roof Slab

Fig. 5A-23

Figure 5A-24 thru 5A-25
(p.5A.FIG-24 thru p.5A.FIG-25)

DELETED

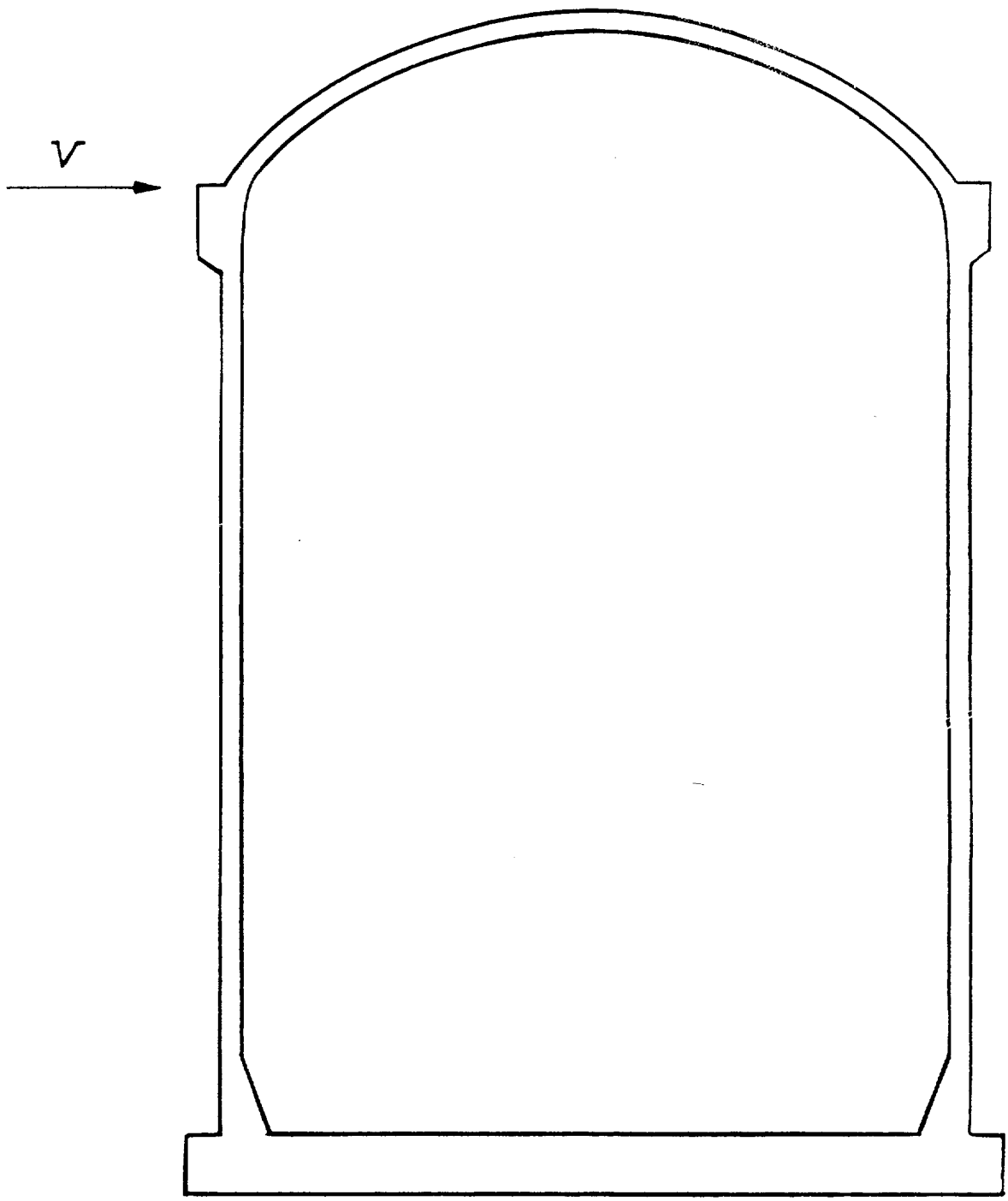

GPU Nuclear
TMI Unit-1

Update -1
7/82

Critical Aircraft Impact-Direction 1

Fig. 5A-26

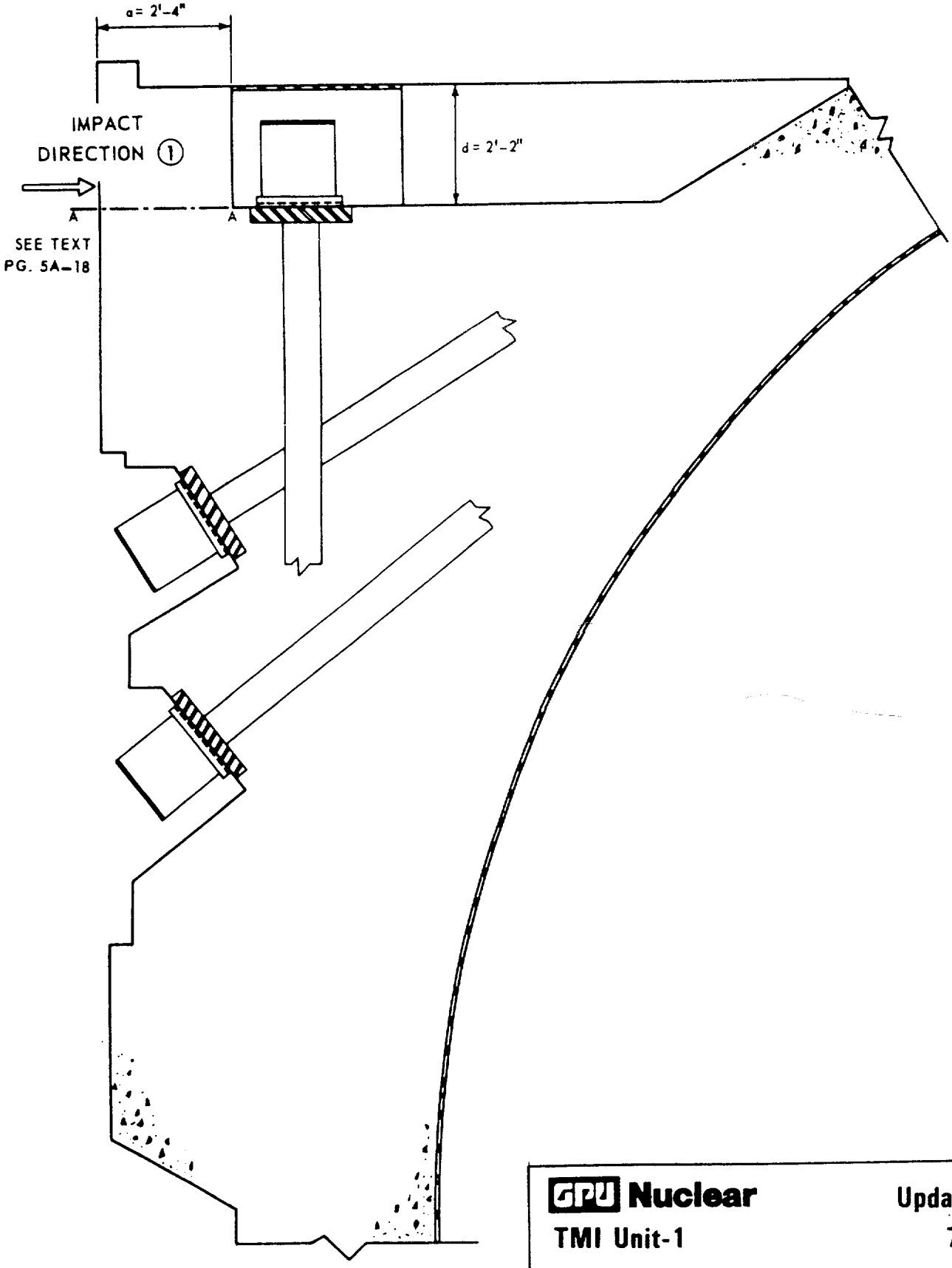

GPU Nuclear
TMI Unit-1

Update -1
7/82

Concrete Cover to Protect Against Aircraft Impact

Fig. 5A-27

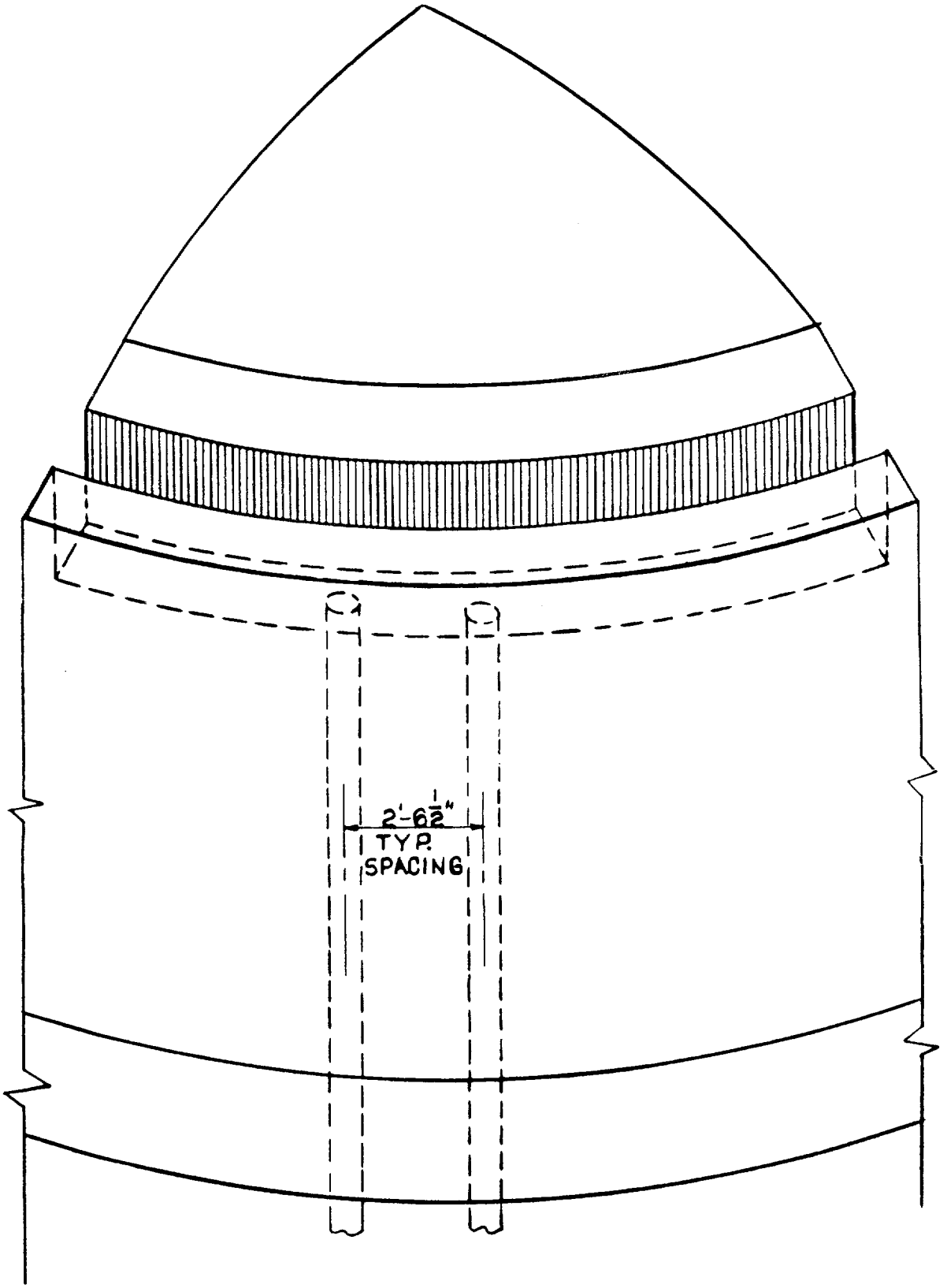

GPU Nuclear
TMI Unit-1

Update -1
7/82

Detail of Anchor Block

Fig. 5A-28

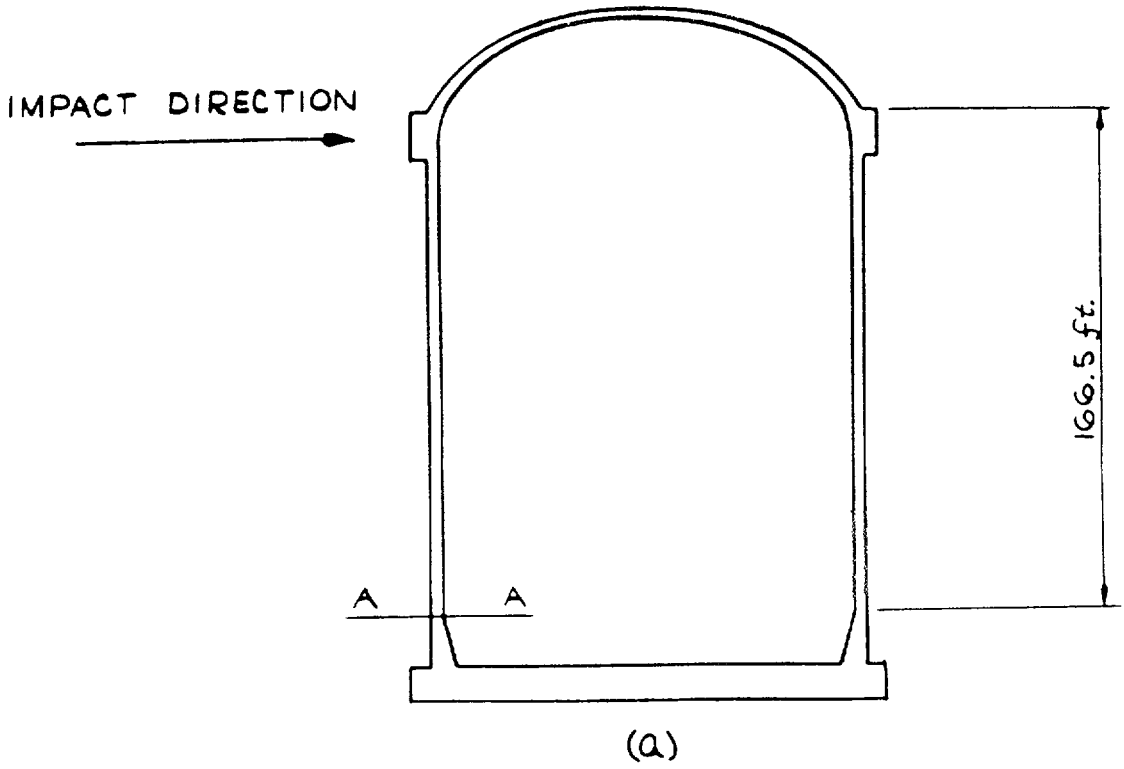

(a)

(b)

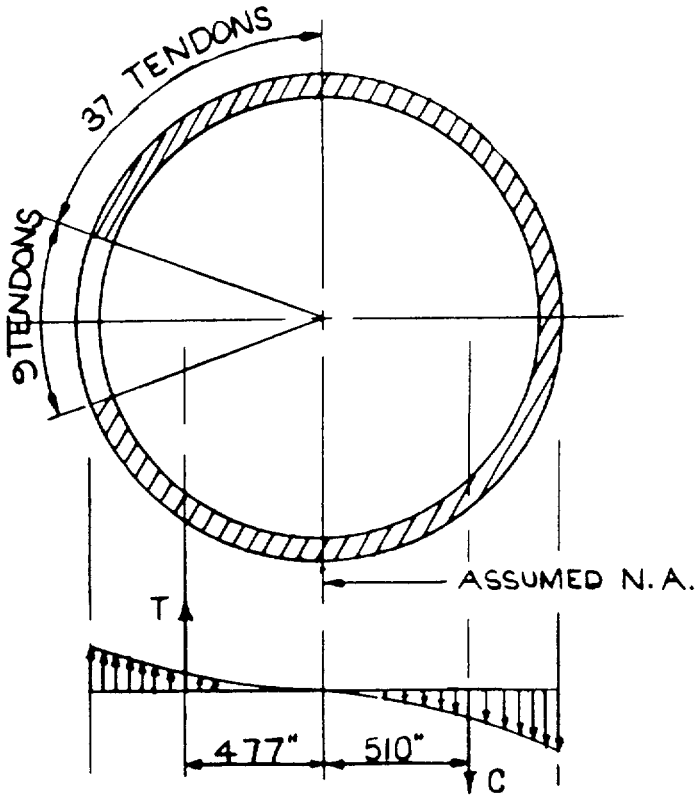

GPU Nuclear
TMI Unit-1

Update -1
7/82

Prestress Stresses after Nine Tendons Fail

Fig. 5A-29

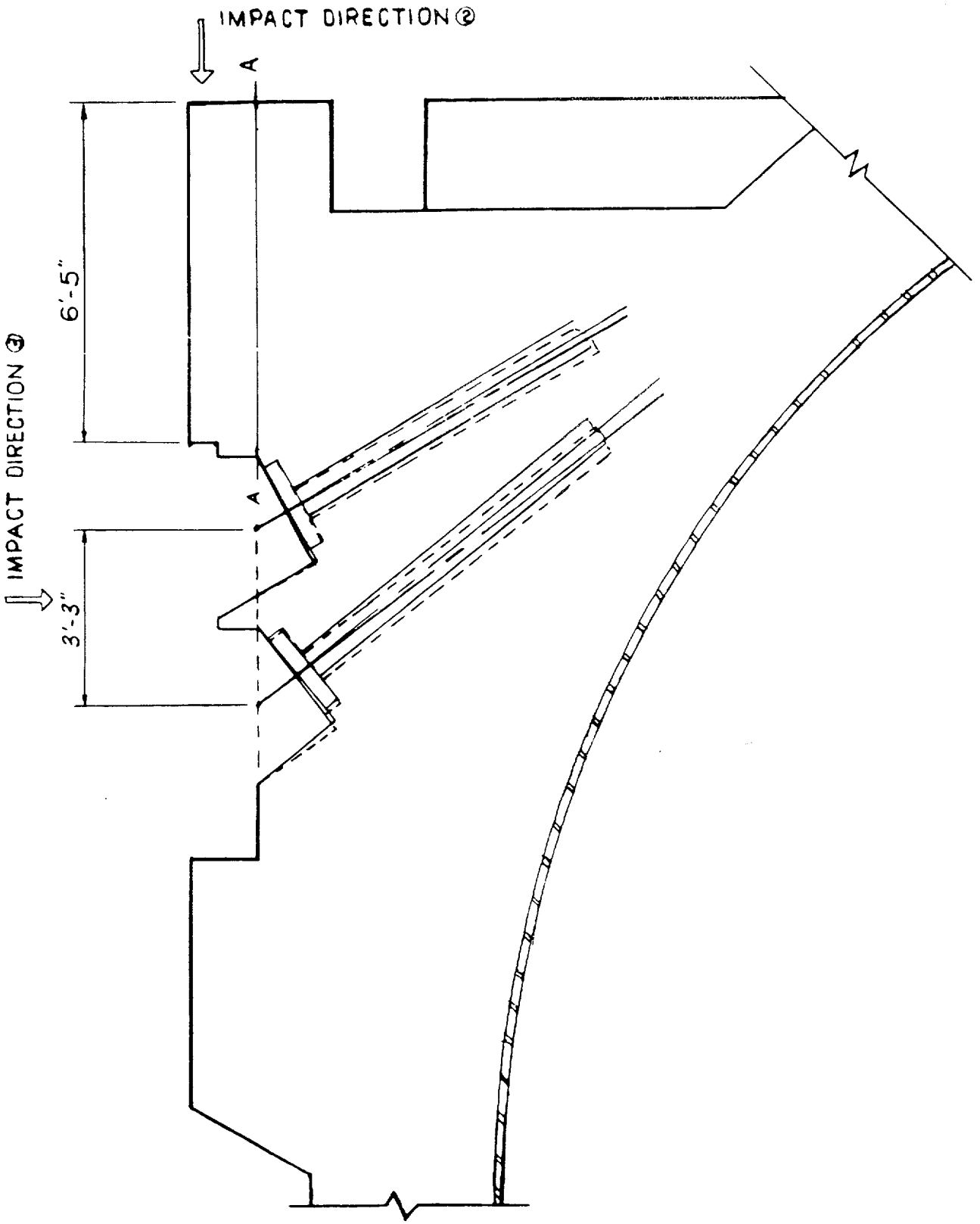

p. 5A.FIG-30

GPU Nuclear
TMI Unit-1

Update -1
7/82

Critical Aircraft Impact - Directions 2 and 3

Fig. 5A-30

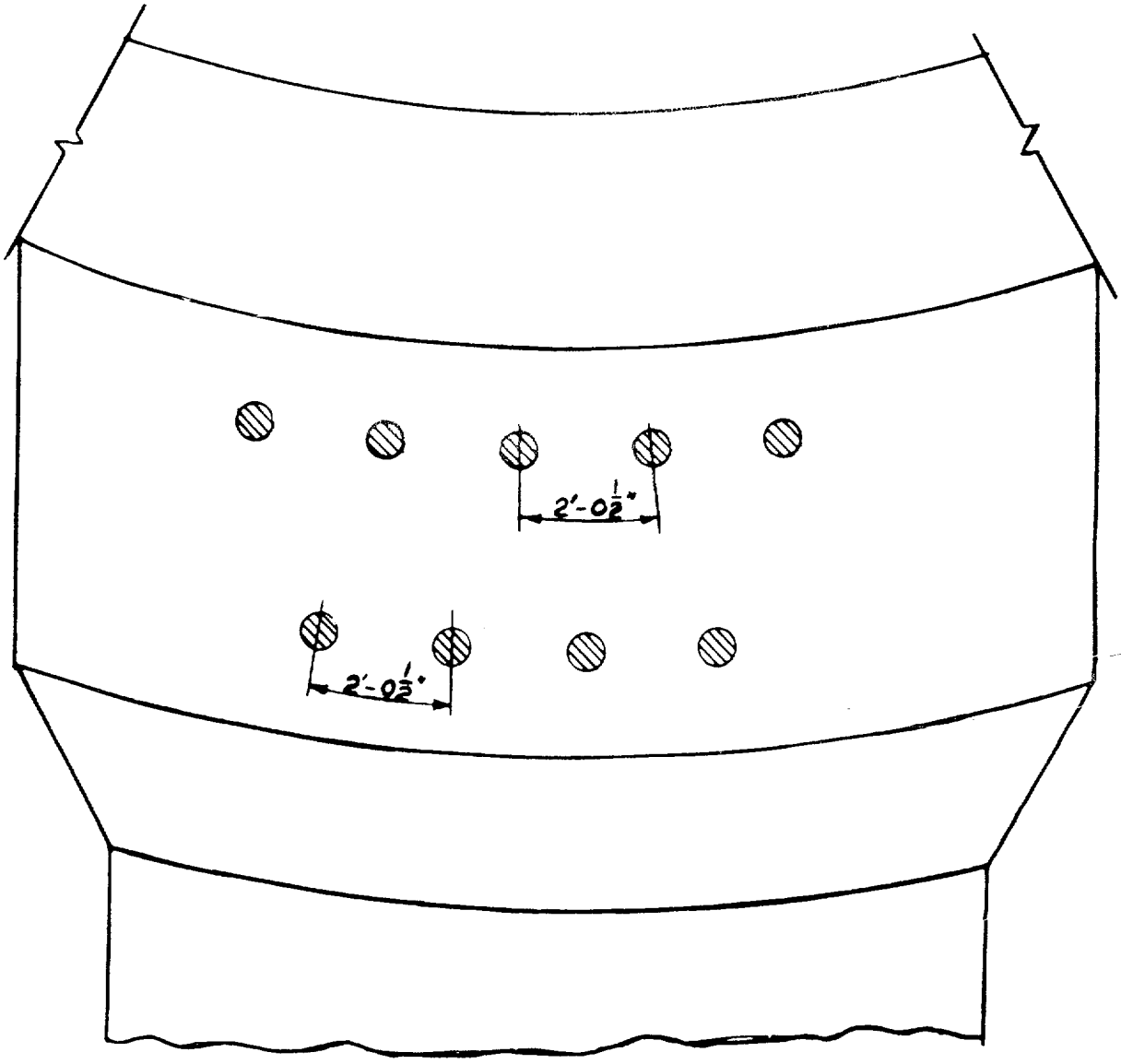

GPU Nuclear
TMI Unit-1

Update -1
7/82

Equal Spacing of Roof Tendons

Fig. 5A-31

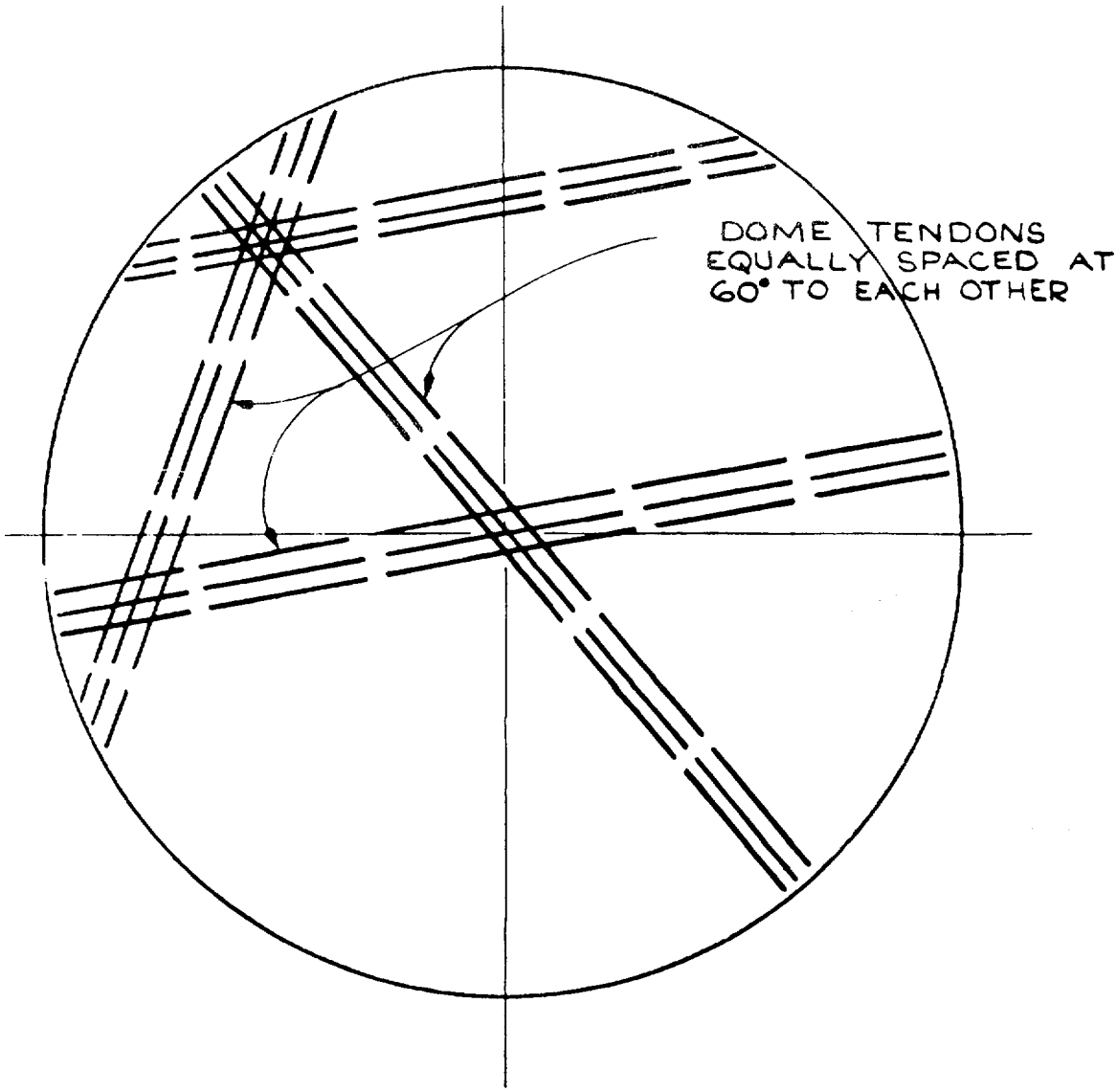

GPU Nuclear
TMI Unit-1

Update -1
7/82

Dome Tendons

Fig. 5A-32

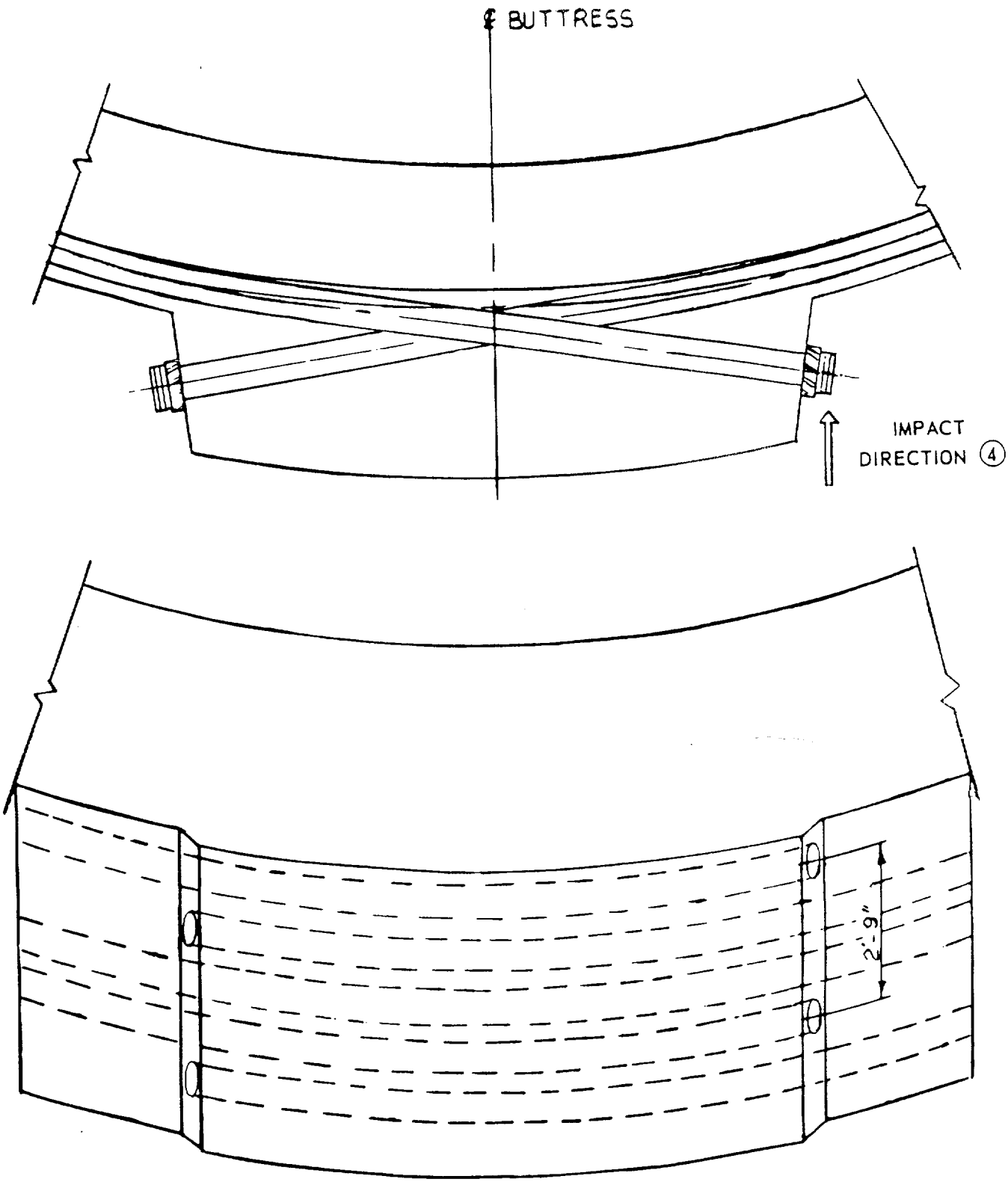

GPU Nuclear **Update -1**
TMI Unit-1 **7/82**

Minimum Spacing of Hoop Tendons

Fig. 5A-33

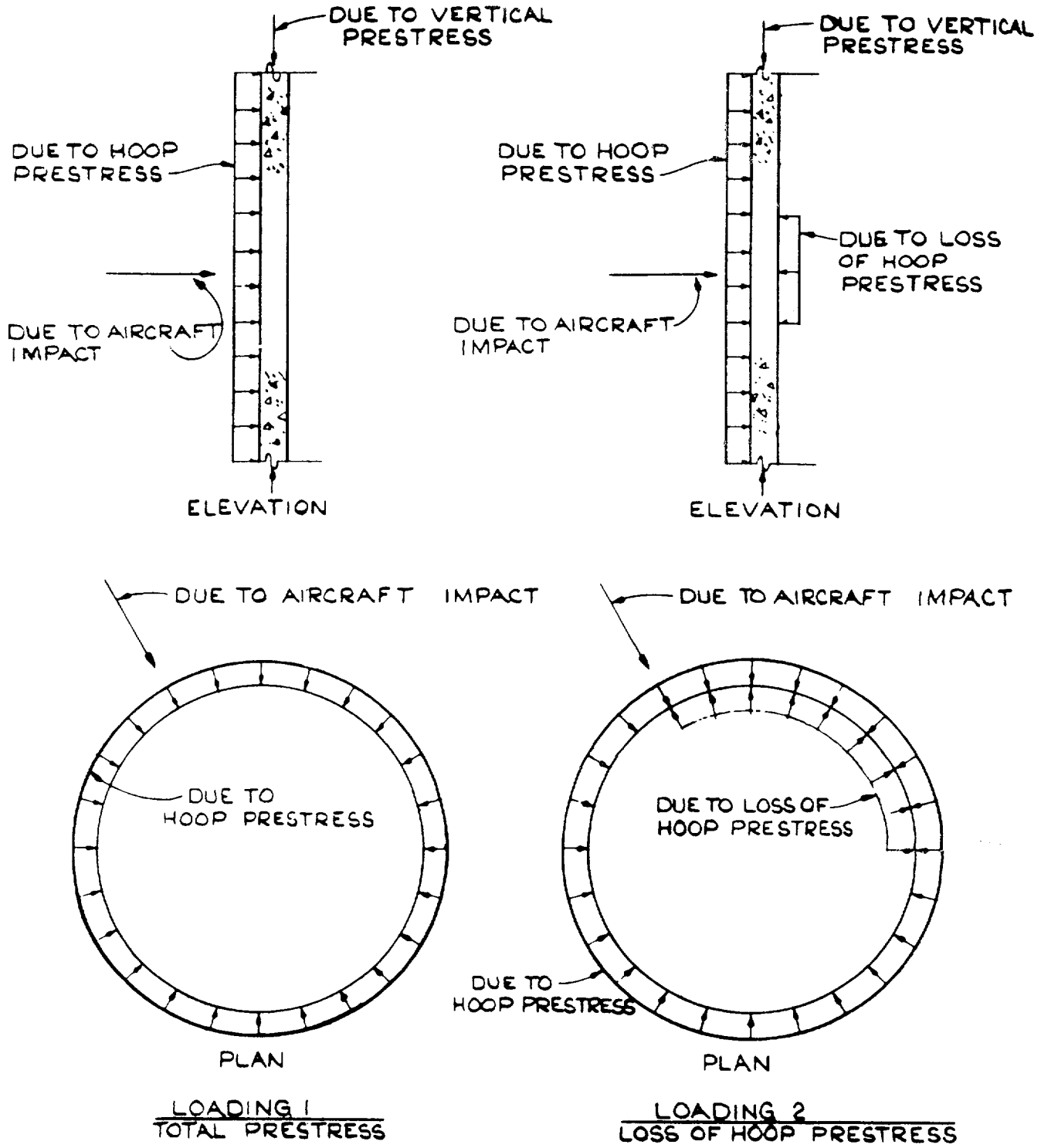

GPU Nuclear	Update -1
TMI Unit-1	7/82
Comparison of Prestress Loading	
	Fig. 5A-34

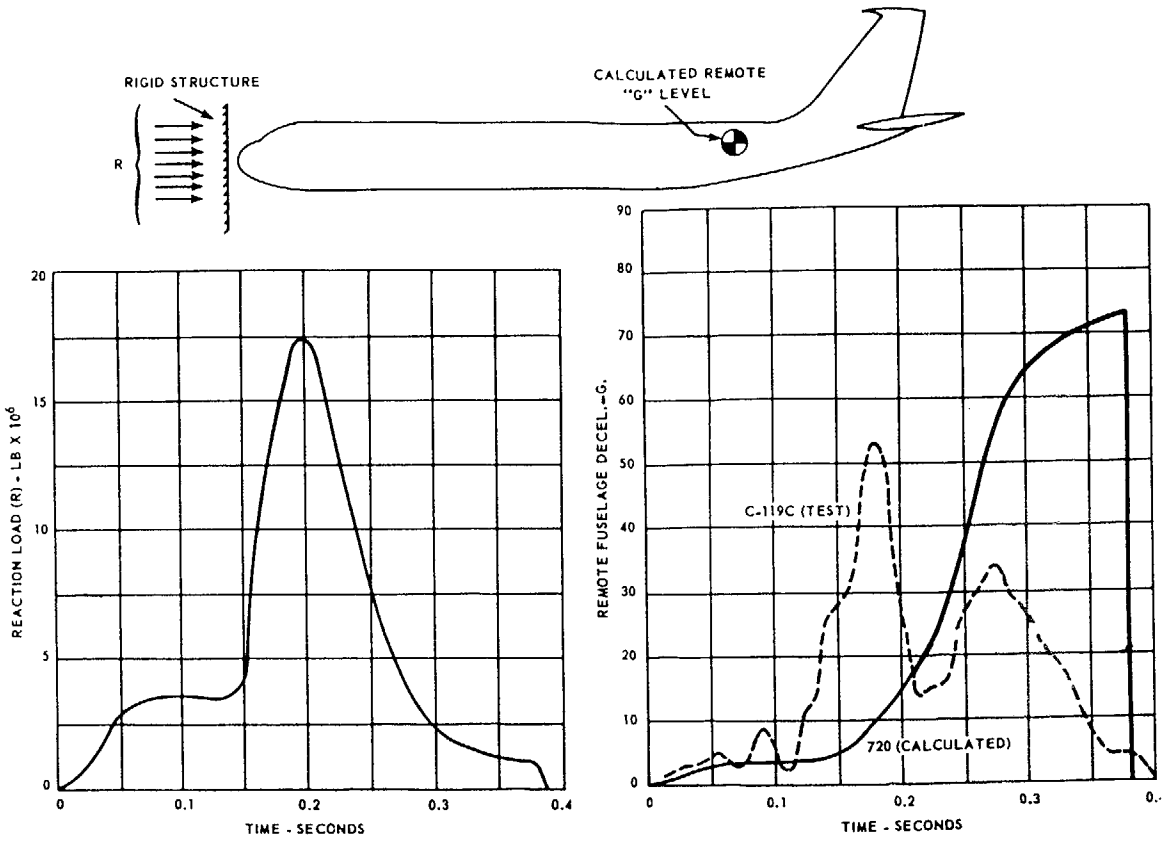

SEE TABLE 5A-7, REACTION LOAD CALCULATIONS
WITH WINGS AND ENGINES ATTACHED

GPU Nuclear
TMI Unit-1

Update -1
7/82

Reaction Load and Fuselage Decel. (Calculated for 720)

Fig. 5A-36

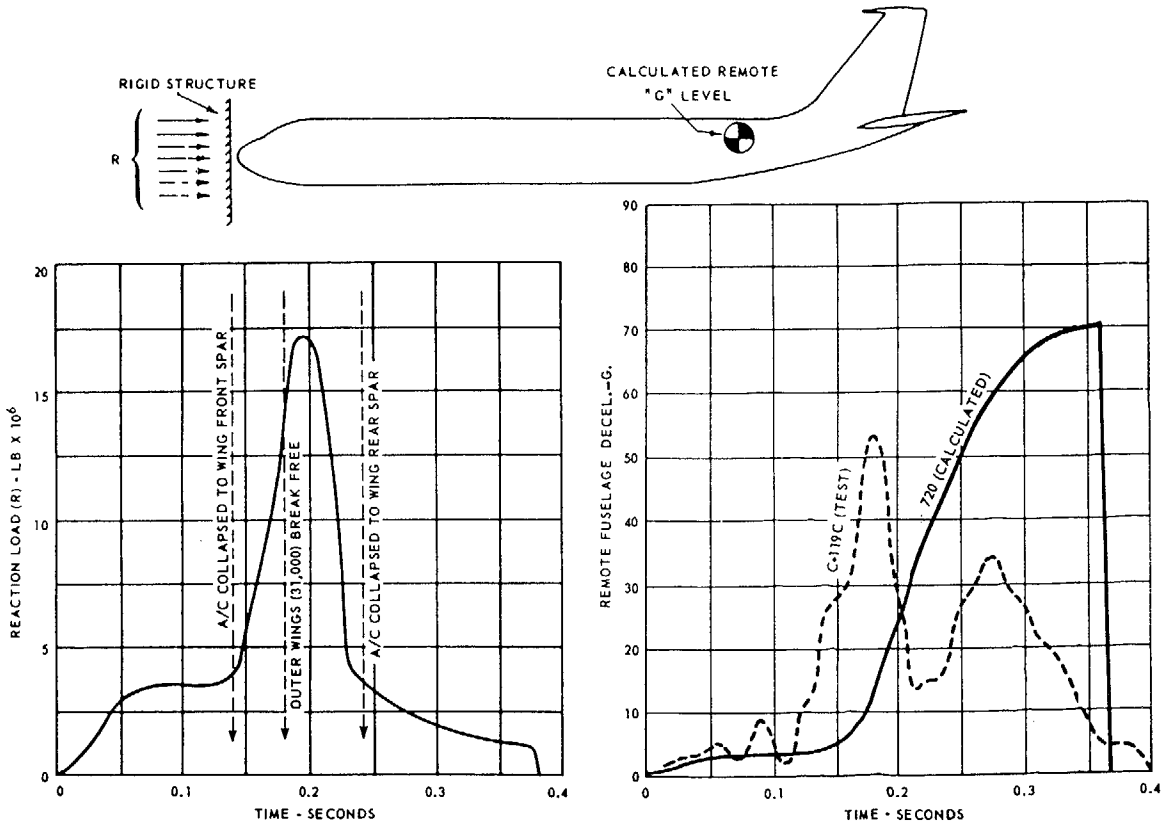

SEE TABLE 5A.6, REACTION LOAD CALCULATIONS
WITH WINGS & ENGINES DETACHED

GPU Nuclear
TMI Unit-1

Update -1
7/82

Reaction Load and Fuselage Decel. (Calculated for 720)

Fig. 5A-35

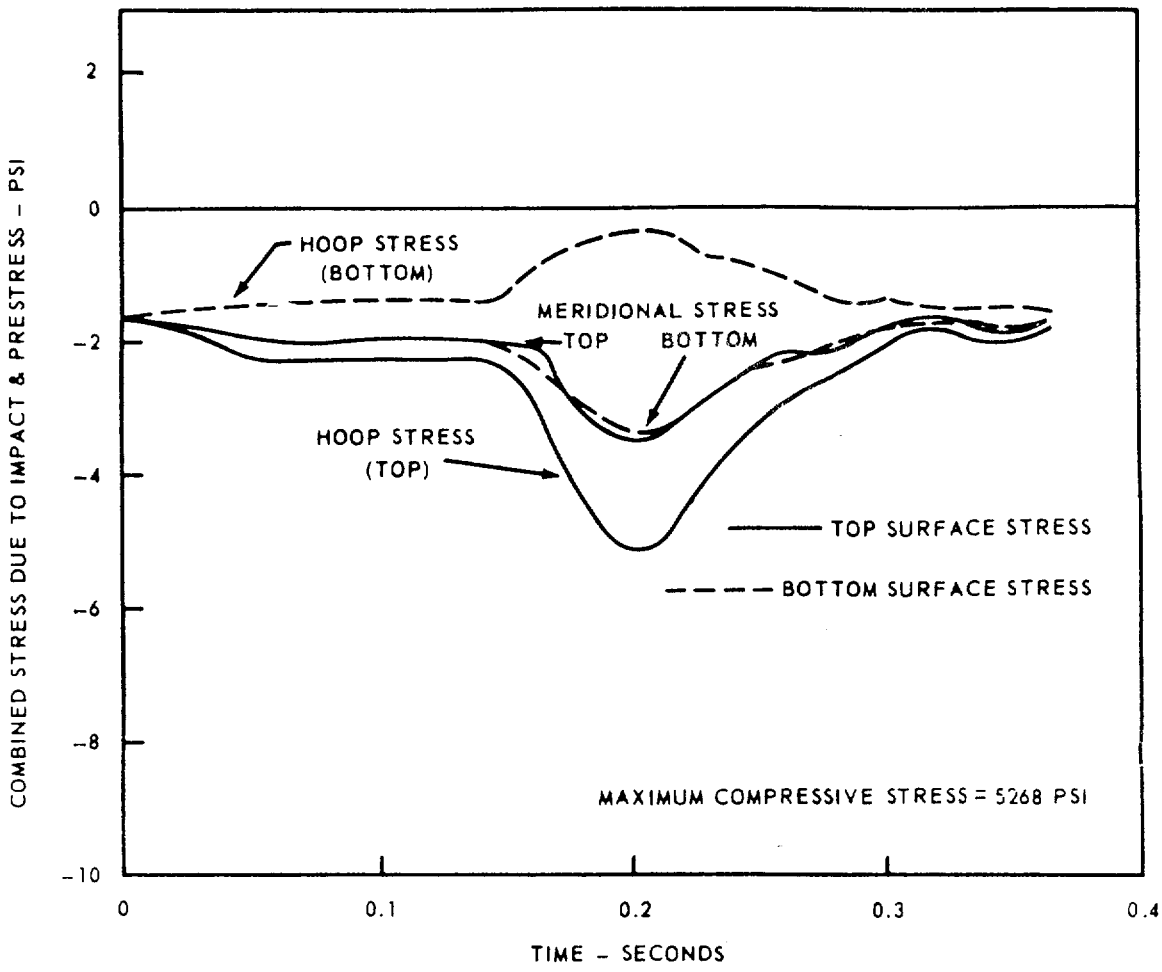

GPU Nuclear — Update -1

TMI Unit-1 — 7/82

Hoop and Meridional Stresses at 36 Inches from the Edge of the Load Area

Fig. 5A-37

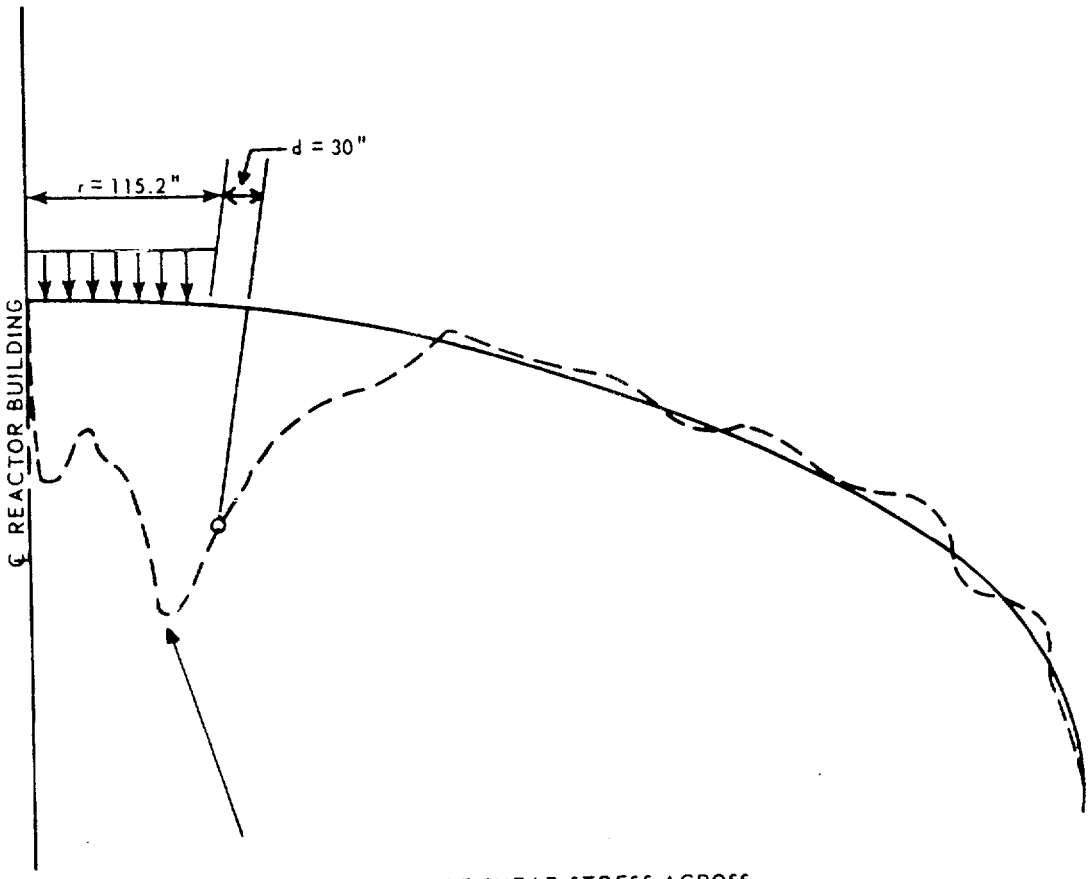

MAXIMUM AVERAGE SHEAR STRESS ACROSS SECTION = 482 PSI

SHEAR AT $r = 145.2" = 354$ PSI

ULTIMATE SHEAR STRESS FROM CHAPTER 26 OF ACI 318 = $v = 3.5\sqrt{f'_c} + 0.3\ f_{pc}$

$v = 3.5 \times 70.7 + 0.3 \times 1600 = 728$ PSI > 354 PSI OK

GPU Nuclear

TMI Unit-1

Update -1

7/82

Average Shear Stress in the Dome at the Time t=0.20 Seconds, Wing and Engines Remain Attached to Fuselage

Fig. 5A-38

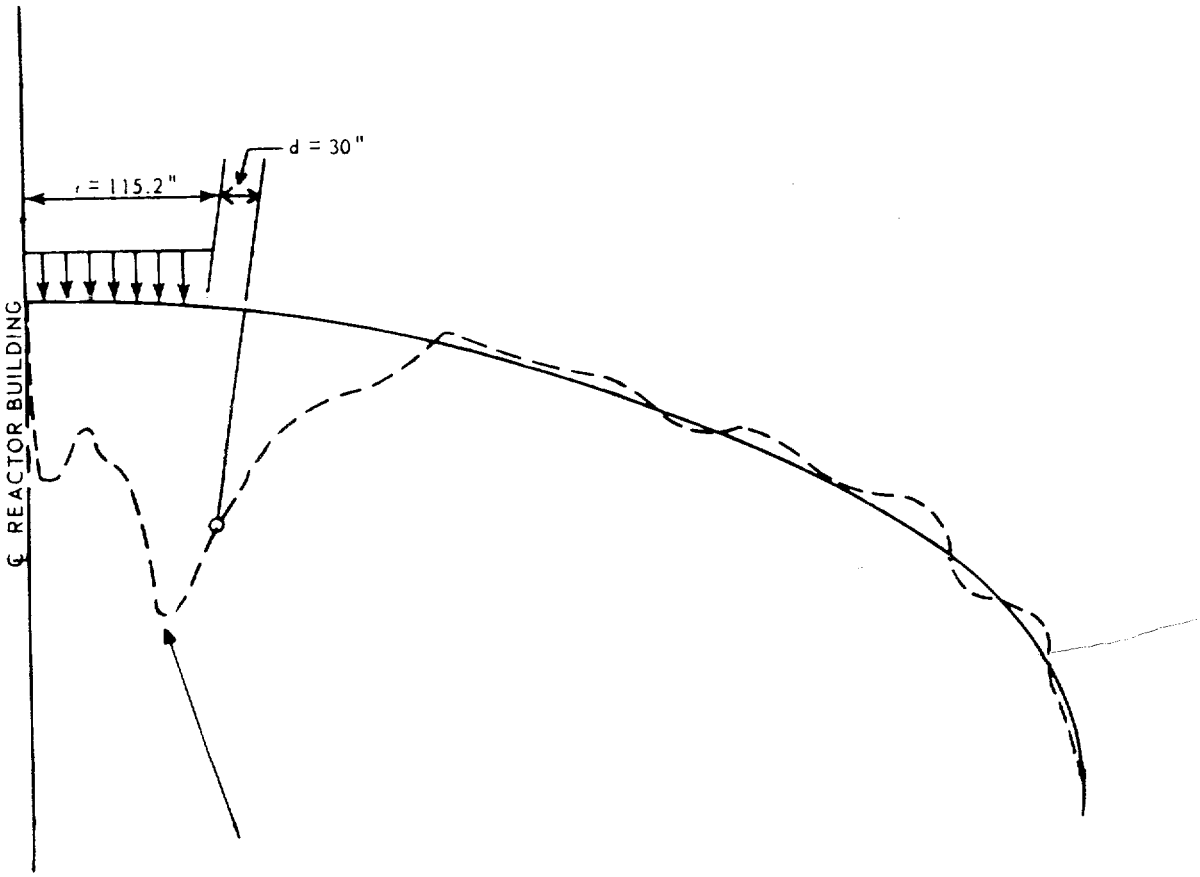

MAXIMUM AVERAGE SHEAR STRESS ACROSS SECTION = 482 PSI

SHEAR AT $r = 145.2"$ = 354 PSI

ULTIMATE SHEAR STRESS FROM CHAPTER 26 OF ACI 318 = $v = 3.5\sqrt{f'_c} + 0.3\ f_{pc}$

$v = 3.5 \times 70.7 + 0.3 \times 1600 = 728$ PSI > 354 PSI OK

GPU Nuclear — Update -1

TMI Unit-1 — 7/82

Average Shear Stress in the Dome at the Time t=0.20 Seconds, Wing and Engines Detached from Fuselage

Fig. 5A-39

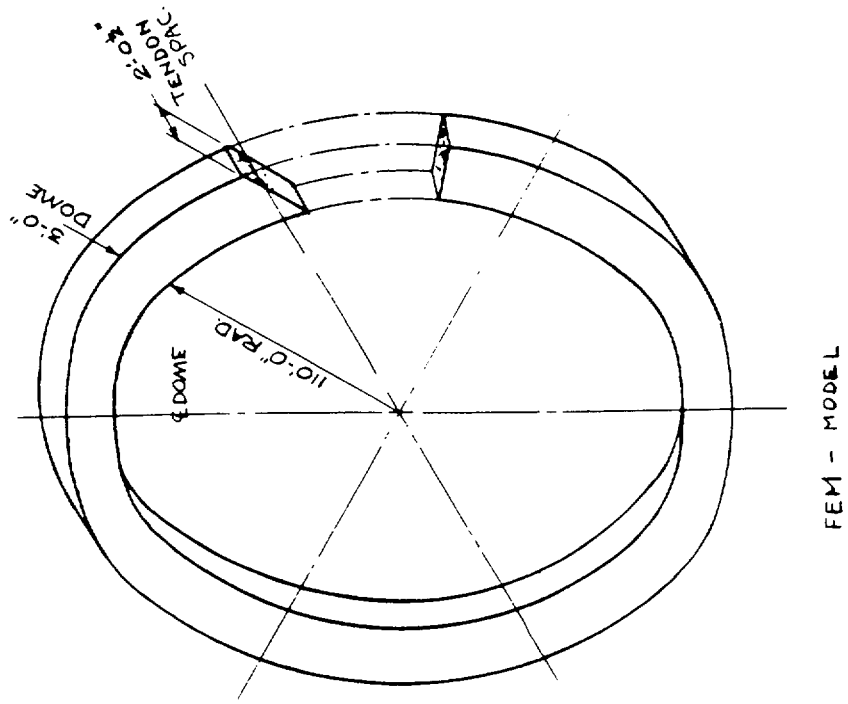

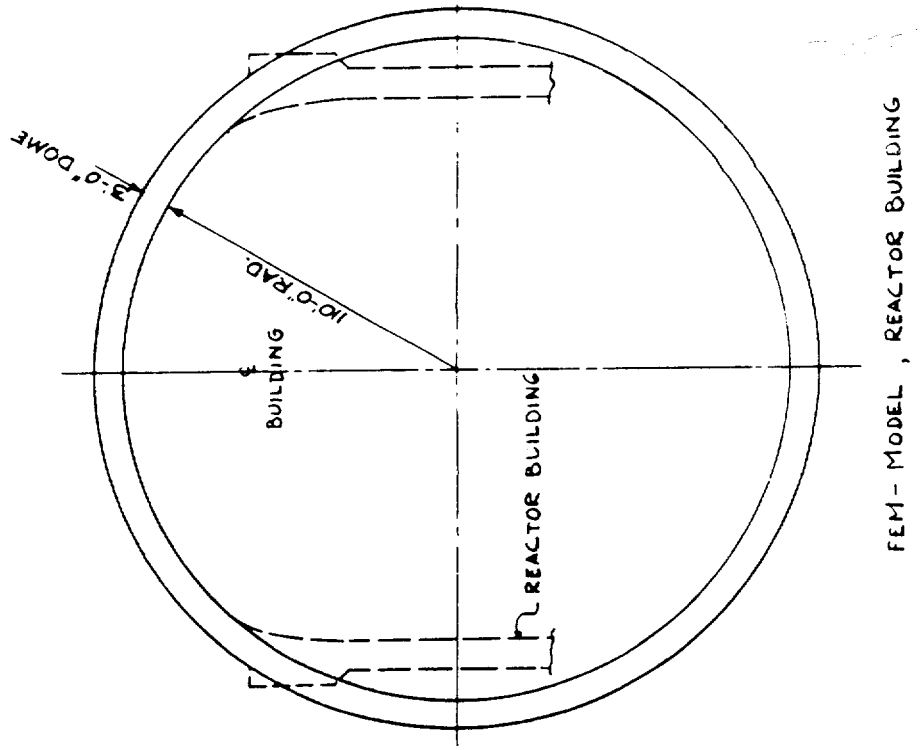

GPU Nuclear **Update -1**

TMI Unit-1 **7/82**

FEM Model-Radial Stresses Due to Prestress and Aircraft

Fig. 5A-40

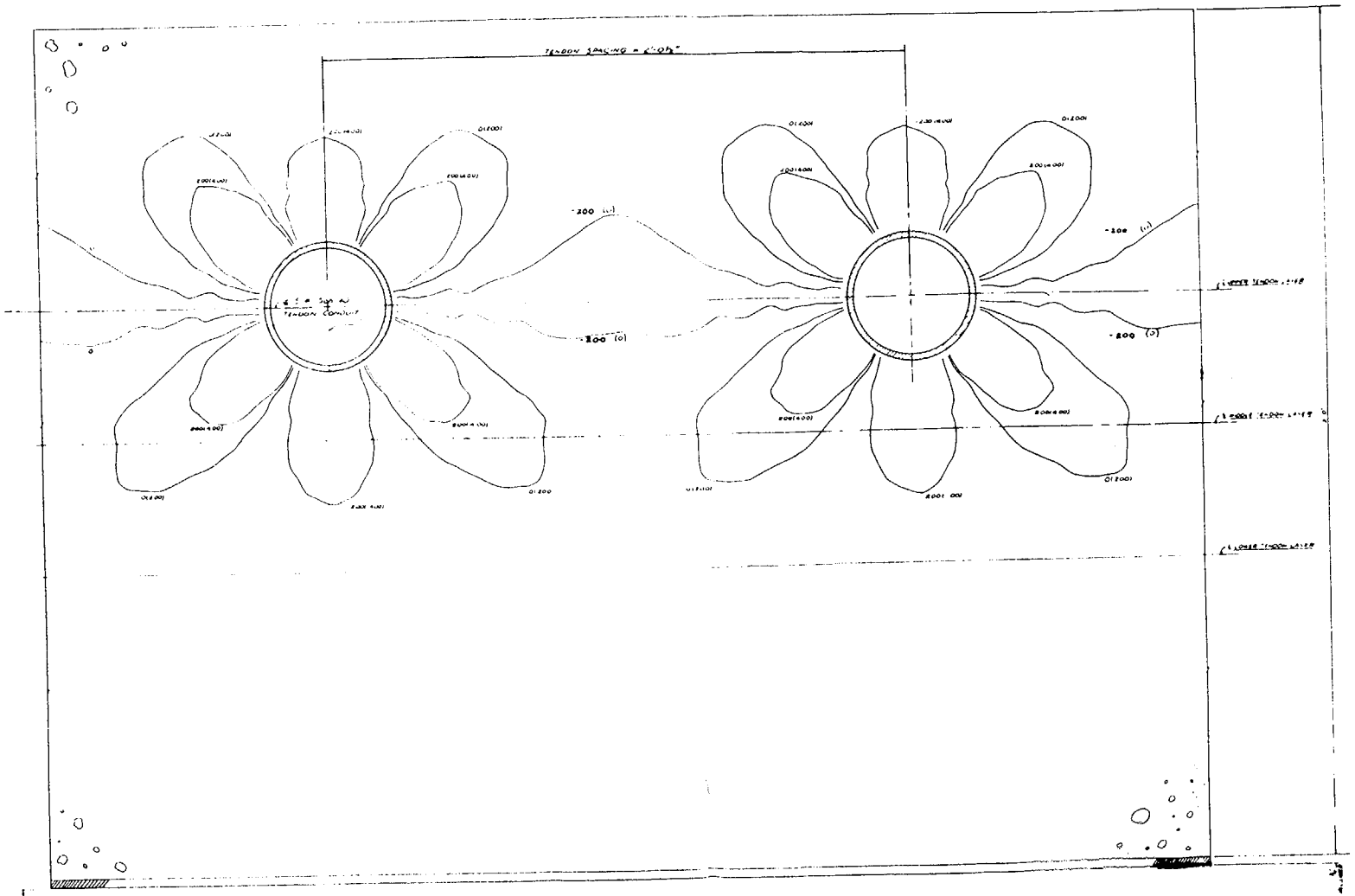

DOME SECTION

GPU Nuclear
TMI Unit-1

Update -1
7/82

Radial Stresses Due to Prestress and Aircraft Impact

Fig. 5A-41

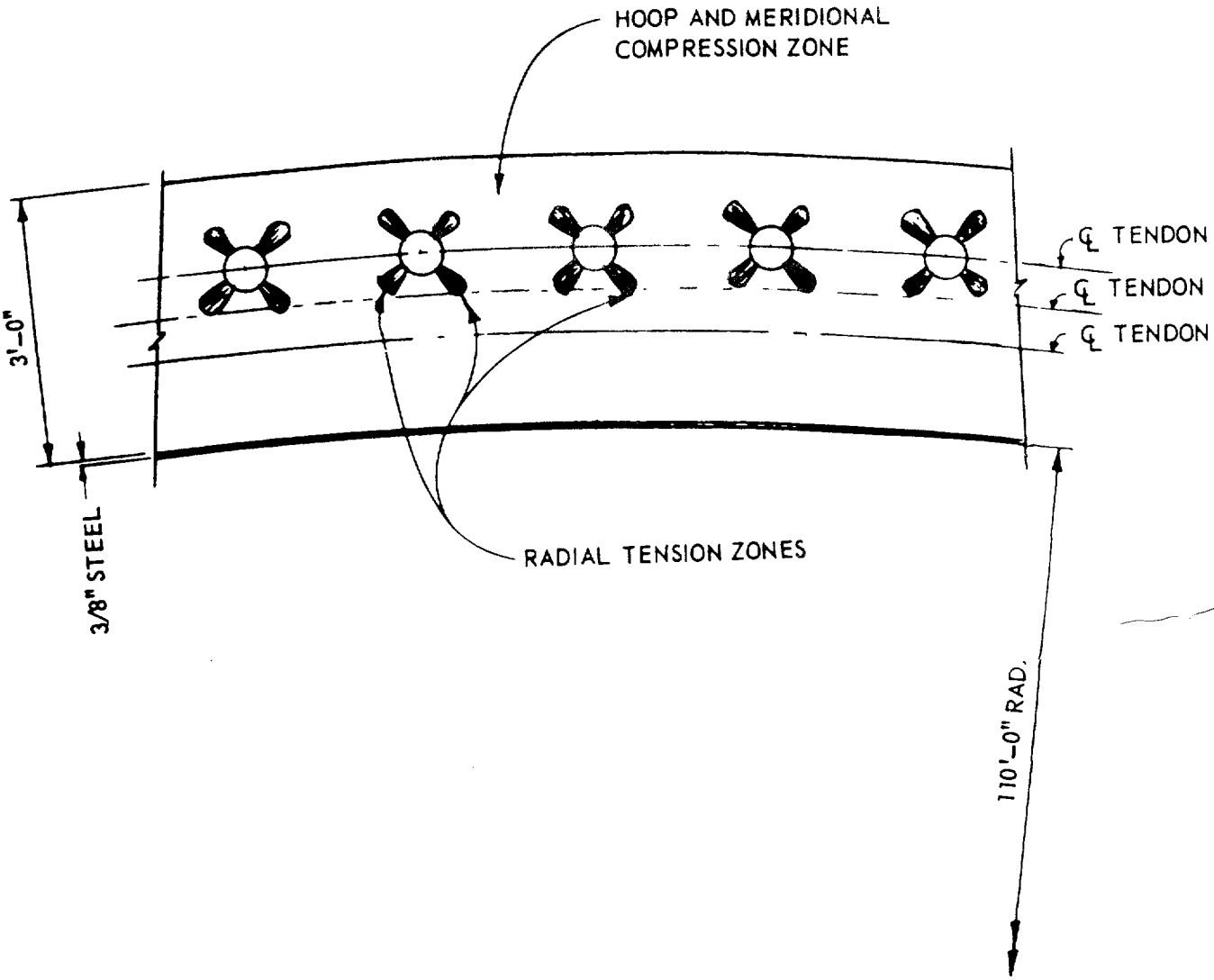

GPU Nuclear
TMI Unit-1

Update -1
7/82

Zones in Compression or Tension Due to Prestress of Aircraft Impact

Fig. 5A-42

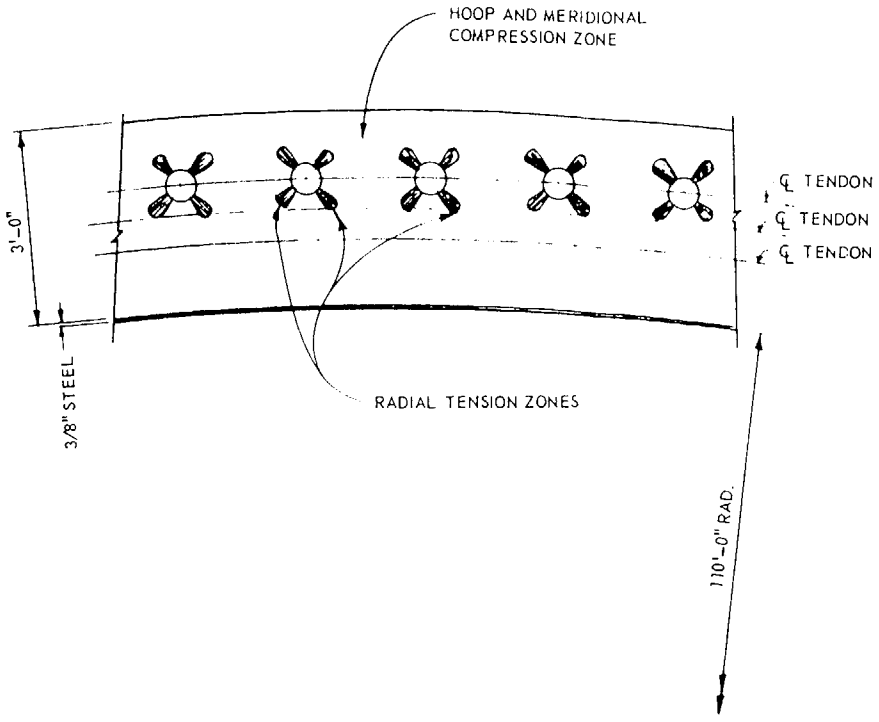

GPU Nuclear
TMI Unit-1

Update - 1
7/82

Zones in Compression or Tension Due to Prestress or Aircraft Impact

Fig. 5A-42